

ELECTRON SPIN RESONANCE OF TRANSITION
METAL COMPLEXES

Thesis for the Degree of Ph. D.

MICHIGAN STATE UNIVERSITY

Henry Anton Kuska

1965



This is to certify that the

thesis entitled

ELECTRON SPIN RESONANCE OF TRANSITION
METAL COMPLEXES

presented by

HENRY ANTON KUSKA

has been accepted towards fulfillment
of the requirements for

Ph. D. degree in CHEMISTRY

Max T Rogers
Major professor

Date Aug. 19 ,1965

ABSTRACT

ELECTRON SPIN RESONANCE OF TRANSITION METAL COMPLEXES

by Henry Anton Kuska

Central metal and ligand nuclear hyperfine splittings and g values were obtained for a number of transition metal complexes by electron paramagnetic resonance spectroscopy. The hyperfine interactions studied include: (1) Carbon-13 ligand hyperfine splittings in $\text{Cr}(\text{CN})_6^{-3}$, $\text{Cr}(\text{CN})_5\text{NO}^{-3}$, $\text{Fe}(\text{CN})_5\text{NO}^{-3}$, and $\text{VO}(\text{CN})_5^{-3}$. (2) copper nuclear hyperfine splittings in a series of substituted acetylacetonate complexes, a series of amino acid complexes, and a series of aliphatic amine complexes, and (3) vanadium nuclear hyperfine splittings in a large number of vanadyl complexes.

The metal-cyanide sigma bonds in $\text{Cr}(\text{CN})_5\text{NO}^{-3}$, $\text{Cr}(\text{CN})_6^{-3}$ and $\text{VO}(\text{CN})_5^{-3}$ were found to have a large amount of covalent character, but the amount of metal-cyanide covalent π bonding appears to be small.

The data for the substituted acetylacetonate complexes of copper (II) indicate that the isotropic hyperfine splittings and g values give the opposite trend of covalent character from that obtained by other methods. This discrepancy was explained by postulating that the isotropic hyperfine splittings are dependent on two contributions, a polarization of filled s orbitals and a fractional occupancy of the empty 4s orbital. The anisotropic hyperfine splittings and g values, which are not dependent on fractional 4s character, did give the expected trend in molecular orbital coefficients. The isotropic g values and hyperfine splittings were found to vary in the same manner

when the complexes were dissolved in more basic solvents as they did when more electronegative groups were substituted in the acetylacetonate structure.

The nitrogen ligand hyperfine splittings in copper (II) glycinate indicate appreciably less covalency in the copper-nitrogen bond than found for copper (II) phthalocyanine.

For the series of copper (II) complexes with amino acids and aliphatic amines a larger isotropic copper nuclear hyperfine splitting correlated with a higher stability constant; however, there were many exceptions which appear to be due to steric effects changing the local symmetry at the copper ion.

For the vanadyl complexes it was possible to correlate the isotropic hyperfine splittings with the ratio of axial to equatorial crystal field. The nuclear hyperfine splitting was found to decrease with increasing covalency and with a lowering of symmetry. The decrease with lowering of symmetry is thought to be due to an increase in the positive contribution of 4s electron density which decreases the net spin density since the polarization of filled s orbitals gives a negative spin density.

ELECTRON SPIN RESONANCE OF
TRANSITION METAL COMPLEXES

by

Henry Anton Kuska

A THESIS

Submitted to
Michigan State University
in partial fulfillment of the requirements
for the degree of

DOCTOR OF PHILOSOPHY

Department of Chemistry

1965

Handwritten text in the top left corner, possibly a signature or title, which is mostly illegible due to blurring.

To my Wife and Parents

ACKNOWLEDGMENTS

The author wishes to express his sincere appreciation to Professor M. T. Rogers for his continued interest, counsel, and encouragement during the course of this investigation.

I would also like to thank Professor B. R. McGarvey, Polytechnic Institute of Brooklyn, and Professor R. G. Hayes, University of Notre Dame, for helpful discussions and pre-prints of related papers.

The experimental assistance of Mr. Lowell Kispert, Mr. John Wreede, Mr. Robert Drullinger, Miss Sandra Bartlett, Mr. Robert Wegener, and Mr. Ward Collins is gratefully acknowledged.

Also I would like to thank the Atomic Energy Commission, the Dow Chemical Company, and the United States Army for financial support during the course of this investigation.

TABLE OF CONTENTS

	Page
INTRODUCTION	1
HISTORICAL	3
Transition Metal Chemistry	3
Review of the Application of Electron Spin Resonance to Transition Metal Complexes	4
Development of the Theory of Obtaining Covalency Parameters from the ESR g Values	6
Theory of Owen	6
Theory of Owen plus Screening Effects	6
Alternate Theory to Owen's Covalent Theory- The Free Ion Theory	10
Present g Value Theory. Inclusion of Charge Transfer and Ligand Spin Orbit Coupling Con- stant Contributions	11
Development of the Theory of Obtaining Covalency Parameters from the ESR Hyperfine Splittings	11
Restricted Hartree-Fock Model-Higher Orbital s Character	11
Unrestricted Hartree-Fock Model-Spin Polarization	11
THEORETICAL	16
Covalent Molecular Orbital Theory of Ligand Hyper- fine Splittings for $\text{Cr}(\text{CN})_6^{-3}$ and CrF_6^{-3}	16
Energy Levels and Molecular Orbitals of $\text{Cr}(\text{CN})_6^{-3}$ and CrF_6^{-3}	16
Experimental ESR Parameters	17
Relationships Between the Experimentally Deter- mined A Values and the Molecular Orbitals	19
Higher Order Considerations and Alternate Theory	21
Covalent Molecular Orbital Theory for the Determina- tion of M.O. Coefficients from the ESR g Values of CrF_6^{-3} and $\text{Cr}(\text{CN})_6^{-3}$	22

	Page
Molecular Orbital Theory of d^1 and Low-Spin d^5 Systems in Tetragonal Field	22
Theory of ESR g Values	22
Metal Ion Hyperfine Splitting Theory	25
Ligand Hyperfine Splittings	25
Molecular Orbital Theory of Ligand Hyperfine Splittings for Copper (II) Complexes and $Fe(CN)_5NO^{3-}$	27
Crystal Field Theory for Tetragonal Symmetry.	28
EXPERIMENTAL	32
ESR System	32
Second Derivative Presentation	32
Measurement of Magnetic Field	32
Measurement of Klystron Frequency	33
Linear, Precalibrated Magnetic Field Sweeps	34
Single Crystal Holder	34
Standard Samples	37
Preparation of Samples.	38
Crystal Growing	38
$K_3Cr(CN)_5NO$ in Alkali Halide Lattices	38
Preparation of Other Single Crystals	39
Equations and Conversion Factors.	39
RESULTS	41
$K_3Cr(CN)_5NO$	41
Electronic Configuration and Optical Spectra.	41
Solution ESR Spectra.	41
Single Crystal Studies.	42
Comparisons of Powder Spectra Data with Single Crystal Data	52
Infrared Spectra	55
$K_3Cr(CN)_6$	55
Crystal Orientation	55
Vanadyl Complexes	62
Ligand Hyperfine Splittings in Vanadyl Com- plexes.	64
Covalency in Vanadyl Complexes.	71

	Page
Copper Complexes	73
Single Crystal Study of Copper Glycinate in Cadmium Glycinate	73
Solution Spectra of Copper Amino Acid Complexes	78
Solution Spectra of Substituted Copper Ace- tylacetonates	78
ESR Study of $[\text{Cr}(\text{NO})(\text{NH}_3)_5]\text{Cl}_3$	88
DISCUSSION	90
$\text{K}_3\text{Cr}(\text{CN})_5\text{NO}$	90
Solution ESR Spectra	90
Electronic Configuration and Optical Spectra	91
Molecular Orbital Coefficients From Single Crystal Data	94
Anisotropic ^{13}C Splittings	98
Variation of ESR and Infra-Red Data with the Various Alkali Halide Matrices	98
$\text{K}_3\text{Cr}(\text{CN})_6$	99
Covalent Bonding	99
Determination of g_y , D, and E	100
^{53}Cr Hyperfine Splittings	102
ESR Studies of Copper Glycinate	102
Solution Spectra of Substituted Copper Acetylac- etonates	104
Solution Spectra of Substituted Vanadyl Acetylac- etonates	110
Correlation of Optical Spectra With The ESR <u>A</u> Values	112
ESR Spectra of Vanadyl Complexes	117
Solution Spectra of Copper (II) Amino Acid Com- plexes	118
SUMMARY	126
APPENDIX I-GLOSSARY	127
REFERENCES	130

LIST OF TABLES

Table	Page
1. Electron distribution in the metal d and ligand p orbitals due to metal-ligand overlap	8
2. Reduction of spin-orbit coupling constants for transition metal hydrates	9
3. Spin density in KNiF_3	15
4. σ_x and π_x values for Co III ions	31
5. Experimental ESR data for $\text{K}_3\text{Cr}(\text{CN})_5\text{NO}$ in H_2O . .	43
6. Data for $\text{Cr}(\text{CN})_5\text{NO}^{-3}$ in various lattices	53
7. Comparison of powder and crystal ESR data . . .	54
8. Infrared data for $[\text{M}(\text{CN})_5\text{NO}]^x$ compounds	56
9a. Direction cosines between the principle magnetic axes (x,y,z) and the crystallographic axes (a,b,c) for $\text{K}_3\text{Co}(\text{CN})_6$	59
9b. Direction cosines between the molecular axes (α, β, γ) and the crystallographic axes (a,b,c) for $\text{K}_3\text{Co}(\text{CN})_6$	59
10. ^{13}C ESR data for $\text{Cr}(\text{CN})_6^{-3}$ in $\text{K}_3\text{Co}(\text{CN})_6$	62
11. Solution ESR spectra of substituted vanadyl acetylacetonates	63
12. ESR and optical data for vanadyl oxalate	64
13. ESR data for vanadyl complexes	65
14. ^{13}C hyperfine splittings in $\text{VO}(\text{CN})_5^{-3}$	71
15. Molecular orbital coefficient for vanadyl xy orbital	73
16. ESR data for bis-(glycino)-copper (II)·xH ₂ O . .	74

Table	Page
17. ESR hyperfine splittings for copper (II) amino acid complexes	78
18. Isotropic and anisotropic A values for substituted copper (II) acetylacetonates	79
19. s orbital spin density (f_s) in sigma ligand orbitals	92
20a. Possible energy level assignment for $\text{Cr}(\text{CN})_5\text{NO}^{-3}$	93
20b. Alternate energy level assignment for $\text{Cr}(\text{CN})_5\text{NO}^{-3}$	94
21. $\text{K}_3\text{Co}(\text{CN})_6$ vibration frequencies	99
22. Values of g_y , D , and E for $\text{K}_3\text{Cr}(\text{CN})_6$ in $\text{K}_3\text{Co}(\text{CN})_6$	101
23. Comparison of ligand spin densities for copper complexes	103
24. ESR hyperfine splitting constants and other data for copper acetylacetonates	105
25. Comparison of copper (II) phthalocyanine and copper (II) glycinate ESR data	109
26. ESR A values for Cu^{+2} and VO^{+2} adsorbed on ion exchange resins	111
27. Energy levels, hyperfine splittings, and ρ values for vanadyl complexes	113
28. σ and π electrostatic interactions for VYX_5 compounds	116
29. Comparison of the ESR data for $\text{VO}(\text{CN})_5^{-3}$ and $[\text{VS}_6\text{C}_6(\text{CN})_6]$	118
30. Literature ESR A values for VO^{+2} complexes	119
31. Group overlap integrals for some vanadyl complexes	121
32. ESR data and literature data for copper amino acid complexes	122
33. ESR and stability constants for copper (II) amine complexes	125

LIST OF FIGURES

Figure	Page
1. Energy level diagram for Cr^{+3} ions	18
2. Energy level diagram for a d^1 transition metal ion in an octahedral and in a tetragonal field	24
3. Crystal field splittings for V^{+4}	29
4. Hall probe schematic	35
5. Adjustable single crystal holder	36
6. Energy level diagram for $\text{K}_3\text{Cr}(\text{CN})_5\text{NO}$	44
7. Orientation dependence of $\text{Cr}(\text{CN})_5\text{NO}^{-3}$ ESR data	46
8. Saturation of the g_{\parallel} position of $\text{K}_3\text{Cr}(\text{CN})_5\text{NO}$ in KBr single crystal at 77°K	47
9. Saturation of g_{\parallel} spectrum but not the g_{\perp} spectrum for $\text{K}_3\text{Cr}(\text{CN})_5\text{NO}$ in KBr single crystal at 77°K	47
10. Collapse of nitrogen lines by overmodulation of the 100 Kc unit for g_{\parallel} position of 15.5% ^{13}C enriched $\text{K}_3\text{Cr}(\text{CN})_5\text{NO}$ in KCl	49
11. Superposition of the g_{\parallel} ESR spectrum of 15.5% enriched ^{13}C $\text{K}_3\text{Cr}(\text{CN})_5\text{NO}$ in KBr single crystal and in ^{13}KCl single crystal	50
12. ^{13}C splittings of 15.5% enriched ^{13}C $\text{K}_3\text{Cr}(\text{CN})_5\text{NO}$ in g_{\perp} plane	51
13. Infrared spectra, from $5,000\text{ cm}^{-1}$ to $1,100\text{ cm}^{-1}$ of $\text{K}_3\text{Cr}(\text{CN})_5\text{NO}$ in various hosts	57
14. Infrared spectra, from $5,000\text{ cm}^{-1}$ to $1,100\text{ cm}^{-1}$ of $\text{Fe}(\text{CN})_5\text{NO}^{-2}$ in various hosts	58
15. ESR spectrum of 15.5% ^{13}C enriched $\text{Cr}(\text{CN})_6^{-3}$ in $\text{K}_3\text{Co}(\text{CN})_6$	60

Figure	Page
16. Single crystal ESR spectrum of $\text{VO}(\text{CN})_5^{-3}$ in KBr	69
17. ESR spectrum of $\text{VO}(\text{NCS})_5^{-3}$ in CHCl_3 solution .	70
18. Aqueous solution spectrum of 15.5% ^{13}C enriched $\text{VO}(\text{CN})_5^{-3}$	72
19. ESR spectra of copper (II) glycinate	75
20. Second derivative ESR spectrum at g_{\parallel} position (lines two and three) of a copper (II) glycinate-cadmium (II) glycinate single crystal	76
21. Second derivative ESR spectrum at g_{\perp} position of a copper (II) glycinate-cadmium (II) glycinate single crystal	77
22. Frozen CHCl_3 solution ESR spectra of copper (II) hexafluoroacetylacetonate	80
23. Frozen CHCl_3 solution ESR spectra of copper (II) trifluoroacetylacetonate	81
24. Frozen CHCl_3 solution ESR spectra of copper (II) benzoylacetonate.	82
25. Frozen CHCl_3 solution ESR spectra of copper (II) 3-methylacetylacetonate	83
26. Frozen CHCl_3 solution ESR spectra of copper (II) acetylacetonate	84
27. Frozen CHCl_3 solution ESR spectra of copper (II) benzoyltrifluoroacetone	85
28. Frozen CHCl_3 solution ESR spectra of copper (II) dibenzoylmethane	86
29. Hyperfine structure observed between g_{\parallel} lines two and three in a frozen CHCl_3 ESR spectrum of copper (II) dibenzoylmethane	87
30. ESR spectra of $\text{Cr}(\text{NO})(\text{NH}_3)_5^{+3}$ in NH_4Cl single crystal	89
31. Solvent and substituent effects on copper (II) acetylacetonates	108

Figure	Page
32. Correlation of ratio of axial to equatorial crystal field, ρ , and ESR A values for a number of vanadyl complexes	115
33. Plot of $A_{ }$ versus $g_{ }$ for a number of vanadyl complexes	120

INTRODUCTION

During the past ten years our knowledge of transition metal complexes has grown considerably. Experimentally, visible, infrared, and electron spin resonance (ESR) spectroscopy have provided the data required to test old theories and formulate new ones. Theoretically, a combination of crystal field and molecular orbital theory have been developed to explain the experimental data. This new theory called ligand field theory, is now generally accepted and is at present being refined to the point that quantitative calculations of the various observables are being made with reasonable success.¹ In this thesis the ESR spectra of a number of transition metal systems have been studied, the data have been interpreted in terms of present theory, and correlations of the ESR data with other types of measurements have been made.

At the beginning of this investigation there was a sizeable literature of ESR work on transition metal fluoro-complexes which indicated that fluorine-metal bonds were not ionic as had been assumed, but had a definite fraction of covalent character.^{1,2} It was decided that a comparison of ESR data for compounds normally considered to be covalent, such as the cyanides, with data for the fluoro-complexes would provide a basis for interpreting the significance of the reported covalent character in the fluoro-complexes. A relative comparison was considered desirable since there were indications that the approximations involved in the ESR theory were such that the amount of covalent character was being overestimated.³

However, in making such a comparison an additional factor had to be considered. The theory of hyperfine interactions had been developed for the nearly ionic case; in the

extension of this theory to highly covalent cases, additional terms may be significant. Because of this uncertainty, it was desirable to have ESR data from an addition series of compounds which had been well characterized by other physical methods and were known to be intermediate in covalency between the fluorides and the cyanides.

For the extremely covalent series, the cyanides and nitrosyls were chosen. The series consisted of the t_{2g}^1 compound $\text{VO}(\text{CN})_5^{-3}$, the t_{2g}^3 compounds $\text{Cr}(\text{CN})_6^{-3}$ and $\text{Cr}(\text{NO})(\text{NH}_3)_5^{-3}$, the t_{2g}^5 compounds $\text{Cr}(\text{CN})_5\text{NO}^{-3}$ and $\text{Fe}(\text{CN})_6^{-3}$ and the $t_{2g}^1 e_g^1$ compound $\text{Fe}(\text{CN})_5\text{NO}^{-2}$.

ESR spectra of several series were studied for the intermediate covalency situation. Substituted acetylacetonate complexes of Cu^{+2} and VO^{+2} were chosen to observe the effect on ESR parameters of having the electron in an orbital of σ (for Cu^{+2}) or π (for VO^{+2}) symmetry. The acetylacetonates were chosen because there exists a large amount of other types of physical data to correlate with the ESR data. Several amino-acid complexes of Cu^{+2} were investigated, and the ESR data were compared with other physical data from the literature. Several vanadyl complexes with bonding intermediate in character between ionic and covalent were investigated, and the ESR data were compared with recently published infrared and optical data.

For ionic complexes published data were utilized for all of the fluoro-complexes with the exception of VOF_5^{-3} for which measurements are reported here.

HISTORICAL

Transition Metal Chemistry

The general field is covered by several excellent books and many recent review articles. Ballhausen's book⁴ gives an excellent introduction and review of ligand field theory in general with an excellent balance of theory and chemical applications. A pair of complementary books, one by Orgel⁵ and the other by Griffith⁶ provide an exhaustive pre-1961 coverage of ligand field theory. Orgel's book is a concise review of the qualitative correlations of the theory with experimental data, while Griffith's book is a complete presentation of the mathematical and physical development of ligand field theory. Jorgensen has two recent books, one discusses the pre-1960 field of optical spectroscopy from a ligand field view-point,⁷ while the second is a pre-1964 survey of the general scientific literature of transition metal complexes.⁸ Jorgensen also has three comprehensive review articles. The two most interesting from the standpoint of the work of this thesis are a pre-1963 review and development of the nephelauxetic series⁹ and a review and further development of the application of ligand field theory to optical spectroscopy.¹⁰ The third is a more general review of the application of spectroscopy to chemical bonding.¹¹ The applications of group theory to ligand field theory are well reviewed and explained by Cotton.¹² The theory and pre-1963 applications of infrared spectroscopy to transition metal chemistry are comprehensively reviewed by Nakamoto.¹³

Optical and infrared spectroscopy and ligand field theory have received comprehensive and authoritative reviews so they will not be generally reviewed in this thesis and

only the basic ideas needed to correlate with the present work will be presented.

Since the application of electron spin resonance to transition metal complexes does not have the benefit of a recent comprehensive review article, the following section will be primarily devoted to this area.

Review of the Application of Electron Spin Resonance to Transition Metal Complexes

A review of the early development of electron spin resonance, ESR, has been given by previous theses¹⁴⁻¹⁷ from this department and will not be duplicated.

In addition to the early reviews and books, see Faber,¹⁴ a number of recent reviews and books have appeared which adequately cover the basic fundamentals and the pre-1960 literature. Pake's book¹⁸ is a textbook covering the theory of ESR from the viewpoint of a physicist. It does not discuss experimental details or, in general, chemical applications. It is especially useful as an abstract of, and a reference source to, the early theoretical papers. A slightly older but extremely useful book is that of Low.¹⁹ This book is more restricted than that of Pake in that it only covers the ESR of solids, but it is extremely thorough in its coverage of this area and therefore is also useful as a source-book. A recent book by Slichter²⁰ is useful as a textbook presenting the theoretical development of ESR of the solid state. The book that is the nearest comparison to the comprehensive optical and infrared books discussed earlier is that by Al'tshuler and Kozyrev.²¹ It is a translation of a 1961 book; and, therefore, its usefulness is limited to the literature and theory of that period.

To partially fill the gap between the limitations of the above books and the general literature there are several excellent reviews. Anderson²² has written a very good general

review of the experimental developments with well chosen examples of experimental applications. Stevens²³ has reviewed the use of the spin Hamiltonian (the mathematical shorthand used to describe the ESR experimental observables). This review provides detailed mathematical examples of the application of the spin Hamiltonian. A useful introductory article covering the application of ESR theory to transition metal compounds is that of Carrington and Longuet-Higgins.²⁴ Jarrett²⁵ has written a detailed review of the theoretical treatment of ESR which serves as an excellent recent review and textbook of advanced ESR. Robertson²⁶ has written an excellent review article in which he discusses in detail representative examples of the application of ESR to transition metal complexes with organic ligands. There are also several concise reviews^{27,28,29} in the annual review literature which, in general, abstract the important ESR literature of that year with a limited amount of critical comment.

As a concentrated source of recent experimental papers, there are several published proceedings of conferences which dealt with ESR³⁰⁻³⁶. A source of comprehensive reviews of particular aspects of ESR is the recent Ph.D. thesis literature. Of particular interest are ESR studies of those transition metal ions which give narrow lines at room temperature or at liquid nitrogen temperature, 77°K. These ions normally are of the outer electronic configuration $3d^1$, $3d^5$, $3d^9$, or $5f^1$. In general the theory of each of these cases is different. Fortunately there is available a Ph.D. thesis which covers each of these configurations. Faber's thesis¹⁴ concerns the random orientation spectra of d^1 , d^5 , and d^9 ions. Feltham's highly diverse investigation³⁷ covered solution ESR spectra, optical spectra, and ligand field theory of d^1 and d^9 complexes. A good source of the present state of ESR of d^5 ions in single crystals is the thesis of Drumheller.³⁸ Neiman's thesis³⁹ is a very useful thesis covering the theory of powder spectra and molecular orbital analysis of d^9 Cu complexes. The theory of ligand hyperfine splitting in d^3

fluoride complexes is presented in Guzzo's thesis⁴⁰ and subsequent publications,^{41,42} but in Guzzo's publications the analysis of the data has been changed from that given in the thesis. Two theses from the University of California^{43,44} report an investigation of the optical and ESR properties of protactinium in single crystals. Hayes' thesis⁴⁵ gives a complete review of the theory of line widths of paramagnetic ions in solution.

Development of the Theory of
Obtaining Covalency Parameters
from the ESR g Values.

Theory of Owen

Owen⁴⁶ found by utilizing optical and magnetic data that the spin-orbit coupling constant λ in the equation

$$g = 2.0023 - \frac{8\lambda}{\Delta} \quad (1)$$

was smaller by 20 to 30% than the free ion λ value. In equation 1 Δ is the energy separation between the ground state and the first excited state and g is the electron gyromagnetic ratio. He interpreted this reduction by saying that partial covalent bonding forces some of the unpaired electron out on the ligands.

Theory of Owen plus Screening Effects

Murao⁴⁷ noted that the decrease in λ is greater for metal ions of smaller atomic number and larger valency. He attributed this to screening by the additional 3d electron density produced by the admixture of 3d wave function into the bonding orbitals. The bonding orbitals are of the form

$$\phi_b = M(\psi_p + b\psi_d) \quad (2)$$

and the antibonding orbitals are of the form

$$\phi_a = N(\psi_d - c\psi_p) \quad (3)$$

where b and c are small coefficients.

Assuming that there is one electronic charge in the d orbital and that the electronic charge in the ϕ_a orbital is distributed among the ψ_p and ψ_d orbitals in proportion to the squares of the ψ_p and ψ_d coefficients, Murao obtained the electron distribution given in Table 1.

The ϕ_b orbital having two electrons increases the d orbital electron density by Δn where

$$\Delta n = \sum_n \frac{c_n^2}{1 + c_n^2} \quad (4)$$

This increase of d orbital electron density causes a reduction in the effective nuclear charge seen by a d electron

$$Z = Z_0 - \alpha \Delta n \quad (5)$$

where Z_0 is the effective nuclear charge for the free ion and α is the d - d screening constant. Based on a hydrogen-like model he determined that

$$\frac{\lambda}{\lambda_0} \propto \left(\frac{Z}{Z_0} \right)^4 \equiv \left[1 - \left(\frac{\alpha \Delta n}{Z_0} \right) \right]^4 \quad (6)$$

Since $\frac{\lambda}{\lambda_0}$ also was proportional to the probability of the unpaired d electron being found on the metal ion the final equation was found to be

$$\frac{\lambda}{\lambda_0} = N^2 \left[1 - \frac{\alpha \Delta n}{Z_0} \right]^4 \quad (7)$$

Murao determined the values of $\frac{\lambda}{\lambda_0}$ given in Table 2. N^2 and C were assumed constant and obtained by making the Cu^{+2} values fit the experimental value.

TABLE 1.--Electron distribution in the metal d and ligand p orbitals due to metal-ligand overlap.

	Contribution from Antibonding Orbital	Contribution from Bonding Orbital	Total Electron Density
Density in Metal d Orbital	$\frac{1}{1 + C^2}$	$\frac{2C^2}{1 + C^2}$	$\frac{2C^2 + 1}{1 + C^2}$
Density in Ligand p Orbital	$\frac{C^2}{1 + C^2}$	$\frac{2}{1 + C^2}$	$\frac{2 + C^2}{1 + C^2}$

TABLE 2.--Reduction of spin-orbit coupling constants for transition metal hydrates.

	Ti ⁺²	V ⁺²	Cr ⁺²	Mn ⁺²	Fe ⁺²	Co ⁺²	Ni ⁺²	Cu ⁺²	V ⁺³	Cr ⁺³	Mn ⁺³
Δn	1.10	0.97	0.83	0.69	0.55	0.41	0.28	0.14	1.10	0.97	0.83
λ	<hr/>										
λ_0	<hr/>										
(calculated)	55	62	68	72	76	79	82	84	61	66	70
λ	<hr/>										
λ_0	<hr/>										
(experiment)	--	≈80	--	--	--	81 ^a	83	84	62	63	--

^aEstimated

An alternate procedure for considering screening effects appears to be currently more popular. This method consists of using the tabulated spin-orbit coupling constants of Dunn⁴⁸ for the various possible oxidation states of the metal to calculate the covalency parameters for that particular oxidation state and then choosing the set of covalency parameters which gives a spin density on the metal in closest agreement with the corresponding assumed oxidation state.

Alternate Theory to Owen's Covalent Theory -
The Free Ion Theory

Although Murao was able to obtain good agreement between the theoretical and experimental reductions in the spin-orbit coupling constants, Marshall and Stuart⁴⁹ felt that the amount of covalency required was too large. They proposed a theory based on an ionic model. In an ionic model there is no covalent character to the wave functions and c in equation 3 is just equal to the metal-ligand overlap integral. They postulated that the decrease in λ is due to an overall shift of the d wave function outward due to a repulsion between the d electron density and the $2p$ electron density which overlaps the metal ion. They supported this theory by citing a neutron diffraction study which reported that the $3d$ wave function was expanded by 10% over the free ion wave function. Using 10% expanded wave functions they were able to obtain good agreement between the experimental fluorine hyperfine splittings for MnF_2 and their calculated values.

Marshall and Stuart's theory is known as the free ion theory since covalent bonding is not considered in their model. Their theory has been reviewed by Anderson⁵⁰ and by Shulman and Sugano.⁵¹

Shulman and Sugano point out that the agreement of Marshall and Stuart's theory with the experimental MnF_6^{-4} data was fortuitous and could not be extended to other ions. Anderson discusses the theoretical justifications given by Marshall and Stuart in proposing their model and concludes that their interpretation is not the only possible one.

Present g Value Theory. Inclusion of
Charge Transfer and Ligand Spin Orbit
Coupling Constant Contributions

Several investigators⁵²⁻⁵⁴ have recently corrected the theory of Owen to include charge transfer and ligand spin-orbit coupling constant contributions. A published comparison of the estimates of covalency obtained with these contributions and the estimates of covalency obtained from optical data indicates⁵⁵ that the former g value theory without charge transfer terms overestimated the degree of covalency.

Development of the Theory of
Obtaining Covalency Parameters
from the ESR Hyperfine Splittings

Restricted Hartree-Fock Model-
Higher Orbital s Character

In $3s^2 3d^n$ transition metal ions one would not predict an isotropic nuclear hyperfine splitting since the 3d orbitals have a node at the metal ion nucleus. The earliest explanation of the observed splitting is that in the ground state there is a small admixture of $3s^1 3d^n 4s^1$ character. Since an s electron has a high electron density at the nucleus, only a small percentage of $3s^1 3d^n 4s^1$ character is required to account for the observed splittings. This theory was introduced by Abragam and Pryce⁵⁶ and utilized by Van Wieringen¹⁶⁷ to explain the observed variations of the Mn^{+2} nuclear hyperfine splittings in a series of Mn^{+2} complexes.

Unrestricted Hartree-Fock Model-
Spin Polarization

For Metal Ion Nuclear Splittings

Although the theory of Abragam and Pryce was able to quantitatively account for the magnitude of the splitting, subsequent investigations showed that it predicted the wrong sign for the splittings.^{57,58,59} This discrepancy was accounted

for by theoretical unrestricted Hartree-Fock calculations of the exchange polarization mechanism which showed that an unpaired 3d electron will polarize the core s electrons to give a net spin at the nucleus of opposite sign to the unpaired electron. For example, Freeman and Watson⁵⁷ reported for vanadium metal that the contributions of the various orbitals were +0.05 (1s), -4.85(2s), +1.6.(3s) and +2.74(4s) to give an overall effective field at the nucleus of -0.45 atomic units.

Matamura⁶⁰ for Mn^{+2} , and Title⁶¹ for Fe^{+3} and Cr^{+1} , were able to interpret the \underline{A} values using only spin polarization and covalency. They plotted the experimental \underline{A} values versus estimated percentage ionicity⁶² and extrapolated back to 100% ionicity. The \underline{A} values at 100% were in close agreement with the calculated values of Freeman and Watson.⁵⁷ The agreement for Mn^{+2} is impressive, but for Cr^{+1} and Fe^{+3} additional data are needed.⁶²

Konig⁶³ has interpreted the isotropic \underline{A} values of Cr^{+1} and $V(0)$, both d^5 low spin cases using a combination of the spin polarization theory and the higher s-state contribution theory. He calculated the exchange polarization contributions to be +26.4 and -134 gauss for Cr^{+1} and $V(0)$ respectively. Since the experimental values of \underline{A} were +21.8 and -83.5 gauss, he calculated the 4s contribution to be -4.6 gauss and +50.5 gauss by the following relationship: $A(\text{experimental}) = (A \text{ exchange polarization}) + A(4s \text{ character.})$ He calculated that one electron in a 4s orbital would cause a splitting of -422.5 and 923.1 gauss for Cr^{+1} and $V(0)$, respectively. He was then able to calculate the 4s spin density as 0.0109 and 0.0547, respectively. Because of the uncertainties in the calculation of exchange polarization and 4s character and the lack of consideration of the effects of covalent bonding on the calculated parameters, the 4s spin densities cannot be considered as quantitatively significant. Additional experimental data are needed. For example chromium metal is $3d^5 4s^1$; since there is an unpaired electron in the

4s orbital, a large 4s contribution is expected. Childs et al.⁶⁴ report that the experimental value for chromium metal is 29.47 gauss. This value is only slightly larger than the Cr splittings when there are only 3d unpaired electrons. This result casts considerable doubt on Konig's estimation of -422.5 gauss for a 4s Cr⁺¹ electron. Childs et al. calculate -51 gauss for the 4s splitting. As a further example of the qualitative nature of this type of treatment, Davison, et al.⁶⁵ estimate the 4s splitting by Cr to be -1170 gauss.

Another illustration of the use of both the 4s contribution and the spin polarization is the published interpretation of the unusually low value ($25.7 \times 10^{-4} \text{ cm}^{-1}$) of the vanadium hyperfine splitting found in bis-cyclopentadienyl vanadium.⁶⁶ Since proton NMR spectra of the complex rule out the possibility that the electron is predominately localized on the ligand, the small vanadium splitting cannot be attributed to a large covalency. The small splitting was explained by partial cancellation of the negative spin polarization contribution by a positive 4s contribution.

Evidence which appears to support the combined polarization and 4s character theory is the large difference in hyperfine splitting constants reported for Cu⁺² in two non-equivalent sites in an NH₄Cl single crystal.⁶⁷ Since the g values for both sites are near 2, the difference cannot be due to a large orbital contribution. Also, the observation of an additional 13-line superhyperfine structure due to 4 equivalent Cl⁻ ions rules out a large difference in covalency between the two sites. The hyperfine splittings for one of the sites have a pronounced temperature dependence. All of these observations can be explained by assuming that the amount of 4s character is dependent on the local crystal field symmetry.

For Ligand Hyperfine Splittings

Two early theories were proposed to account for the observed ligand hyperfine splittings. Mukherji and Das,⁶⁸ Marshall and Stewart,⁴⁹ and Freeman and Watson⁶⁹ utilized ionic

models and were able to quantitatively account for the magnitudes of the splittings by polarization of the ligand orbitals due to overlap of the metal-ligand wave functions. However, subsequent experiments⁵¹ which determined the sign of the hyperfine splittings and the dependence of the splittings on whether the unpaired electron was in an orbital of σ or π symmetry indicated that covalent contributions must be considered.

The covalent contribution at first was considered to arise from covalency of the antibonding unpaired electron. Using this model Shulman and Sugano⁵¹ were able to obtain good agreement between the observed and theoretical fluorine hyperfine splittings in KNiF_3 . However, Watson and Freeman⁷⁰ have recently claimed that the model used by Shulman and Sugano is incorrect. They propose that the covalent contribution arises from spin unpairing in the bonding molecular orbitals rather than the antibonding molecular orbitals. The numerical parameters calculated by them did not give as good agreement with the experimental parameters as the theoretical values calculated by Shulman and Sugano; however, a more recent paper by Ellis⁷¹ has reconsidered Watson and Freeman's theory and found additional contributions so that the theoretical and experimental values are now in better agreement; as illustrated in Table 3.

An additional mechanism which can account for observed ligand hyperfine splittings has been proposed by Kivelson and Lee.⁷² This mechanism is a configuration interaction whereby a bonding electron is promoted from its spin paired orbital to the corresponding antibonding orbital leaving a net negative spin density in the original bonding orbital. This mechanism predicts a ligand hyperfine splitting even when the unpaired electron is in an ionic orbital which does not overlap the ligand in question.

TABLE 3.--Spin density in KNiF_3 .

Spin Density f_i	Shulman and Sugano ⁵¹	Watson and Freeman ⁷⁰	Ellis ⁷¹	Experiment ⁵¹
f_s Spin Overlap	0.0022	0.0021	0.0022	--
f_s Spin Covalent	<u>0.0020</u>	<u>0.0010</u>	<u>0.0041</u>	--
Total f_s	0.0042	0.0031	0.0063	0.0054
f_σ Spin Overlap	0.0041	0.0037	0.0041	--
f_σ Spin Covalent	<u>0.0480</u>	<u>0.0060</u>	<u>0.0148</u>	--
Total f_σ	0.0521	0.0189	0.0097	0.0378

THEORETICAL

COVALENT MOLECULAR ORBITAL THEORY OF LIGAND HYPERFINE SPLITTINGS FOR $\text{Cr}(\text{CN})_6^{-3}$ AND CrF_6^{-3}

For a more general discussion of this theory the reader is referred to Anderson's⁵⁰ review article and Shulman and Sugano's⁵¹ paper. The $\text{Cr}(\text{CN})_6^{-3}$ and CrF_6^{-3} ions will be used to illustrate the application of the theory to complexes in which only molecular orbitals (M.O.'s) of π symmetry contain unpaired metal electrons in the ground state.

Energy Levels and Molecular Orbitals of $\text{Cr}(\text{CN})_6^{-3}$ and CrF_6^{-3}

The energy levels of $\text{Cr}(\text{CN})_6^{-3}$ and CrF_6^{-3} are given in Figure 1. The cubic field splits the five degenerate chromium 3d orbitals into a higher energy e_g doublet and a lower energy t_{2g} triplet. The separation between the e_g and t_{2g} levels is called Δ . For the CrF_6^{-3} complex the chromium t_{2g} levels form molecular orbitals with the occupied $2p_\pi$ orbitals of fluorine. The bonding t_{2g} molecular orbitals are occupied by the paired fluorine electrons forcing the unpaired metal t_{2g} electrons into the antibonding t_{2g}^* molecular orbitals thereby decreasing Δ . See Figure 1. For $\text{Cr}(\text{CN})_6^{-3}$ the low energy p_π carbon orbitals are utilized in carbon to nitrogen π bonding leaving only an empty high energy antibonding carbon orbital to form π molecular orbitals with the metal d orbitals. Since the carbon p_π orbital is empty and less stable than the metal d orbitals, the metal electrons are stabilized by the interaction and form a t_{2g} molecular orbital which is slightly

bonding. This causes an increase in Δ ($\Delta \text{Cr}(\text{CN})_6^{-3} > \Delta$ in cubic field $> \Delta$ in CrF_6^{-3}).

Therefore, for CrF_6^{-3} the π molecular orbitals containing the three unpaired electrons are antibonding, while for $\text{Cr}(\text{CN})_6^{-3}$ the π molecular orbitals are bonding.

The molecular orbitals are:

$$\phi_{\sigma}^* = N_{\sigma} (\psi_{3d_{z^2}} - \lambda_{2s} \psi_{2s} - \lambda_{p_{\sigma}} \psi_{p_{\sigma}}) \quad (8)$$

$$\phi_{\pi_1} = N_{\pi_1} (\psi_{3d_{zx}} \pm \lambda_{\pi_1} \psi_{\pi_1}) \quad (9)$$

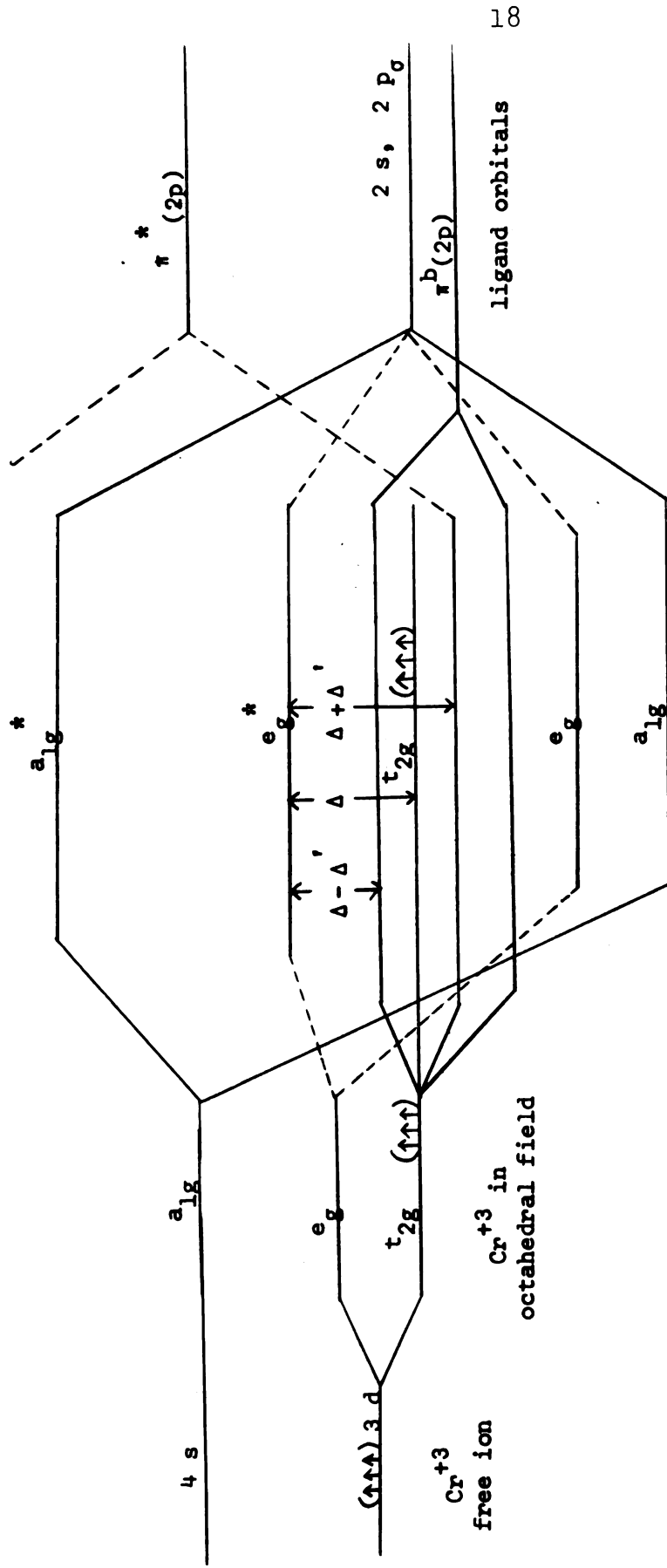
$$\phi_{\pi_2} = N_{\pi_2} (\psi_{3d_{yz}} \pm \lambda_{\pi_2} \psi_{\pi_2}) \quad (10)$$

The negative signs in equations (9) and (10) are for CrF_6^{-3} ; the positive signs are for $\text{Cr}(\text{CN})_6^{-3}$. For $\text{Cr}(\text{CN})_6^{-3}$ there is an additional negative (antibonding) term in equations (9) and (10) due to a contribution from the bonding occupied carbon p_{π} orbitals.⁷³ If this term was kept there would not be sufficient experimental data to solve for the M.O. coefficients. Since the stability of transition metal cyanides increases as the number of d_{π} electrons increases the important term must be the positive (bonding) term and as an approximation the antibonding term was set equal to zero and not included in equations (9) and (10).

Experimental ESR Parameters

If the ESR absorption lines are narrow and if the ligand nuclei have nuclear magnetic moments, it is sometimes possible to observe a splitting of the main lines. This splitting is due to unpaired electron density reaching the ligand nucleus. The spectra can be fitted to the equation:

$$H-H_0 = (A_{\parallel}^2 \cos^2 \theta + A_{\perp}^2 \sin^2 \theta)^{\frac{1}{2}} m_I \quad (11)$$



Cr^{+3} and ligand molecular orbitals

$\Delta - \Delta'$ is the splitting for CrF_6^{-3} and is representative of ligand to metal π bonding.

Δ is the splitting for Cr^{+3} with no π bonding.

$\Delta + \Delta'$ is the splitting for $\text{Cr}(\text{CN})_6^{-3}$ and is representative of metal to ligand π bonding.

Figure 1. Energy level diagram for Cr^{+3} ions.

where H_0 is the peak center in gauss before splitting by the ligand, H is the position of the split peak, m_I is the projection on H_0 of the ligand nuclear spin and is equal to $I, I-1, \dots, -I+1, -I$. θ is the angle between H_0 and the metal-ligand sigma bond. $A_{||}$ and A_{\perp} are defined by the following:

$$A_{||} = A_s + 2A_p \quad (12)$$

$$A_{\perp} = A_s - A_p \quad (13)$$

A_s is the isotropic splitting and is due to an unpairing of the ligand s electrons.

A_p is the anisotropic splitting and is due to spin unpairing in the p_{σ} and p_{π} orbitals and to a direct dipole interaction, A_D .

Relationships Between the Experimentally Determined A Values and the Molecular Orbitals^{41,42,49,51}

$$A_p = A_{\sigma} - A_{\pi} + A_D N_{\pi}^2 \quad (14)$$

$$A_{\sigma} = \frac{2 \mu_n \beta_n}{5 (2S) I_n} (f_{\sigma} - f_{\pi}) \left\langle \frac{1}{r^3} \right\rangle \quad (15)$$

$$A_{\pi} = \frac{2 \mu_n \beta_n}{5 (2S) I_n} (f_{\pi_1} - f_{\pi_2}) \left\langle \frac{1}{r^3} \right\rangle \quad (16)$$

A_{π} is zero for cylindrical symmetry around the metal-ligand bond since $f_{\pi_1} = f_{\pi_2}$. Cylindrical symmetry is found in CrX_6^{-3} ligand-metal bonds because each of the three t_{2g} orbitals contains one unpaired electron.

$$A_D = \frac{\mu_n \beta_n C}{I_n R^3} \quad (17)$$

C is a correction factor due to the fact that the magnetic electrons cannot be treated as point dipoles.⁴²

$$A_S = \frac{8\pi \mu_n \beta_n N_\sigma^2 \lambda_{2s}^2}{3 \cdot 2S I_n} \psi(0)^2 \quad (18)$$

β_n is the nuclear magneton, μ_n is the magnetic moment of the ligand nucleus, S is the total electron spin of the complex and A_D is the point dipole term.

The molecular orbital coefficients are related to γ where γ is a measure of the covalency in the bond formed by the central metal ion 3d orbital and the x orbital of the ligand by the following:¹

$$\lambda_{2s} = \gamma_s + \sqrt{3} S_{3d,2s} \quad (19)$$

$$\lambda_p = \gamma_\sigma + \sqrt{3} S_{3d,p_\sigma} \quad (20)$$

$$\lambda_\pi = \gamma_\pi + 2 S_{3d,p_\pi} \quad (21)$$

where $S_{d,x}$ is the metal 3d orbital-ligand x orbital atomic overlap integral.

N_σ and N_π are the normalization coefficients and are given by

$$N_\sigma = (1 - 2\sqrt{3}\lambda_\sigma S_{d,p_\sigma} + \lambda_\sigma^2)^{-\frac{1}{2}} \quad (22)$$

$$N_\pi = (1 \pm 4\lambda_\pi S_{d,p_\pi} + \lambda_\pi^2)^{-\frac{1}{2}} \quad (23)$$

where the plus sign in equation (23) is for bonding molecular orbitals, as in $\text{Cr}(\text{CN})_6^{-3}$, and the negative sign is for antibonding molecular orbitals, as in CrF_6^{-3} .

The unpaired spin density in the ligand σ and π orbitals, f_σ and f_π , respectively, are related to the molecular orbital coefficients and to the experimental hyperfine splittings by the following equations:⁵¹

$$f_\sigma = \frac{\lambda_\sigma^2 N_\sigma^2}{3} = \frac{2S A_s}{A_s'} \quad (24)$$

$$f_\pi = \frac{\lambda_\pi^2 N_\pi^2}{4} = \frac{2S A_\sigma}{A_\sigma'} \quad (25)$$

$$f_s = \frac{2S A_s}{A_s'} \quad (26)$$

$$A_s' = \frac{8}{3} \frac{\mu_n \beta_n}{I_n} [\psi(0)_{2s}^2] \quad (\text{in gauss}) \quad (27)$$

$$A_\sigma' = \frac{2}{5} \frac{\mu_n \beta_n}{I_n} \left\langle \frac{1}{r^3} \right\rangle_{2p} \quad (28)$$

Higher Order Considerations and Alternate Theory

The above theory is only a first order theory; there are several higher order effects which have been examined in the literature. The ESR theory for CoF_3^{-1} has been extended to include the effects of unquenched orbital momentum and mixing of excited states.⁷⁴

Marshall⁷⁵ has investigated higher order contributions for Cr^{+3} and Ni^{+2} and finds that terms from spin-orbit interactions which produce unquenched orbital moment on the ligand and also modify the spin distribution are sometimes important.

Helmholz, Guzzo, and Sanders⁴² give equations which take into consideration that the magnetic field at the ligand has components perpendicular to the external field of the unpaired electrons.

Simanek and Sroubek⁷⁶ and also Watson and Freeman⁷⁰ have considered an alternate theory to the theory used in this thesis. They consider that the unpaired spin density reaches the ligands through the bonding electrons and is of opposite sign to the unpaired metal electrons. This theory has been developed, at present, only for the d^8 case so that a comparison of its use for Cr^{+3} with the theory used in this thesis is not yet possible.

COVALENT MOLECULAR ORBITAL
THEORY FOR THE DETERMINATION
OF M.O. COEFFICIENTS FROM THE
ESR g VALUES OF CrF_6^{-3} AND
 $Cr(CN)_6^{-3}$

The theory for the determination of the M.O. coefficients from the g values has been presented by Lacroix and Emch⁵² and by McGarvey.⁵³ It will not be presented here since it was not used in this research.

MOLECULAR ORBITAL THEORY FOR d^1 AND LOW-
SPIN d^5 SYSTEMS IN A TETRAGONAL FIELD

Theory of ESR g Values

In a tetragonal field for the d^1 and low-spin d^5 cases the experimental g values can be related to the molecular orbital coefficients by:^{72,77}

$$g_{\parallel} = 2.0023 - \frac{8\lambda N_{\pi_2}^2 N_{\sigma_2}^2}{\Delta b_2 \rightarrow b_1 (I)} \left[1 - \frac{1}{2} (\lambda_{\pi_2} \lambda_{\sigma_2}) T(n) \right. \\ \left. - \sqrt{3} \lambda_{\sigma_2} S_{d, \sigma_2} - 2\lambda_{\pi_2} S_{d, \pi_2} \right] - \frac{8\lambda N_{\pi_2}^2 (1 - N_{\sigma_2}^2)}{\Delta b_2 \rightarrow b_1 (II)} \quad (29)$$

$$g_{\perp} = 2.0023 - \frac{2\lambda N_{\pi_2}^2 N_{\pi_1}^2}{\Delta b_2 \rightarrow e \text{ (I)}} [1 - (\frac{1}{2})^{\frac{1}{2}} \lambda_{\pi_1}^e \lambda_{\pi_2} - 2S_{d,\pi_2} \lambda_{\pi_2}^e - (\frac{1}{2})^{\frac{1}{2}} 2S_{d,\pi_2} \lambda_{\pi_1}^e - S_{d,\pi_1} \lambda_{\pi_1}^a] - \frac{2\lambda N_{\pi_2}^2 (1 - N_{\pi_1}^2)}{\Delta b_2 \rightarrow e \text{ (II)}} \quad (30)$$

where $T(n)$ is defined by Kivelson and Lee,⁷² S_{d,π_2} is the metal d, ligand p_{π_2} atomic overlap integral, $\lambda_{\pi_1}^e$ and $\lambda_{\pi_1}^a$ are the xz, yz molecular orbital coefficients for the equatorial and axial ligands, respectively, and λ is the spin-orbit coupling constant. The spin-orbit coupling constant is positive if the transition is one where an unpaired electron goes from a half-filled orbital to an unoccupied orbital and is negative if the transition is from a filled orbital to a half-filled orbital. The latter type of transition is commonly called a hole transition. Transitions I and II are the d-d and the charge transfer transitions, respectively. $\Delta b_2 \rightarrow b_1$ and $\Delta b_2 \rightarrow e$ are determined from optical spectroscopy with the aid of the energy level diagram given in Figure 2.

The g values are obtained from the experimental spectrum with the use of the following equations:^{78,38}

$$\text{For } g \text{ isotropic} \quad g = \frac{h\nu}{\beta H_0} \quad (31)$$

$$H_0 = H_{(m)} + A \cdot m + \frac{A^2}{2 H_{(m)}} [I(I+1) - m^2] + \frac{A^3}{4 H_{(m)}^2} \quad (32)$$

$$\text{For } g_{\parallel} \quad H_0 = H_{(m)} + A_{\parallel} \cdot m + \frac{A_{\parallel}^2 [I(I+1) - m^2]}{2 H_{(m)}} \quad (33)$$

$$\text{For } g_{\perp} \quad H_0 = H_{(m)} + A_{\perp} \cdot m + \frac{(A_{\parallel}^2 + A_{\perp}^2) [I(I+1) - m^2]}{4 H_{(m)}} \quad (34)$$

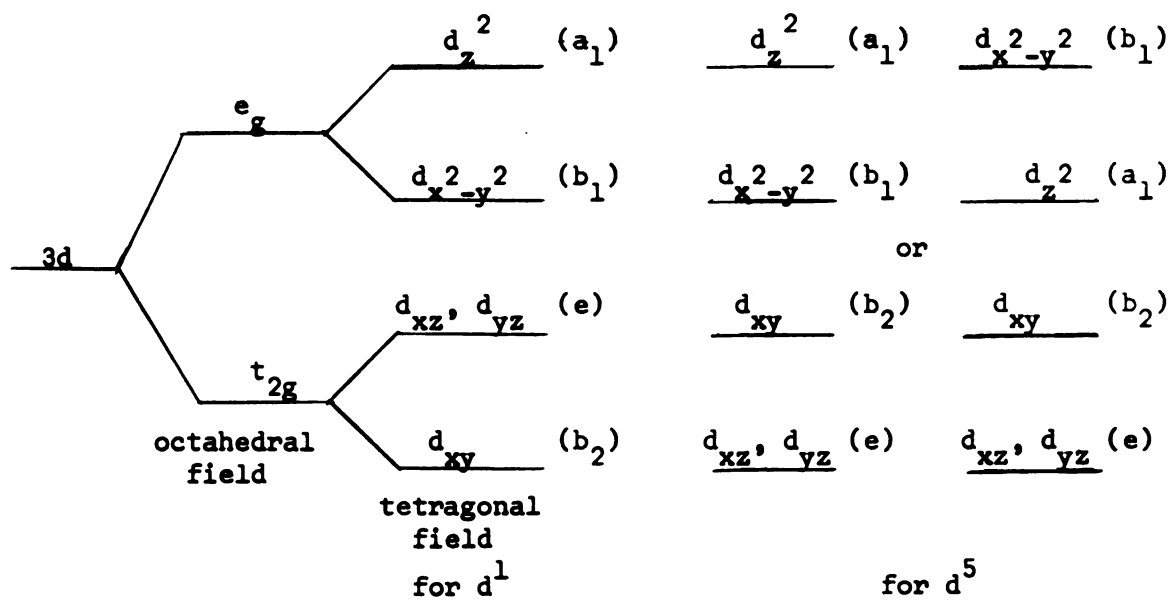


Figure 2. Energy level diagram for a d^1 transition metal ion in an octahedral and in a tetragonal field.

Here $H_{(m)}$ is the magnetic field position of the ESR line due to the component (m) of the nuclear magnetic moment (I), ν is the klystron frequency in megacycles and A , A_{\parallel} , and A_{\perp} are the nuclear hyperfine splitting constants.

Metal Ion Hyperfine Splitting Theory

The experimental metal ion nuclear hyperfine splitting is related to the molecular orbitals by the equations:⁷²

$$A_{\parallel} = -\frac{4}{7} N_{\pi_2}^2 A_0 - A - \frac{8\lambda N_{\pi_2}^2 N_{\sigma_2}^2 A_0}{\Delta b_2 + b_1 (I)} - \frac{6}{7} \frac{\lambda N_{\pi_2}^2 N_{\pi_1}^2 A_0}{\Delta b_2 + e (I)} \quad (35)$$

$$A_{\perp} = -\frac{2}{7} N_{\pi_2}^2 A_0 - A - \frac{11}{7} \frac{\lambda N_{\pi_2}^2 N_{\pi_1}^2 A_0}{\Delta b_2 + e (I)} \quad (36)$$

where $A = \frac{2}{3} A_{\perp} + \frac{1}{3} A_{\parallel}$ and $A_0 = \frac{\mu_n \beta_n}{I_n} \left\langle \frac{1}{r^3} \right\rangle$. Estimation of $\left\langle \frac{1}{r^3} \right\rangle$ values. $\left\langle \frac{1}{r^3} \right\rangle$ can be found in the literature, if available, or calculated from the semiempirical method of Korol'kov.⁷⁹

$$\left\langle r^{-3} \right\rangle = \frac{\lambda}{5.84Z} [C + 0.09 \ln \left(\frac{\left\langle r^{-3} \right\rangle}{Z} \right)]^{-1} \quad (37)$$

C is calibrated with a similar known ion. λ is the spin orbit coupling constant. Z is the atomic number of the metal ion.

To determine an unknown $\left\langle r^{-3} \right\rangle$ value, solve for $\left\langle r^{-3} \right\rangle$ using the correct Z and λ then use the $\left\langle r^{-3} \right\rangle$ value in $\ln\left(\frac{\left\langle r^{-3} \right\rangle}{Z}\right)$ term of a known similar ion. Take the calculated $\left\langle r^{-3} \right\rangle$ put it back in the right side of Equation (37) and repeat the calculation; continue until $\left\langle r^{-3} \right\rangle$ does not change.

Ligand Hyperfine Splittings

For the equatorial ligands the ligand hyperfine splittings are given by the following equations for a spin = $\frac{1}{2}$ system:⁴⁹

$$A_Z^c = A_S - f_{\sigma_2} A'_p - N_{\pi_2}^2 A_D + 2 f_{\pi_1} A'_p - f_{\pi_2} A'_p \quad (38)$$

$$A_{\sigma}^c = A_S + 2 f_{\sigma_2} A'_p + 2 N_{\pi_2}^2 A_D - f_{\pi_1} A'_p - f_{\pi_2} A'_p \quad (39)$$

$$A_{\pi}^c = A_S - f_{\sigma_2} A'_p - N_{\pi_2}^2 A_D - f_{\pi_1} A'_p + 2 f_{\pi_2} A'_p \quad (40)$$

where the z-axis is along g_{II} , the σ -axis is along the metal-ligand bond, and the π -axis is perpendicular to z and σ in the xy plane.

$$f_{\sigma_2} = \frac{\lambda_{\sigma_2}^2 N_{\sigma_2}^2}{3} \quad (41)$$

$$f_{\pi_2} = \frac{\lambda_{\pi_2}^2 N_{\pi_2}^2}{4} \quad (42)$$

$$f_{\pi_1} = \frac{\lambda_{\pi_1}^2 e N_{\pi_1}^2}{2} \quad (43)$$

An isotropic hyperfine splitting, A_S , is not expected since the ground state orbital is an orbital of π symmetry. The observed A_S values have been attributed by Kivelson and Lee⁷² to configuration interaction in which an electron is promoted from a bonding orbital to an antibonding orbital. Specifically, the promotions of importance are:

$$(x^2 - y^2)^{\uparrow\downarrow}(b) (xy)^{\uparrow} (*) \rightarrow (x^2 - y^2)^{\downarrow}(b) (x^2 - y^2)^{\uparrow} (*) (xy)^{\uparrow} (*) \quad (44)$$

$$(z^2)^{\uparrow\downarrow}(b) (xy)^{\uparrow} (*) \rightarrow (z^2)^{\downarrow}(b) (z^2)^{\uparrow} (*) (xy)^{\uparrow} (*) \quad (45)$$

The superscript b indicates a bonding orbital and * indicates an antibonding orbital. For the equatorial ligands the first promotion is the important one. The isotropic splitting is given by:

$$A_s = - \frac{N_{\sigma_2}^2 (1 - N_{\sigma_2}^2) (d_{xy}, d_{x^2-y^2}) A_s'}{2\Delta E (x^2 - y^2)^b + (x^2 - y^2)^*} \quad (46)$$

where $(d_{xy}, d_{x^2-y^2})$ is an exchange integral and the $\frac{1}{2}$ comes from the assumption that the sigma ligand orbital is an s-p hybrid. A similar equation applies for the isotropic nitrogen splittings except that the promotions involve the z^2 orbitals. The approximations involved in equation (46) are such that molecular orbital coefficients cannot be calculated from them; however, the spin density at the ligand can be calculated with the use of equation (26).

An alternate mechanism also considered by Kivelson and Lee⁷² is that the A_s values are due to polarization of the ligand by unpaired spin density in the ligand π orbitals.

MOLECULAR ORBITAL THEORY OF
LIGAND HYPERFINE SPLITTINGS
FOR COPPER (II) COMPLEXES
AND $\text{Fe}(\text{CN})_5\text{NO}^{-3}$

For the equatorial ligands in copper(II) complexes and the axial ligands in $\text{Fe}(\text{CN})_5\text{NO}^{-3}$ the unpaired electron is in an orbital of σ symmetry. Equations (11) through (28) are applicable with the assumption that

$$A_\sigma \approx \frac{2 \mu_n \beta_n}{5 (2s) I_n} f_\sigma \left\langle \frac{1}{r_3} \right\rangle$$

in equation (15) and that $A_\pi \approx 0$ in equation 16.

CRYSTAL FIELD THEORY FOR
TETRAGONAL SYMMETRY

A crystal field of tetragonal symmetry is obtained by compression or elongation of an octahedron along a four-fold axis. An octahedral field causes the free ion degenerate d orbital energy levels to be split into a triplet and a doublet as shown in Figure 3. The addition of a tetragonal distortion splits the doublet into two singlets and the triplet into a doublet and a singlet.

The energies of the orbitals can be represented in terms of three crystal field parameters D_s , D_q and D_t by the following equations:⁸⁰

$$E(z^2) = 6 D_q - 2D_s - 6 D_t \quad (47)$$

$$E(x^2 - y^2) = 6 D_q + 2D_s - D_t \quad (48)$$

$$E(xy) = - 4 D_q + 2D_s - D_t \quad (49)$$

$$E(xz, yz) = - 4 D_q - D_s + 4 D_t \quad (50)$$

where D_q , D_s , and D_t are defined as:

$$D_q = \frac{1}{6} \rho_4^{xy} \quad (51)$$

$$D_s = \frac{1}{7} (2\rho_2^{xy} - \rho_2^{+z} - \rho_2^{-z}) \quad (52)$$

$$D_t = \frac{1}{21} (2\rho_4^{xy} - \rho_4^{+z} - \rho_4^{-z}) \quad (53)$$

$$\rho_n = \text{eq}\left(\frac{r^n}{R^{n+1}}\right) \quad (54)$$

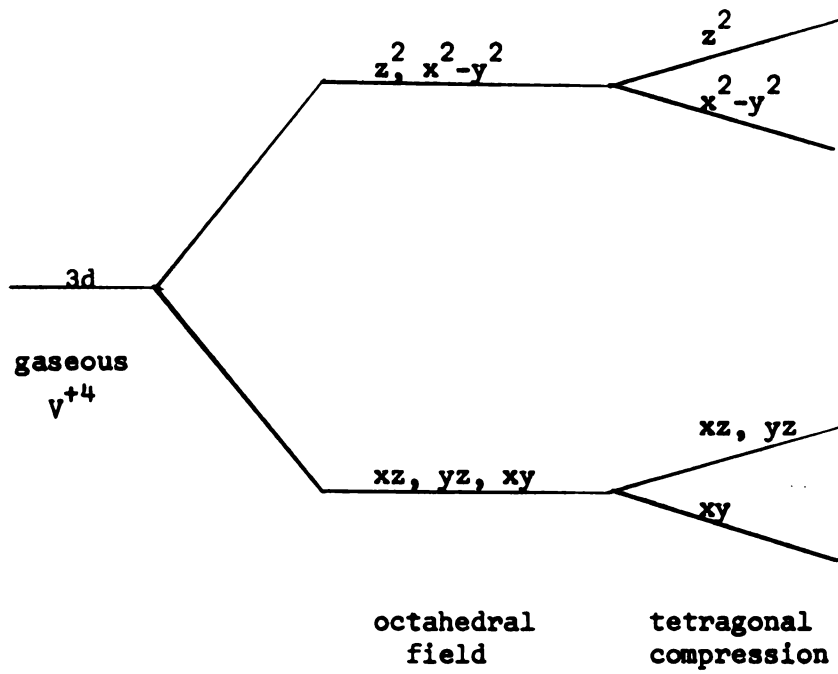


Figure 3. Crystal field splittings for V^{+4} .

e and r are the electronic charge and radius, and q and R are the effective ligand charge and the internuclear distance.

In this thesis we are interested in the ratio of the axial field to the equatorial field, ρ :⁸¹

$$\rho = \frac{\rho_4^{+z} + \rho_4^{-z}}{2 \rho_4^{xy}} \quad (55)$$

For d^1 vanadyl complexes ρ is obtained from the experimental optical spectrum by use of the equation:⁸¹

$$\rho = \frac{3 (E_{xy} + z^2) - 4 (E_{xy} + xz, yz)}{2 (E_{xy} + x^2 - y^2)} - \frac{1}{2} \quad (56)$$

In addition to the ratio of the axial to equatorial field strength it is also possible to determine the field strength of the various ligands using the expressions of Yamatera.⁸² Defining σ_x as the σ electrostatic effect due to the σ -bond between ligand x and M and π_x as the electrostatic effect due to the π bond between ligand x and M, he obtains the following expressions for the d orbital energy levels for MX_5Y type ions:

$$E_{xz} = E_{yz} = \frac{3}{4} \pi_x + \frac{1}{4} \pi_y \quad (57)$$

$$E_{x^2 - y^2} = \sigma_x \quad (58)$$

$$E_{z^2} = \frac{2}{3} \sigma_x + \frac{1}{3} \sigma_y \quad (59)$$

Some of the σ_x and π_x values for Co^{+2} complexes are listed in Table 4.^{10x}

TABLE 4.-- σ_x and π_x values for Co III ions.

	Example	σ_x	π_x
C ⁺²	CN ⁻	24,000 cm ⁻¹	-8,000 cm ⁻¹
N ⁺³	NO ₂ ⁻	20,000	-6,000
N ⁰	NH ₃	22,000	0
N ⁻	N ₃ ⁻	24,000	10,000
O ⁰	H ₂ O	25,000	8,000
O ⁻	OH ⁻	32,000	16,000
	Oxalate	23,000	6,000
O ⁻²	O ⁻²	39,000	24,000
F ⁻	F ⁻	26,000	10,000
Cl ⁻	Cl ⁻	24,000	10,000
Br ⁻	Br ⁻	23,000	10,000
I ⁻	I ⁻	21,000	10,000

EXPERIMENTAL

ESR SYSTEM

Second Derivative Presentation

A Varian⁸³ model 4500 spectrometer with 100 kc field modulation was used in this research. It was modified so that the sample could be modulated at both 100 kc and 400 cycles, and the resulting signal doubly detected by the two lock-in amplifiers. This procedure gives a second derivative presentation of the signal. Second derivative presentation is useful when there are overlapping lines. A disadvantage is that the sensitivity is lowered by a factor of approximately 16 from first derivative 100 kc operation.

Measurement of Magnetic Field

A small proton marginal oscillator⁸⁴ was used to measure the magnetic field. The proton frequency was measured with a Hewlett-Packard⁸⁵ Electronic Counter, Model 524 C, which has an accuracy of ± 20 cps.

When operating the spectrometer in the second derivative mode, the proton signal was passed through a variable attenuator into a Hewlett-Packard Model 460 AR Wide Band Amplifier. The output from this amplifier was fed to the Y axis input of the ESR console oscilloscope. With the function switch in position 2 the signal is fed to the 400 cycle lock-in amplifier where it is detected and amplified. The second derivative of the proton signal then appears in the recorded spectrum superimposed on the second derivative of the ESR signal, while the first derivative of the proton signal appears on the scope. The frequency is recorded by

the H.P. Counter by setting the display time on infinity and pressing the recount button when the chart and scope signal appear. The proton oscillator is then changed to another frequency down field (for down field sweeps) and the process repeated. The magnetic field in gauss is calculated from the following equation:

$$H \text{ in gauss} = 2.3486855 \times (\nu_1) \times 10^{-4} \quad (50)$$

ν_1 is the frequency of the proton resonance at the magnet field in question.

Measurement of Klystron Frequency

Three methods of measuring the klystron frequency are available.

(a) A Waveline 698 Wave Meter⁸⁶.--The normal accuracy is ± 1 mc, however wave meters are temperature dependent and it has been in error by as much as ± 2 mc. Other disadvantages are that it is insensitive at low klystron powers and that it is not calibrated directly in megacycles. The frequency is obtained by interpolation from a table of actual frequencies versus wave meter readings.

(b) A TS-148/UP U.S. Navy Spectrum Analyzer.--The spectrum analyzer also operates on the wavemeter principle but is preferable to method (a) since the dial is calibrated directly in megacycles and the instrument does not lose sensitivity at low klystron powers. Although the accuracy of calibration as checked against method (c) is only ± 2 mc., the precision of measurement is ± 0.5 mc so that an initial calibration before a series of runs by method (c) followed by the use for each spectrum of the spectrum analyzer has proven satisfactory.

(c) A Micro-Now Model 101 frequency calibrator.--The klystron frequency is allowed to beat with a harmonic of a Micro-Now⁸⁷ Model 101 Frequency Calibrator and the difference

frequency is tuned with a National⁸⁸ NC-173 communications receiver. The difference frequency can be read from the calibrated dial to ± 0.05 mc on the low frequency band and to ± 0.5 mc on the highest frequency band. An output is provided after the first R.F. amplification stage of the communications receiver so that the signal can be fed to the Hewlett-Packard wide band amplifier and then to the Hewlett-Packard Electronic Counter, Model 524 C. The frequency read on the counter, minus 455 ± 2 kc (The I.F. frequency of the communications receiver) gives the difference between the klystron frequency and the harmonic of the Micro-Now to an accuracy greater than presently needed for ESR experiments.

Linear, Precalibrated Magnetic Field Sweeps

A Hall probe⁸⁹ was used in constant current mode to drive the x - axis of an x-y recorder. The experimental setup is given in Figure 4. In constant current operation the output of the Hall probe is directly proportional to the applied magnetic field. At 3000 gauss the output is approximately 0.16 volts. Most of the 0.16 volts are bucked out by the feedback network shown in Figure 3 so that a change of twenty gauss at a magnetic field of 3000 gauss will cover the full x axis of the recorder on the 7.5 mv. scale. The method allowed the use of precalibrated standards to determine the A values of a series of samples by running the known before the first and after the last sample of the series. The reproducibility has consistently been at least one part in two hundred for narrow lines.

Single Crystal Holder

The single crystal holder is pictured in Figure 5. It permits rotation of the crystal in two mutually perpendicular directions in the cavity. Its design and operating principles are as follows:

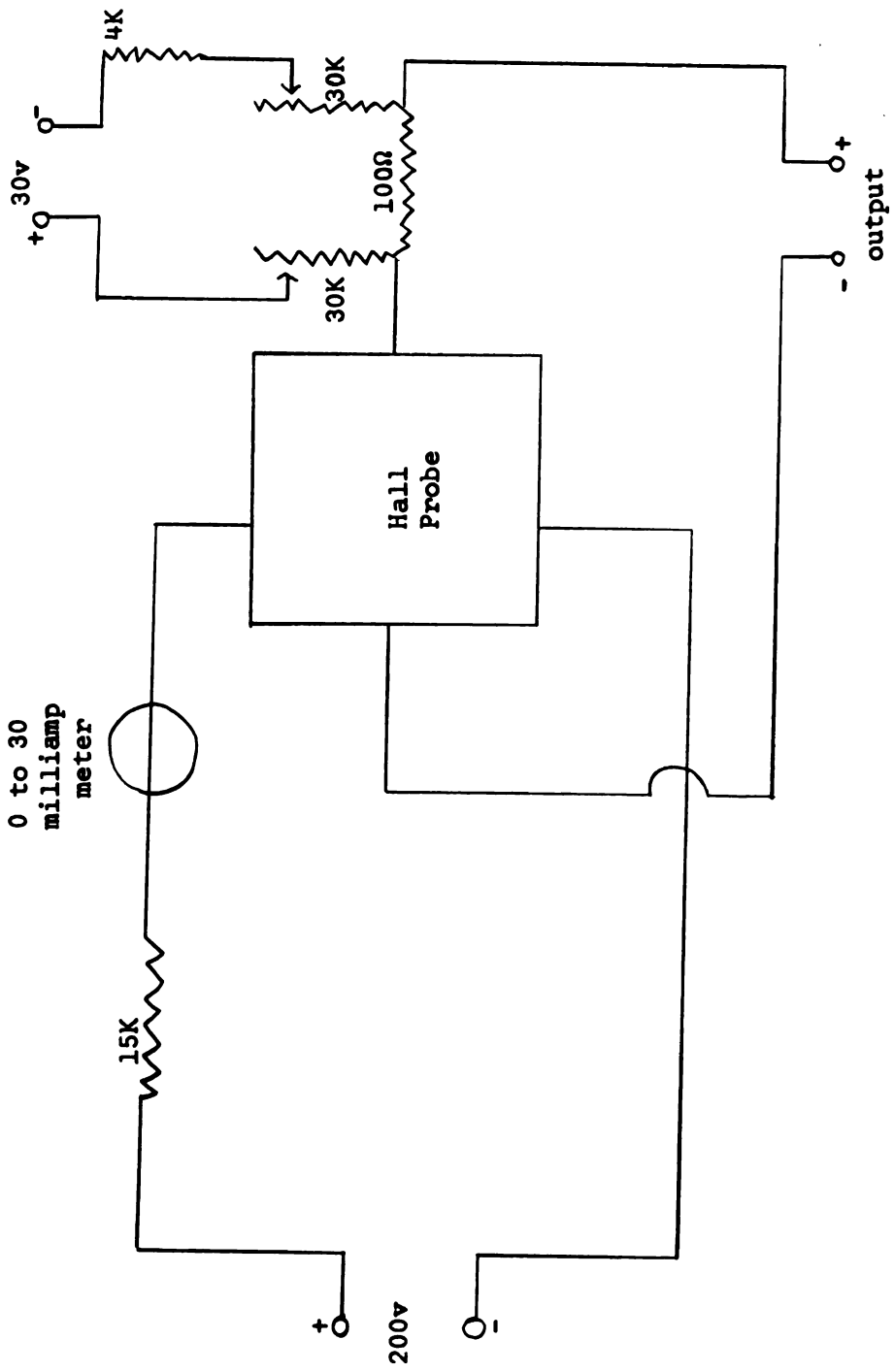


Figure 4. Hall probe schematic.

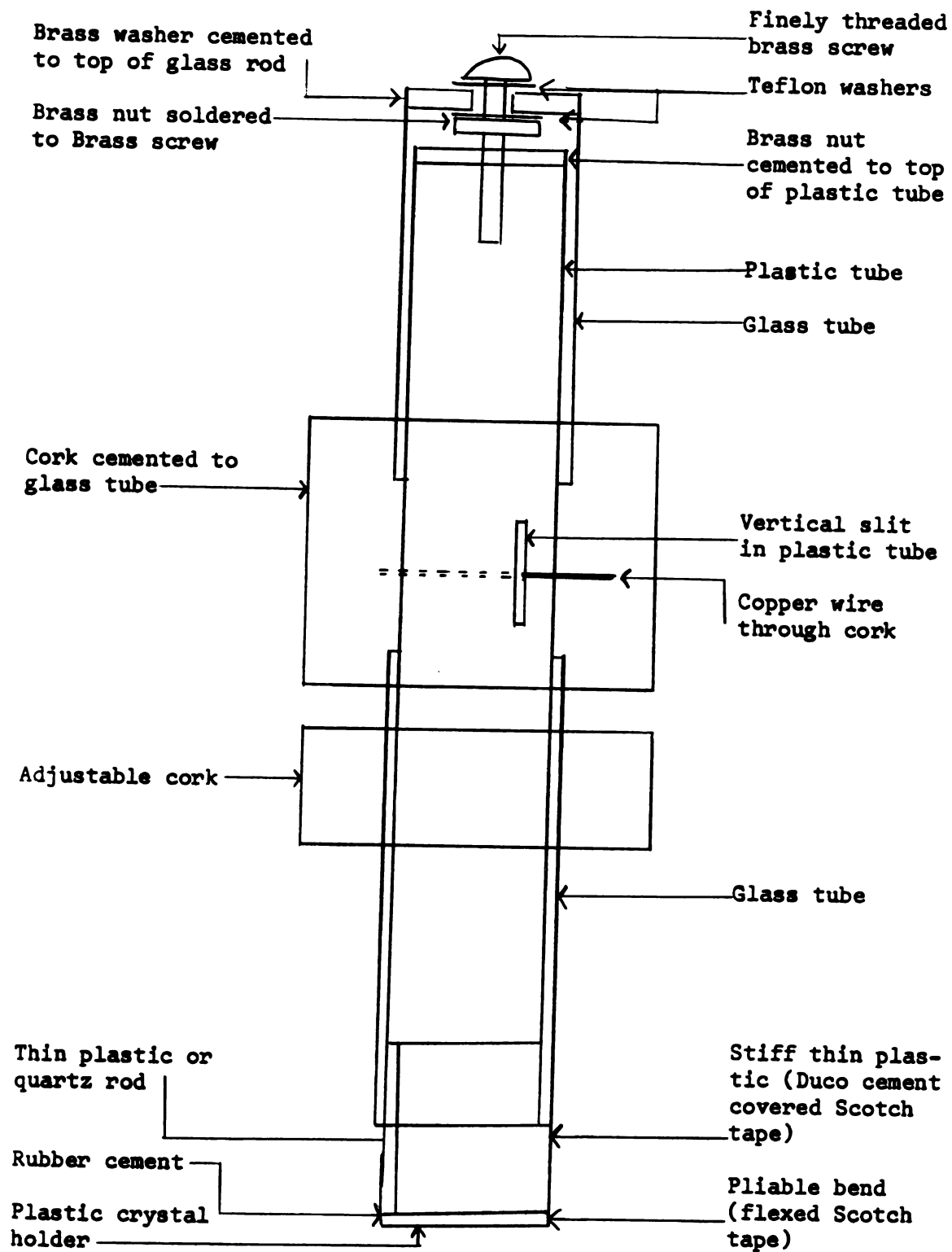


Figure 5. Adjustable single crystal holder.

The holder body consists of two concentric pieces of tubing, the outer one of glass and the inner one of plastic. The inner tube has a nut cemented to its top and a vertical slit in its body. The outer has a screw secured to its top such that the screw can be rotated but not raised or lowered. This outer tube consists of two pieces which are held together by the fixed cork. The division is necessary so that the heavy copper wire can be drawn through the cork and the vertical slit in the inner plastic tube. The copper wire prevents the inner tube from rotating when the screw is turned. Since the inner tube cannot rotate, it will move vertically as the screw is turned. The left end of the plastic crystal holder (see diagram) will be raised or lowered while the right side acts as a hinge thereby giving a vertical rotation. The adjustable cork is used to position the holder so that the crystal will be in the center of the microwave cavity.

Standard Samples

Several standard samples were used to check the calibration of the x- axis of the xy recorder and the klystron frequency readings. They are:

$$\begin{aligned} & \text{Aqueous peroxyamine disulphonate} \\ & \hline g = 2.00550 \pm 0.00005, A(\text{high field}) & = 13.110 \text{ gauss} \\ & A(\text{low field}) = 13.031 \text{ gauss}^{90} \end{aligned}$$

Varian standard sample of pitch in KCL
 $g = 2.0028, 10^{13}$ spins for the 0.00033% sample per cm. of length and 3×10^{15} spins for the 0.1% sample $\pm 25\%$ accuracy for the number of spins. Line width (separation of peaks of the derivative) ≈ 1.7 gauss.⁹¹

$$\begin{aligned} & \text{Aqueous } K_3Cr(CN)_5NO \\ & \hline g = 1.99454 \pm 0.00005, A^N = 5.265 \pm 0.05^{90,92} \end{aligned}$$

Aqueous VOSO_4

$A = 116.13 \pm 0.2$ gauss (separation between the fourth and fifth line)⁹³

DPPH in KCL

$g = 2.0036$ ²²

PREPARATION OF SAMPLES

Substituted copper acetylacetonates. The preparation of the substituted acetylacetonates is described by Burdett.⁹⁴ The copper complexes were prepared by adding copper acetate to a solution of the ligand in CHCl_3 .

$\text{K}_3\text{Cr}(\text{CN})_6$. The method of Cruser and Miller⁹⁵ was used to prepare the potassium hexacyanochromate.

$\text{K}_3\text{Cr}(\text{CN})_5\text{NO}$. This compound was prepared by the method of Griffith et. al.⁹⁶

$\text{VO}(\text{CN})_5^{-3}$. This complex ion was prepared in water solution by adding excess KCN to a solution of VOSO_4 .⁹⁷

$\text{K}_3\text{VO}(\text{NCS})_4$. This complex was prepared by adding KNCS to a water solution and extracting with ethyl acetate.⁹⁸

$\text{Cr}(\text{NO})(\text{NH}_3)_5\text{Cl}_3$. This complex was prepared by the method of Mori et. al.⁹⁹

The vanadyl acetylacetonates were prepared by adding the appropriate substituted acetylacetonate to vanadyl sulphate in dimethylformamide (DMF) or by the method of Feltham.³⁷

The copper salts of the amino acids were prepared by adding CuCO_3 to an aqueous solution of the amino acid and boiling.¹⁰⁰

The other vanadyl complexes were prepared by the methods of Holmes.⁹⁷

CRYSTAL GROWING

$\text{K}_3\text{Cr}(\text{CN})_5\text{NO}$ in Alkali Halide Lattices

Single crystals of alkali halides containing about 0.1% $\text{Cr}(\text{CN})_5\text{NO}^{-3}$ were grown from saturated aqueous solutions.

The KBr crystals were very easy to grow. KCl crystals were moderately easy to grow. KI crystals were easy to grow, but they often were inhomogenous and contained visible areas of trapped water and visible areas of high concentrations of $K_3Cr(CN)_5NO$. NaCl crystals were very hard to grow and only small (2-3 mm on a side) crystals were obtained. The NaCl crystals were not cubes but contained a combination of the cubic and octahedron faces.

The crystals were grown in a desiccator kept at $23 \pm 2^{\circ}C$. Small seed crystals of the respective alkali halide were grown from solutions left standing in open beakers for KCl and NaCl. For KBr and KI small crystals from the reagent bottle were used as seeds. The seed crystals were suspended in the mother liquor by a fine piece of nylon thread. In order to prevent capillary action in the thread and the deposit of rings of the alkali halide on the side of the beaker, both the thread and the entire inside of the beaker were coated with Dow Corning high-vacuum silicone grease.

Preparation of the Other Single Crystals

The other single crystals used in this investigation were also prepared by the desiccator evaporation method described above. The $K_3Cr(CN)_6, K_3Co(CN)_6$ crystals were relatively easy to grow as were the copper glycinate, cadmium-glycinate crystals. The $Cr(NO)(NH_3)_5^{+3}$, NH_4Cl single crystals had to be grown very slowly. $VO(CN)_5^{-3}$ could be grown in KBr only if there was an excess of KCN in the solution to prevent decomposition of the $VO(CN)_5^{-3}$ ion.

EQUATIONS AND CONVERSION FACTORS

The following equations and conversion factors are included for convenient reference.¹⁰¹

$$g = 7.14489 \times 10^{-7} \frac{v}{H} \quad (51)$$

ν is in megacycles and H is in gauss.

$$\left[\Delta\left(\frac{\nu}{c}\right)\right] \text{ in cm}^{-1} = \left(\frac{\beta}{hc}\right) g \Delta H(\text{in gauss}) \quad (52)$$

$$\beta = 0.92732 \times 10^{-20}$$

$$h = 6.6256 \times 10^{-27}$$

$$c = 2.997925 \times 10^{10}$$

$$\Delta\left(\frac{\nu}{c}\right) \text{ in cm}^{-1} = (4.668567 \times 10^{-5}) g \Delta H(\text{in gauss}) \quad (53)$$

$$\Delta H \text{ in gauss} = (2.141984 \times 10^4) \frac{1}{g} \left[\Delta\left(\frac{\nu}{c}\right)\right] \text{ in cm}^{-1} \quad (54)$$

$$\nu(\text{megacycles}) = 1.3996 g H(\text{in gauss}) \quad (55)$$

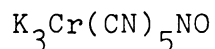
$$\nu (\text{cm}^{-1}) = 3.3356 \times 10^{-5} (\text{Mc}) \quad (56)$$

$$1 \text{ gauss} = 1 \text{ oersted (for air)} \quad (57)$$

$$1 \text{ a.u.} = 5.29167 \times 10^{-9} \text{ cm} \quad (58)$$

$$\text{a.u.}^{-3} \times 6.74872 \times 10^{24} = \text{cm}^{-3} \quad (59)$$

RESULTS



Electronic Configuration and Optical Spectra

This complex is t_{2g}^5 low spin. The possible orderings of the energy levels are given in Figure 6. At present it is not possible to assign the relative positions of the d_{z^2} and the $d_{x^2 - y^2}$ levels.

Optical spectra of KBr single crystals and of the water solution were obtained with a Beckman Model DB Spectrometer. Visible peaks were observed at $13,700 \text{ cm}^{-1}$, $22,000 \text{ cm}^{-1}$, and a shoulder at about $30,400 \text{ cm}^{-1}$. These are in good agreement with the published solution data.^{102,103} In addition a faint peak was observed which varied from $16,400$ to $17,100 \text{ cm}^{-1}$ in the two KBr crystals used. U.V. peaks were observed at $\approx 37,000 \text{ cm}^{-1}$ and $\approx 44,000 \text{ cm}^{-1}$.

Solution ESR spectra

The ESR data for $\text{K}_3\text{Cr}(\text{CN})_5\text{NO}$ in water solution are given in Table 5. The nitrogen hyperfine splittings were measured from samples containing natural abundance ^{13}C while the carbon hyperfine splittings were measured from samples enriched to 15.5% ^{13}C . The ^{53}Cr hyperfine splittings were measured from samples containing natural abundance ^{53}Cr . For the measurements of the relative intensity ratios of the axial and equatorial ^{13}C splittings the experimental spectra were taken on the low field side of the natural abundance (10%) ^{53}Cr lines to avoid overlapping of the ^{53}Cr and ^{52}Cr sets. No splittings of the ^{13}C lines due to the cyanide nitrogen was observed even in D_2O solution. In concentrated

H_2SO_4 only a single line of width four gauss was present. In DMF the splittings were about the same as in H_2O except that over several months a second peak (or peaks) appeared.

Single Crystal Studies

Angular Dependence of ESR Spectra

The spectra obtained using KBr, KCl, and NaCl as host lattices are similar and the triplet separation, due to hyperfine splitting by the ^{14}N (of the NO group), varies with angular setting as shown in Figure 7. When the host lattice was KI no angular variation was observed at room temperature and the spectrum was similar to the aqueous solution spectrum. Some KI samples showed an angular dependence at lower temperatures (-10 to -20°C) while others gave the same spectrum as a powdered crystal. The KI crystals chosen were desiccator dried for several months, were uniform in appearance and did not contain visible areas of trapped water; nor did they show, by infrared analysis, any greater percentage of water than the KBr crystals. However, the low temperature spectra indicate that the complex ion has not completely entered the lattice in all the crystals.

In describing the crystal spectra it is assumed that the complex ion has replaced an MX_6^{-5} group of the MX alkali halide host lattice and that the complex ions are arranged with the Cr-N-O direction randomly distributed among the six possible positions (which are also the cubic axes of the crystal). The vertical axis, about which our rotations were made, is chosen as the z-axis and was always a cubic axis of the crystal; the x and y axes are then the Cr-C-N directions in the plane $\perp z$. The applied field H_0 is along x initially and θ is the angle between H_0 and x at any given setting. The crystals were oriented by manually adjusting the crystal holder in two mutually perpendicular directions until the g_{\parallel} spectra observed on the oscilloscope were at highest magnetic field; this was seen visually to place H_0 along a cubic axis.

TABLE 5.--Experimental ESR data for $K_3Cr(CN)_5NO$ in H_2O

	This Thesis ⁹⁰	Ref.106-	Ref.104	Ref.105	Ref.102	Ref.107
$A(^{53}Cr)$	18.49 ±0.05	18.39 ±0.05	18.49	18.5		17.25
$A(^{14}N)$	5.26 ± 0.05	5.27 ±0.05	5.26	5.4	5.55	4.9
$A(^{13}C \text{ equatorial})$	12.49 ±0.10	12.64 ±0.2	12.49	11.9		11.9
$A(^{13}C \text{ axial})$	8.43 ±0.20	8.80 ±0.3	8.43			
g	1.99454 ±0.00005		1.9945	1.9950		1.995

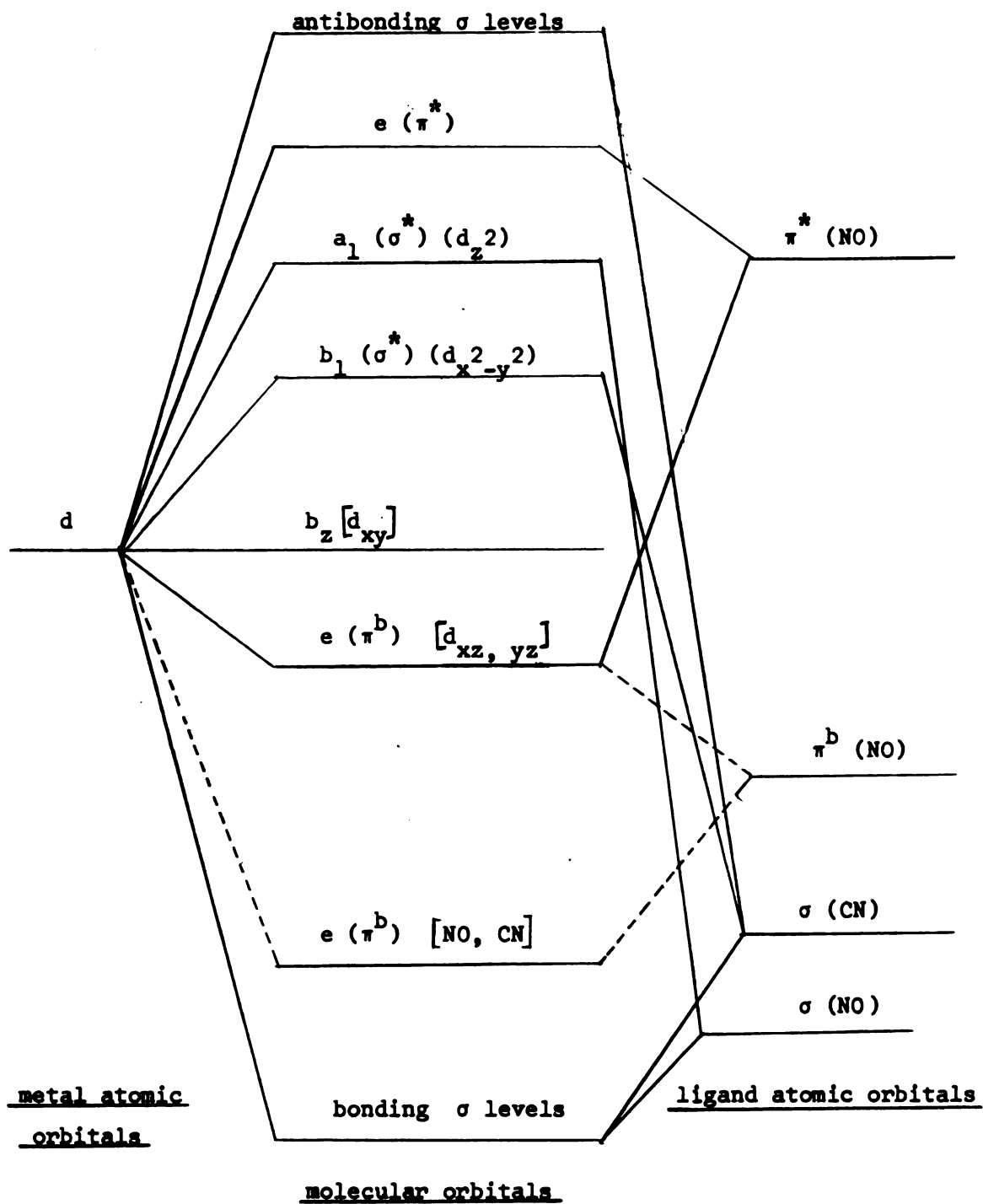


Figure 6. Energy level diagram for $K_3Cr(CN)_5NO$.

Since visual orientation could not be used for the NaCl crystals, which were small and irregular, and since the oscilloscope signal was insensitive over about a 5° range about the maximum, values of $A(N)_{\parallel}$ (Table 6) for NaCl have a larger uncertainty than normal.

As shown in Figure 7 the g_{\perp} lines did not change with angular setting since, when the unique axis of the octahedral ion is perpendicular to H_0 , one third of the octahedral ions are always oriented with their unique axis $\perp H_0$ and give rise to a triplet centered at g_{\perp} which does not shift on rotation about the z-axis. One third of the octahedra are oriented at the initial setting ($H_0 \parallel$ cubic crystal axis) with the unique axis parallel to H_0 ; these give rise to a triplet centered at g_{\parallel} which moves monotonically on rotation until at $\theta = 90^\circ$ it coincides with the g_{\perp} lines. The third triplet coincides with g_{\perp} at $\theta = 0$ and moves on rotation until it is at g_{\parallel} at $\theta = 90^\circ$. The line widths are about 1.5 gauss at g_{\parallel} and 3 gauss at g_{\perp} and neither the widths nor the splittings were altered appreciably from the room temperature values when the KBr crystal was heated to 300°C , although decomposition began. A precise study by Hayes⁴⁵ indicates a small linear increase in line width with temperature over the range 24° to 100°C for $\text{K}_3\text{Cr}(\text{CN})_5\text{NO}$ in water solution.

Spin Lattice Relaxation

The g_{\parallel} lines saturated at about 300 milliwatts, see Figures 8 and 9, but the g_{\perp} lines could not be saturated with our instrument. At present there is no theory for this anisotropic relaxation phenomenon. Dr. Cowen¹⁰⁸ of our Physics Department is studying the dependence of the relaxation on temperature and alkali halide lattice.

Collapse of Nitrogen Splittings

As illustrated in Figure 10 it is possible with over-modulation by the 100 Kc unit (setting of 800 where modulation

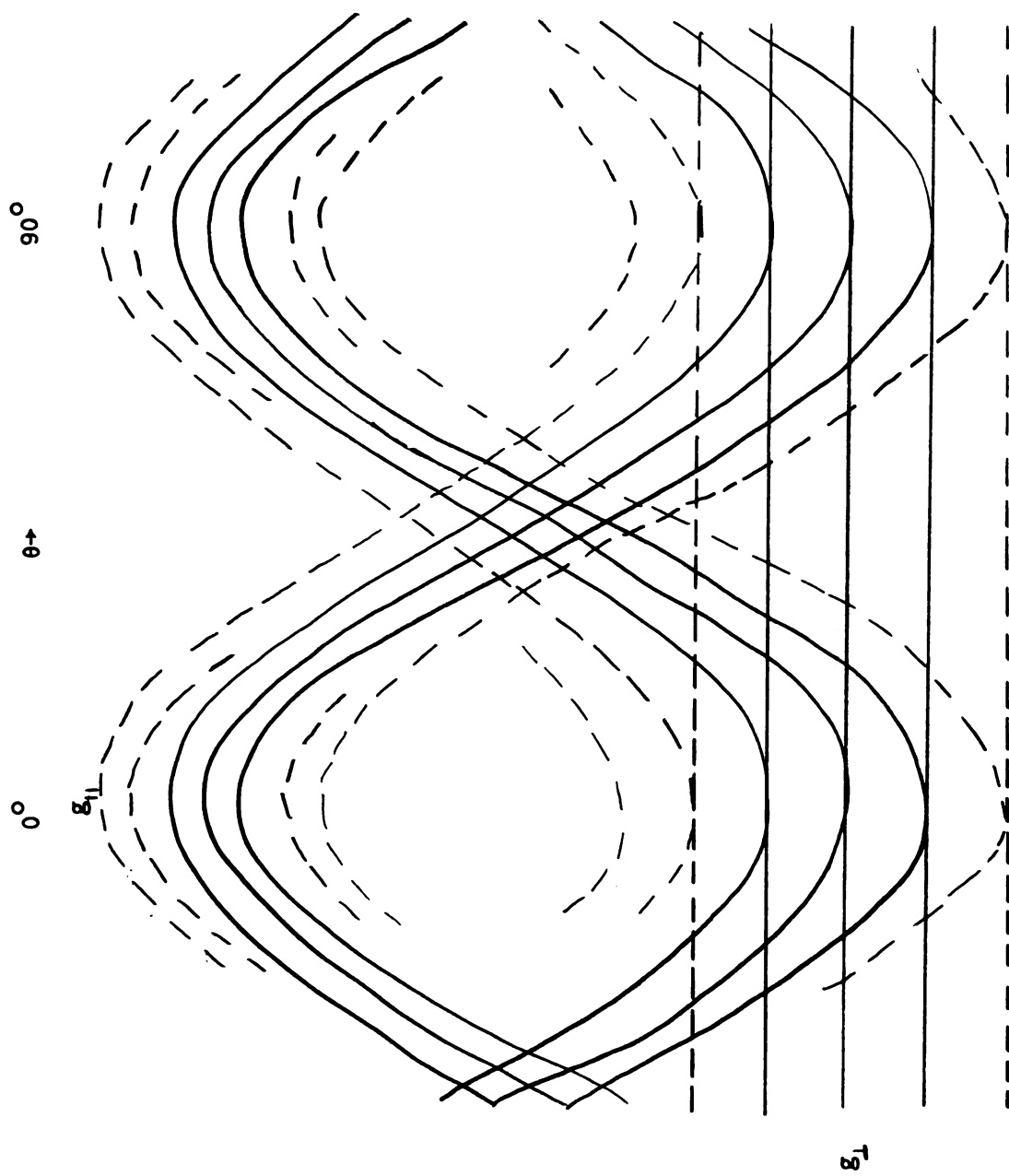


Figure 7. Orientation dependence of $\text{Cr}(\text{CN})_5\text{NO}^{-3}$ ESR data.

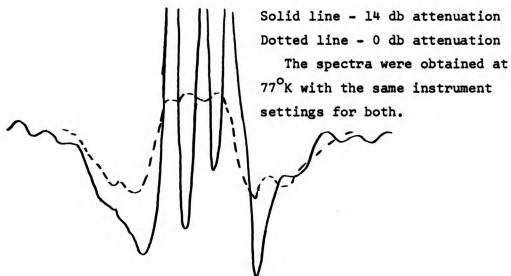


Figure 8. Saturation of the g_{\parallel} position of $\text{K}_3\text{Cr}(\text{CN})_5\text{NO}$ in KBr single crystal at 77°K .

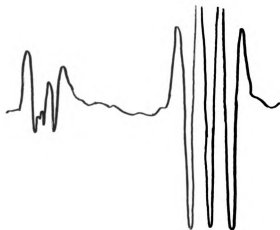


Figure 9. Saturation of g_{\parallel} spectrum but not the g_{\perp} spectrum for $\text{K}_3\text{Cr}(\text{CN})_5\text{NO}$ in KBr single crystal at 77°K .

broadening starts at 125) and second derivative presentation to collapse the nitrogen triplet and leave the ^{13}C splittings undisturbed. This technique is of limited use since the two sets of splittings must be sufficiently different in width so that both sets will not be overmodulated. With this limitation it can be used to resolve overlapping spectra and remove closely spaced fine structure from larger splittings.

^{13}C Splittings

The ^{13}C hyperfine splittings were obtained from samples prepared with KCN enriched to 15.5% in ^{13}C . The splitting in the g_{\parallel} position (see Figure 11) is 12.94 gauss and results from four equatorial carbon atoms for which the Cr-C bonds are perpendicular to H_0 . One axial carbon for which Cr-C is parallel to H_0 should also produce a splitting but this is not seen either because it falls at about the same place as the stronger peak or because it lies beneath a carbon peak from the other nitrogens (the observed line widths are 1.5 to 3 gauss). We symbolize this splitting as $A(^{13}\text{C})_{\perp}$ since H_0 is perpendicular to the Cr-C bonds.

In the g_{\perp} position in KCl two ^{13}C doublets with intensity ratios 3:2 are seen (Figure 12.) If the axial and equatorial ^{13}C splittings were the same, this intensity ratio could be interpreted as the splittings due to the three ^{13}C nuclei of the three Cr-C bonds perpendicular to H_0 and the splittings of the two ^{13}C nuclei of the two Cr-C bonds parallel to H_0 . However, Fortman and Hayes¹⁰⁴ have been able to distinguish the axial ^{13}C splittings from the equatorial for $\text{Cr}(\text{CN})_5\text{NO}^{-3}$ in $\text{Na}_2[\text{Mn}(\text{CN})_5\text{NO}]$ and find that they are not equivalent. Since the behavior of the axial ^{13}C splitting is, no doubt, similar in the two systems, the actual intensity ratio is probably 1 to 1; the observed ratio of 3 to 2 may be due to the overlap of the neighboring more intense nitrogen line which would have the effect of shifting the baseline of the recorded spectrum. The outer peak gives $A(^{13}\text{C})_{\perp} = 12.97$ gauss, as at the g_{\parallel} position; and the inner peak gives

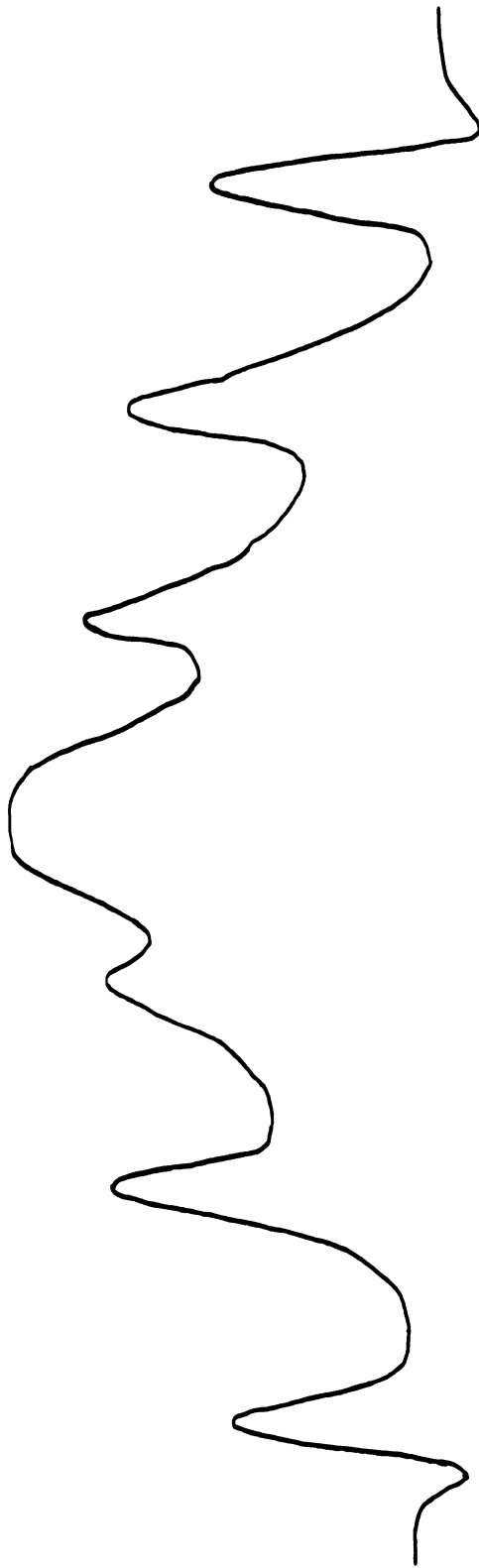


Figure 10. Collapse of nitrogen lines by overmodulation of the 100 kc unit for g_{II} position of 15.5% ^{13}C enriched $\text{K}_3\text{Cr}(\text{CN})_5\text{NO}$ in KCl .

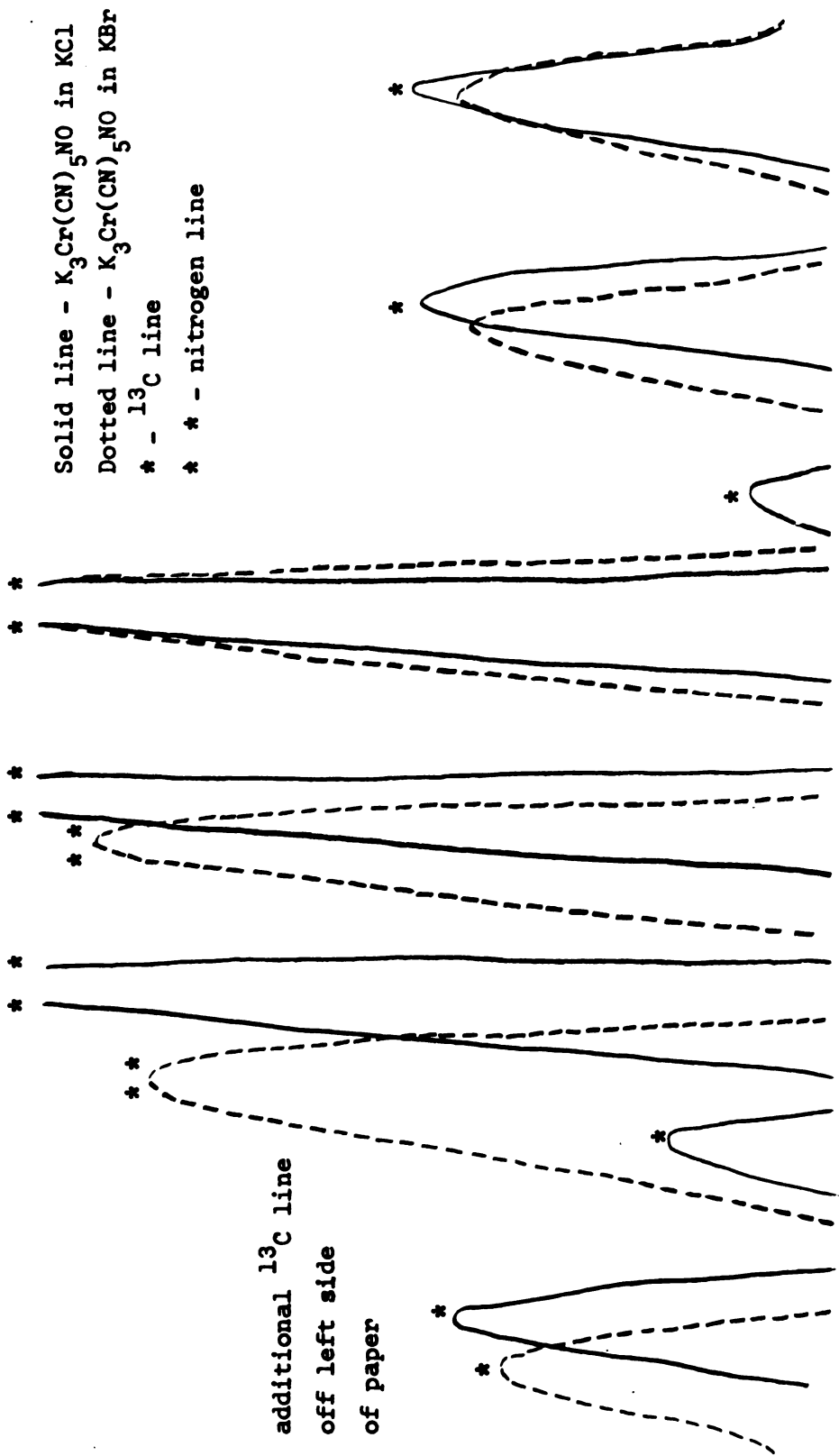


Figure 11. Superposition of the $g_{||}$ ESR spectrum of 15.5% enriched ^{13}C $K_3Cr(CN)_5NO$ in KBr single crystal and in KCl single crystal.

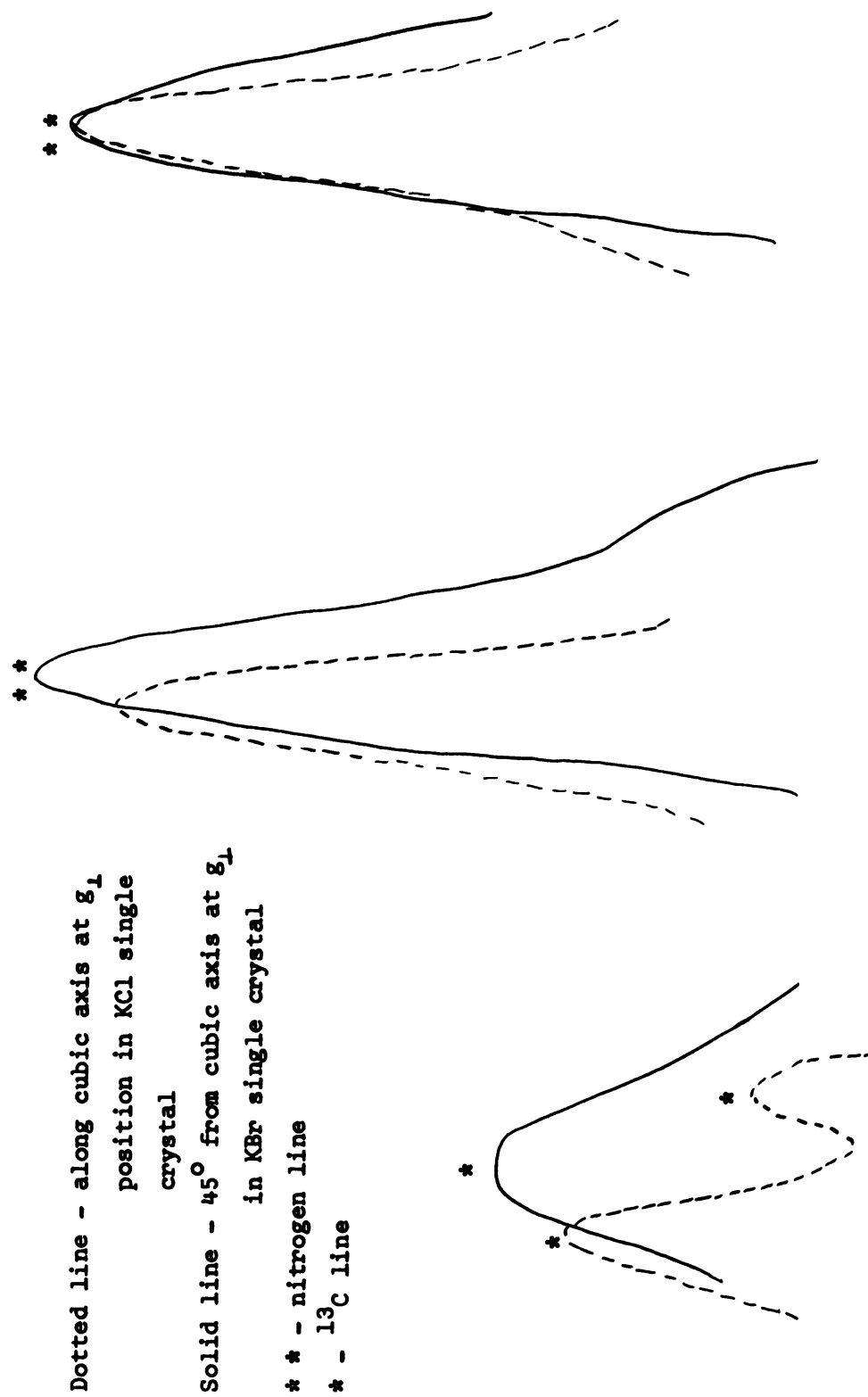


Figure 12. ^{13}C splittings of 15.5% enriched ^{13}C $\text{K}_3\text{Cr}(\text{CN})_5\text{NO}$ in g_{\perp} plane.

$A(^{13}\text{C})_{\parallel} = 9.35$ gauss. In KBr, the ^{13}C lines were not split in the g_{\perp} position. At $\theta = 45^{\circ}$ the four equatorial cyanides should be equivalent. The splitting at this position is 11.35 gauss (labeled $A(^{13}\text{C}_e)_{45^{\circ}}$ in Table 5) and was used along with the $A(^{13}\text{C})_{\perp}$ value to calculate $A_s^{13}\text{C}$ and $A_p^{13}\text{C}$ in KBr.

NO-Cr-CN Angle

For the KBr and KCl crystals the g_{\perp} data were taken at the same crystal orientation as the g_{\parallel} . X-ray spectra of the similar compound $\text{Na}_2\text{Fe}(\text{CN})_5\text{NO}$ indicate that the NO-Fe-CN bonds make an angle of 96° with each other.¹⁰⁹ An attempt was made to check the g_{\parallel} to g_{\perp} angle; however, the g_{\perp} spectrum is made up of two mutually perpendicular orientations which behave differently on rotation. Any rotation of the crystal to see if g_{\perp} would move farther down-field resulted in a broadening of the line which masked any shift which might have been present. The regular structure of the alkali halide lattice would tend to minimize the non-perpendicularity of the NO-Cr-CN bonds. As a check on the assumption that the g_{\parallel} orientation also gave the g_{\perp} orientation the powder spectra of crushed KBr and NaCl crystals were also run.

Comparisons of Powder Spectra Data With Single Crystal Data

Second derivative spectra gave excellent resolution of the g_{\perp} lines in the crushed single crystals but did not resolve the g_{\parallel} splittings. A comparison of the powder data with the single crystal data for KBr is given in Table 6. Within experimental error the data are in agreement. The g_{\perp} and A_{\perp} data for KBr and NaCl listed in Table 5 were obtained from the powder spectra.

TABLE 6.--Data for $\text{Cr}(\text{CN})_5\text{NO}^{-3}$ in various lattices.

Quantity	KI	KBr	KCl	NaCl	$\text{K}_3\text{Mn}(\text{CN})_5\text{NO}^{\text{c}}$
g_{\parallel}	-- --	1.9722 ± 0.0005	1.9722 ± 0.0005	1.9750 ± 0.001	1.9745 --
g_{\perp}	-- --	2.00447 ± 0.0002	2.0044 ± 0.0005	2.0045 ± 0.0005	2.0052 --
g	1.99475 ± 0.0001	1.9937 ± 0.0008	1.9936 ± 0.0008	1.9947 ± 0.001	1.9950 --
A_{\parallel}^{N}	-- --	2.89 ± 0.1	2.41 ± 0.1	2.1 ± 0.2	2.06 --
A_{\perp}^{N}	-- --	7.1 ± 0.2	7.1 ± 0.1	7.12 ± 0.2	6.90 --
A_{S}^{N}	5.27 \pm 0.05 --	-5.71 ± 0.2	-5.53 ± 0.1	-5.4 ± 0.2	-5.29 --
A_{p}^{n}	-- --	+1.41 ± 0.1	+1.57 ± 0.1	+1.70 ± 0.2	1.63 --
$A_{\perp}^{13\text{C}}$	-- --	13.05 ± 0.1	12.95 ± 0.05	-- --	15.0 ^a 8.79 ^b

^aequatorial^baxial^cRef. 104

TABLE 6.--(Continued)

Quantity	KI	KBr	KCl	NaCl	$K_3Mn(CN)_5NO^c$
$A_{ }^{13C}$	--	--	9.35	--	10.78 ^a
	--	--	±0.5	--	7.59 ^b
$A_{45^\circ}^{13C}$	--	11.35	--	--	--
	--	±0.5	--	--	--
A_s^{13C}	--	-11.92	-11.75	--	-12.16
	--	±0.3	±0.2	--	--
A_p^{13C}	--	+1.13	+1.19	--	1.15
	--	±0.3	±0.2	--	--
$A_{ }^{53Cr}$	--	33.4	33.4	--	32.5
	--	±0.8	±0.1	--	--
A_{\perp}^{53Cr}	--	11.9	11.7	--	11.5
	--	±1.0	±0.5	--	--
A^{53Cr}	--	19.1	18.9	--	18.46
	--	±1.0	±0.5	--	--

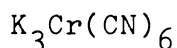
^aequatorial^baxial^cRef. 104

TABLE 7.--Comparison of powder and crystal ESR data.

KBr Powder	KBr Single Crystal
$g_{\perp} = 2.00447$ ±0.0002	$g_{\perp} = 2.0051$ ±0.0010
$A_{\perp}^N = 7.13$ ±0.05	$A_{\perp}^N = 7.05$ ±0.20

Infrared Spectra

Infrared spectra of $K_3[Cr(CN)_5NO]$ and $K_2Fe(CN)_5NO$ in KBr powder in mulls, of KBr single crystals, and of KBr and KCl pellets made from crushed KBr and KCl single crystals were made using Beckman IR 5 and IR 7 IR Spectrometers. Since the NO stretching frequency and a water peak fall in the same region (1600 cm^{-1}) single crystals were also grown from D_2O where the water peak is shifted to 1200 cm^{-1} . The IR data, along with some data from the literature for comparison, are given in Table 8. The IR spectra are given in Figures 13 and 14.



Crystal Orientation

Single crystals of $K_3Co(CN)_6$ containing less than 1% $K_3Cr(CN)_6$ were grown by slow evaporation of the saturated aqueous solution in a desiccator kept at $23 \pm 2^\circ C$. By visual inspection the crystals resembled the crystal illustrated in Figure 256 of Chemische Kristallographie.¹¹⁰ The crystal angles of the apparent m and a faces were measured with a reflecting goniometer. The three principle magnetic axes x, y, z and the crystallographic axes a, b, c are related by the direction cosines in Table 9a.¹¹¹ There are two nonequivalent octahedra which transform into each other by reflection in the ac plane. Each of the two cyanide octahedra has a two-fold axis along the c axis. The four-fold axis normal to the c axis makes an angle of 27° with the b axis. The direction cosines of the molecular axes (α, β, δ) of the two octahedra are given in Table 9b.

The crystals were cemented, in the approximate orientation desired, to a cavity insert which was adjustable in two perpendicular directions as shown in Figure 5. The accurate positioning of the crystal was then accomplished by observing the ESR spectrum on an oscilloscope, adjusting the two probe directions and rotating the electromagnet; also the above

TABLE 8.--Infrared data for $[M(CN)_5NO]^x$ compounds.

	Host	$\nu(NO)$ in cm^{-1}	$\nu(CN)$	$\nu(M-C)$
$[Fe(CN)_5NO]^{-2}$	Mull ^a	1938	--	--
	KBr ^{a,b}	1938	--	--
	KCl ^{a,b}	1925	--	--
	NaCl ^a	1938	--	--
$[Cr(CN)_5NO]^{-3}$	Mull ^a	1616(s) 1634(m)	2116(s) --	-- --
	Ground ^a in KBr	1637(s)	2123(s)	--
	Pellet from ^a KBr Single Crystals	1634(s) 1656(s) --	2123(s) 2101(wtos) --	350 401 434
	Pellet from ^a KCl Single Crystals	1707(s) 1685(s) 1654(s) --	2103(s) 2112(m) -- --	347 351 397 428
	Pellet from ^a NaCl Single Crystals	1696(s) 1666(s) 1648(s)	2118(s) -- --	-- -- --

^aThis work.

^bReference 169.

^cs = strong, m = medium, w = weak.

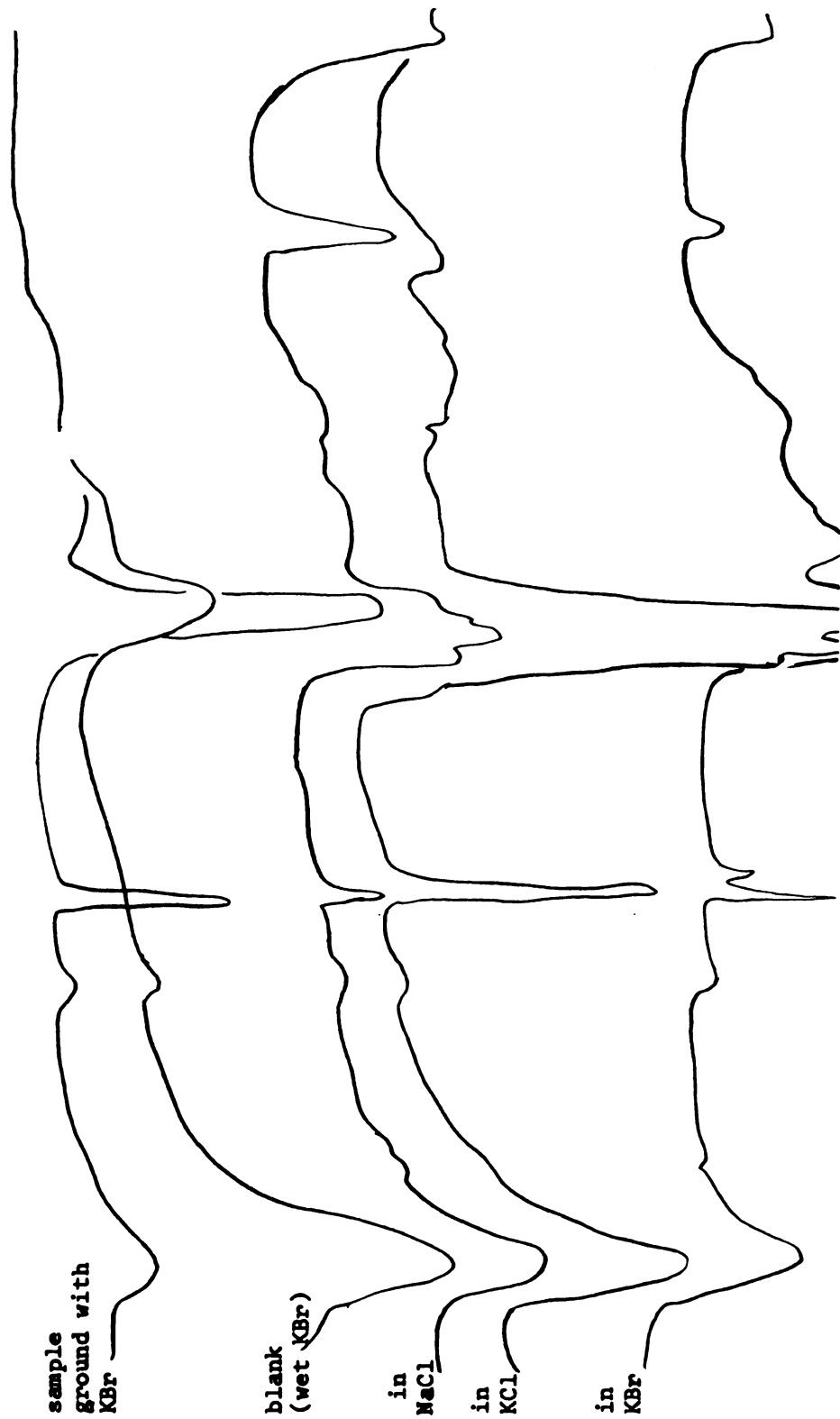


Figure 13. Infrared spectra, from 5,000 cm^{-1} to 1,100 cm^{-1} , of $\text{K}_3\text{Cr}(\text{CN})_5$ in various hosts.

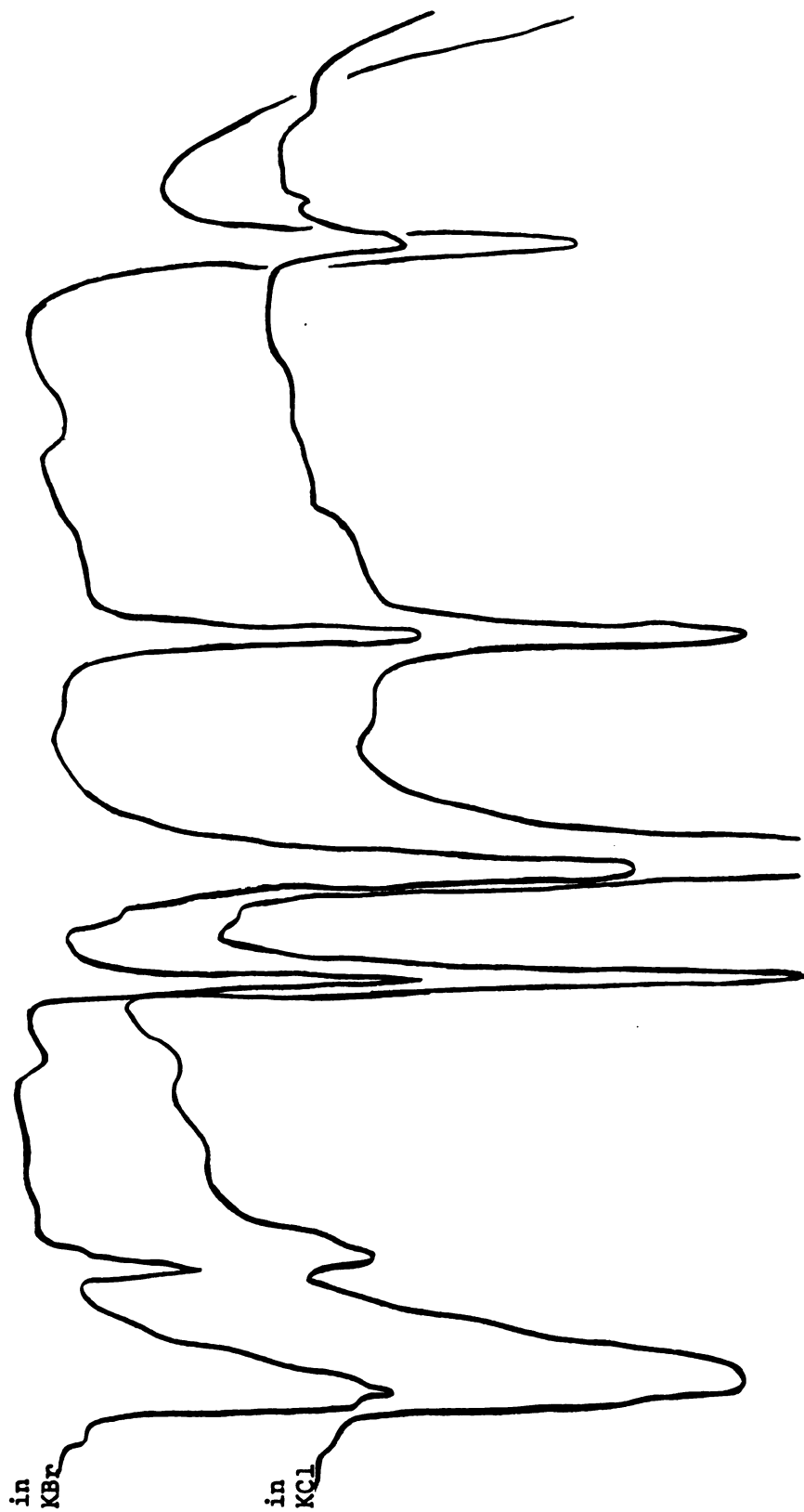


Figure 14. Infrared spectra, from 5,000 cm⁻¹ to 1100 cm⁻¹, of Fe(CN)₅NO⁻² in various hosts.

TABLE 9a.--Direction cosines between the principle magnetic axes (x,y,z) and the crystallographic axes (a,b,c) for $K_3Co(CN)_6$.¹¹¹

	x	y	z
a	0.104	0	0.994
b	±0.994	0	±0.104
c	0	1	0

TABLE 9b.--Direction cosines between the molecular axes (α, β, δ) and the crystallographic axes (a,b,c) for $K_3Co(CN)_6$.¹¹¹

	α	β	δ
a	0.45	-0.63	0.63
b	±0.89	±0.32	±0.32
c	0	0.71	0.71

mentioned relationships between the magnetic and octahedra axes were utilized along with the fact that there are two non-equivalent octahedra that transform by reflection.¹¹¹ The spectra were taken at room temperature and at approximately 126°K. The line width decreased as the temperature decreased, but the ^{13}C splitting remained constant. The spectra were taken in five crystal orientations - the magnetic x, y, and z axes, along a Cr-C bond axis, and at 61° to each of two of the Cr-C axes. Second derivative presentation was used. A typical spectrum is given in Figure 15.

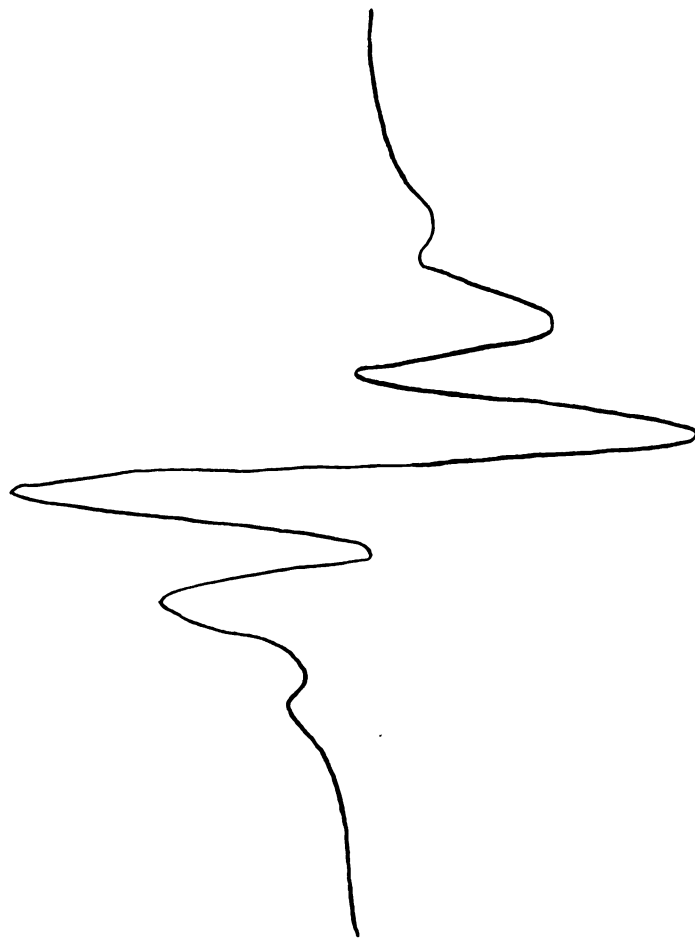


Figure 15. ESR spectrum of 15.5% ^{13}C enriched $\text{Cr}(\text{CN})_6^{-3}$ in $\text{K}_3\text{Co}(\text{CN})_6$.

ESR Spectra

The spectra were fitted to equation (11) where I is the projection on H_0 of the ^{13}C nuclear spin of the complexes containing only one isotropically substituted ^{13}C (which constitute 40% of the total number of complex ions in our case), and is equal to $\pm \frac{1}{2}$. H_0 is the center of the spectrum for the complexes (33% abundance) which contain no ^{13}C .

In each orientation chosen two of the Cr-C bond directions are equivalent and make an angle θ with H_0 . The hyperfine splitting observed is attributed to the cyanide carbon atoms lying along these axes. Any splitting due to the remaining two cyanide carbon atoms would be half the intensity and is neglected. The splittings due to the 9.5% abundant ^{53}Cr isotope and to the complexes containing two or more ^{13}C atoms are neglected; no correction has been applied for distortion of the measured peaks by these or by the central line of the spectrum. Off-diagonal terms in the hyperfine splitting tensor⁴² are also neglected.

The values $A_p = \pm 0.69$ gauss and $A_s = -9.80$ gauss account for the data from four orientations (resolution along the fifth direction, H_0 parallel to the x - axis, was so poor that quantitative measurements could not be made). At least seven spectra were taken for each orientation and the average deviations were ≈ 0.03 gauss. In view of the approximations involved, it appears more realistic to report $A_p = 0.7 \pm 0.2$ gauss and $A_s = -9.8 \pm 0.1$ gauss. The experimental data are given in Table 10.

There is another possible set of solutions to the ESR data. It is $A_s = \pm 3.73$ gauss and $A_p = \pm 6.76$ gauss. This set gives a carbon π spin density of $\approx 60\%$ on each of the six carbon atoms. Since the total spin density in the complex is only three electrons, the value of the total carbon spin density obtained with this set of A_s and A_p values, ≈ 3.6 electrons is physically unacceptable.

TABLE 10.-- ^{13}C ESR data for $\text{Cr}(\text{CN})_6^{-3}$ in $\text{K}_3\text{Co}(\text{CN})_6$

Along the C-Cr bond axis	($\theta = 90^\circ$)	$H - H_0 = 5.26$ gauss
Along the y magnetic axis	($\theta = 45^\circ$)	$H - H_0 = 4.79$ gauss
Along the 50° rotation position	($\theta = 76^\circ$)	$H - H_0 = 4.99$ gauss
Along the magnetic z axis	($\theta = 56^\circ 45'$)	$H - H_0 = 4.93$ gauss

VANADYL COMPLEXES

The isotropic g and A values were obtained from the liquid solution spectra. In solution vanadyl complexes have an eight-line ESR spectra due to the hyperfine splitting by the vanadium nucleus with nuclear spin of $\frac{7}{2}$. The A value is measured as the magnetic field separation between lines 4 and 5. To first order the g value is equal to $\frac{h\nu}{\beta H_{4,5}}$ where ν is the klystron frequency in megacycles and $H_{4,5}$ is the magnetic field in gauss halfway between lines 4 and 5. The second order correction is significant so that the actual magnetic field that is used is:

$$H = H_{4,5} + \frac{31 A^2}{4(H_{4,5})} \quad (60)$$

The anisotropic terms were determined from dilute powder spectra, frozen non-aqueous solutions, or dilute single crystals. $A_{||}$ and A_{\perp} were measured from the separation between their respective lines 4 and 5 when resolution permitted. Otherwise they were determined from the other line separations with the use of equations (26) and (27)

The ESR A values for substituted vanadyl acetylacetonates are given in Table 11. Vanadyl acetylacetonate,

TABLE 11.--Solution ESR spectra of substituted vanadyl acetylacetonates.^c

R'	R''	In Benzene	In CHCl ₃	In Acetone	In DMF
CH ₃	CH ₃	108.3 ^a	106.9 ^a	106.0 ^b	104.6 ^a
φ	CH ₃	107.6 ^a	105.6 ^a	106.0 ^b	107.1 ^a
φ	φ	107.7 ^a	106.0 ^a	106.4 ^b	107.9 ^a
CF ₃	CH ₃	110.4 ^a	108.5 ^a	109.0 ^b	108.8 ^a
CF ₃		111.1 ^a	109.0 ^a	109.6 ^b	109.4 ^a
CF ₃	CF ₃	114.5 ^a	112.6 ^a	113.3 ^a	112.6 ^a

^a \bar{A} value in gauss ± 0.5 .

^b \bar{A} value in gauss ± 1.0 .

^c The ligand is O-CR' - CH - CR'' - O

vanadyl bisbenzoylacetate, and vanadyl bisdibenzoylmethanate slowly decomposed in DMF, as evidenced by the appearance of a second set of peaks.

The ESR A values and optical data for vanadyl oxalate in various solvents are given in Table 12. In DMF and in H_2O excess oxalate ion was needed to slow down the decomposition.

TABLE 12.--ESR and optical data for vanadyl oxalate

Solvent	A (gauss)	Optical Transitions		
		$xy \rightarrow xz, yz$	$xy \rightarrow x^2 - y^2$	$xy \rightarrow z^2$
H_2O	106.6	12,500 cm^{-1}	16,500 cm^{-1}	--
	90.0	--	--	--
DMF	107.2	12,500	16,300	--
DMSO	106.9	12,400	16,000	22,900

The g values and A values for the other vanadyl compounds studied in this project are given in Table 13. A single crystal spectrum and a frozen solution spectrum are given in Figures 16 and 17, respectively.

Ligand Hyperfine Splittings in Vanadyl Complexes

Ligand hyperfine splittings were found only in $VO(CN)_5^{-3}$. The data are given in Table 14. A typical spectrum is given in Figure 18.

TABLE 13.--ESR data for vanadyl complexes

Compound	g	A_{\parallel}^a	g_{\parallel}	A_{\parallel}^a	g_{\perp}	A_{\perp}^a
$\text{VO}(\text{CN})_5^{-3}$ in DMF	1.9786 ± 0.002	81.4 ± 0.5	-- --	-- --	-- --	-- --
$\text{VO}(\text{CN})_5^{-3}$ in H_2O	1.98295 ± 0.0002	77.9 ± 0.5	-- --	-- --	-- --	-- --
$\text{VO}(\text{CN})_5^{-3}$ in KBr Single Crystal	1.9800 ± 0.0005	83.3 ± 2	1.9711 ± 0.0005	149 ± 2	1.9844 ± 0.0005	51 ± 1
$\text{VO}(\text{CN})_5^{-3}$ in KBr Powder	1.981 ± 0.002	83.6 ± 2	1.9735 ± 0.005	150 ± 2	1.98475 ± 0.0005	51.1 ± 0.5
$\text{VO}(\text{CF}_3\text{AcAc})_2$ in DMF	1.965 ± 0.005	108.8 ± 0.5	1.995 ± 0.005	190 ± 2	1.977 ± 0.005	69.5 ± 1
$\text{VO}(\text{hexaFAcAc})_2$ in DMF	1.9635 ± 0.005	112.6 ± 0.5	1.9415 ± 0.005	193 ± 2	1.9745 ± 0.005	70.5 ± 1

TABLE 13.--(Continued)

Compound	δ	A^a	$\delta_{ }$	$A_{ }^a$	δ_{\perp}	A_{\perp}^a
VO(hexaFAcAc) ₂ in Acetone	1.965 ±0.002	113.3 ±0.5	-- --	-- --	-- --	-- --
VO(NCS) ₅ ⁻³ in DMF	1.9687 ±0.002	104.5 ±0.5	1.9475 ±0.005	180 ±2	1.977 ±0.005	66.5 ±1
VO(NCS) ₅ ⁻³ in CHCl ₃	1.9668 ±0.002	107.0 ±1.0	1.9446 ±0.005	185 ±2	-- --	-- --
VO(AcAc) ₂ in CHCl ₃	1.969 ±0.002	106.9 ±0.5	1.9528 ±0.005	182.5 ±2	1.9760 ±0.005	66.9 ±1
VO(ClO ₄) _{4/2} in HClO ₄	-- --	120.0 ±0.5	1.9356 ±0.005	203 ±2	-- --	-- --
VO(DMSO) ₅ (ClO ₄) ₂ in DMSO	-- --	110.5 ±0.5	1.938 ±0.005	196 ±2	1.974 ±0.005	71.5 ±1

TABLE 13.--(Continued)

Compound	g	A ^a	g	A ^a	g _⊥	A _⊥ ^a
VO($\text{C}_6\text{F}_5\text{CF}_3\text{AcAc}$) ₂ in DMF	--	109.4 ±0.5	1.9428 ±0.005	191 ±2	1.9780 ±0.005	71.5 ±1
VOSO ₄ in DMSO	--	112.8 ±0.5	1.9396 ±0.005	196 ±2	-- --	-- --
VO(α, α -Bipyridine) ⁺² ₂ in DMF	--	103.2 ±0.5	-- --	-- --	1.9795 ±0.005	66.3 ±1
VOSO ₄ +pyridine in DMF	--	106.9 ±0.5	-- --	-- --	1.977 ±0.005	66.8 ±1
VO(orthrophen- anthroline) ₂ ⁺² in DMF	--	104 ±1	-- --	-- --	-- --	-- --
VO(NCS) ₅ ⁻³ in DuPont glue	--	-- --	-- --	-- --	1.9746 ±0.002	65.6 ±1.0

TABLE 13.--(Continued)

Compound	g	A ^a	g	A ^a	g _⊥	A ^a _⊥
VO(AcAc) ₂ in DuPont glue	--	--	--	--	1.9770 ±0.002	72.6 ±0.5
VOSO ₄ in DMF	--	114.6 ±0.5	--	--	1.9745 ±0.005	71.9 --
VOCl ₂ in HCl	--	110.9 ±0.5	--	--	--	--
VOF ₅ ⁻³ in HF, H ₂ O	--	116.0 ±0.5	--	--	--	--
VO(AcAc) ₂ in DMF	1.9678 ±0.002	104.6 ±0.5	--	--	--	--
VO(AcAc) ₂ in Benzene	1.969 ±0.002	108.3 ±0.5	--	--	--	--

^aIn gauss

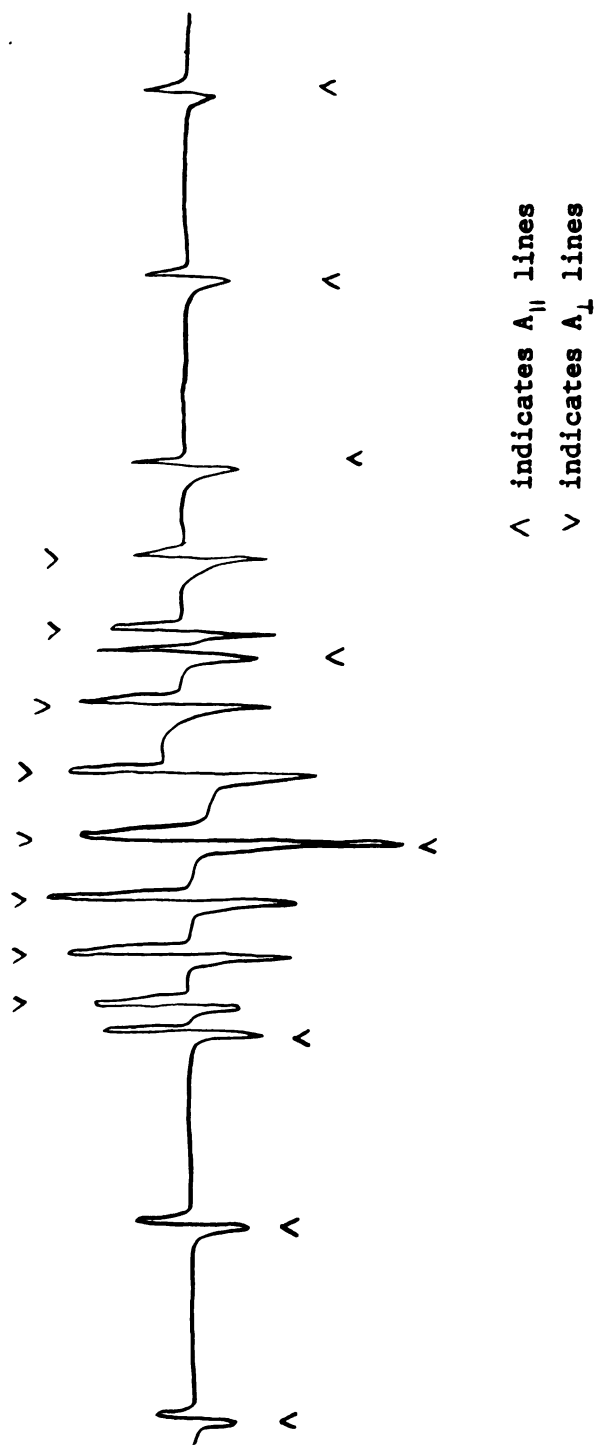


Figure 16. Single crystal ESR spectrum of $\text{VO}(\text{CN})_5^{-3}$ in KBr.

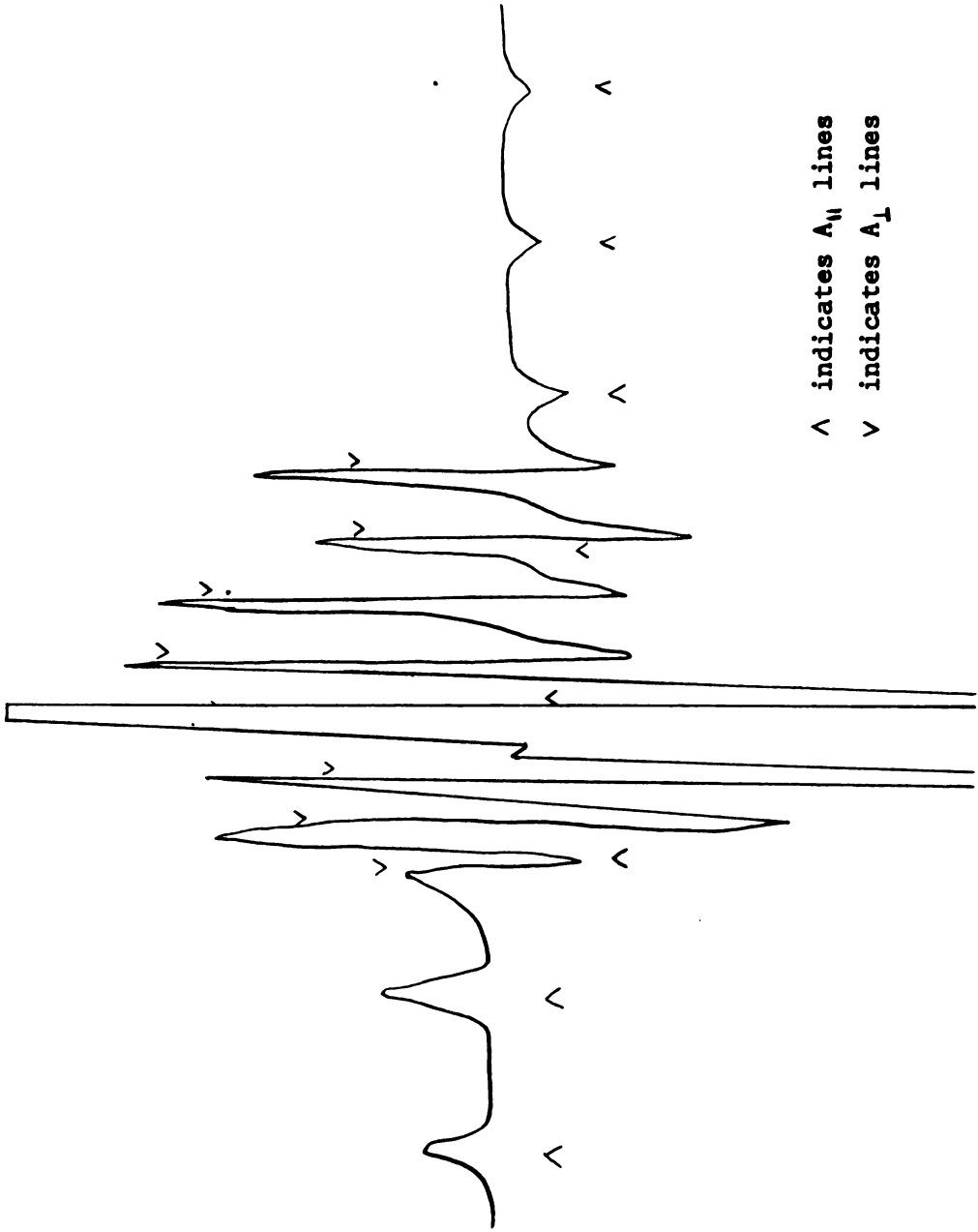


Figure 17. ESR spectrum of $\text{VO}(\text{NCS})_5^{-3}$ in frozen CHCl_3 solution.

TABLE 14.-- ^{13}C hyperfine splittings in $\text{VO}(\text{CN})_5^{-3}$

Solvent or Matrix	<u>A</u>	A(at g_{\perp})	A(at g_{\parallel})
H_2O	11.3 Gauss ± 0.2	--	--
DMF	Not Observed	10.65	9.95 ± 0.05
KBr (Single Crystal)	--	14	11.7 ± 0.5

Covalency in Vanadyl Complexes

The equations used for the determination of the molecular orbital coefficients from the ESR data are equations (29), (30), (35), and (36). Using $\langle \frac{1}{r^3} \rangle = 3.67 \text{ a.u.}$, $^{112} A_0$ (see equation (35) and (36) is equal to 184 gauss. Approximating equation (35) by $A_{\parallel} = -\frac{4}{7} N_{\pi_2}^2 A_0 - A$ one obtains the $N_{\pi_2}^2$ values given in Table 15. This set of $N_{\pi_2}^2$ coefficients indicates considerable xy π covalency for all of the complexes studied. (An $N_{\pi_2}^2$ value of 1 indicates a completely ionic complex and an $N_{\pi_2}^2$ value of 0.5 indicates a completely covalent complex.) Perhaps a closer approximation to the actual covalency can be obtained by setting A_0 at the value which gives $N_{\pi_2}^2 = 1$ for $\text{VO}(\text{H}_2\text{O})_5^{+2}$ and calculating the molecular orbital coefficient for the remaining complexes on this basis. These values are listed as $N_{\pi_2}^{2'}$. For comparison the molecular orbital coefficients obtained from the ratio of $A_{\text{isotropic}}$ for the complex over $A_{\text{isotropic}}$ for $\text{VO}(\text{H}_2\text{O})_5^{+2}$ are included. These values are listed as $N_{\pi_2}^{2''}$.

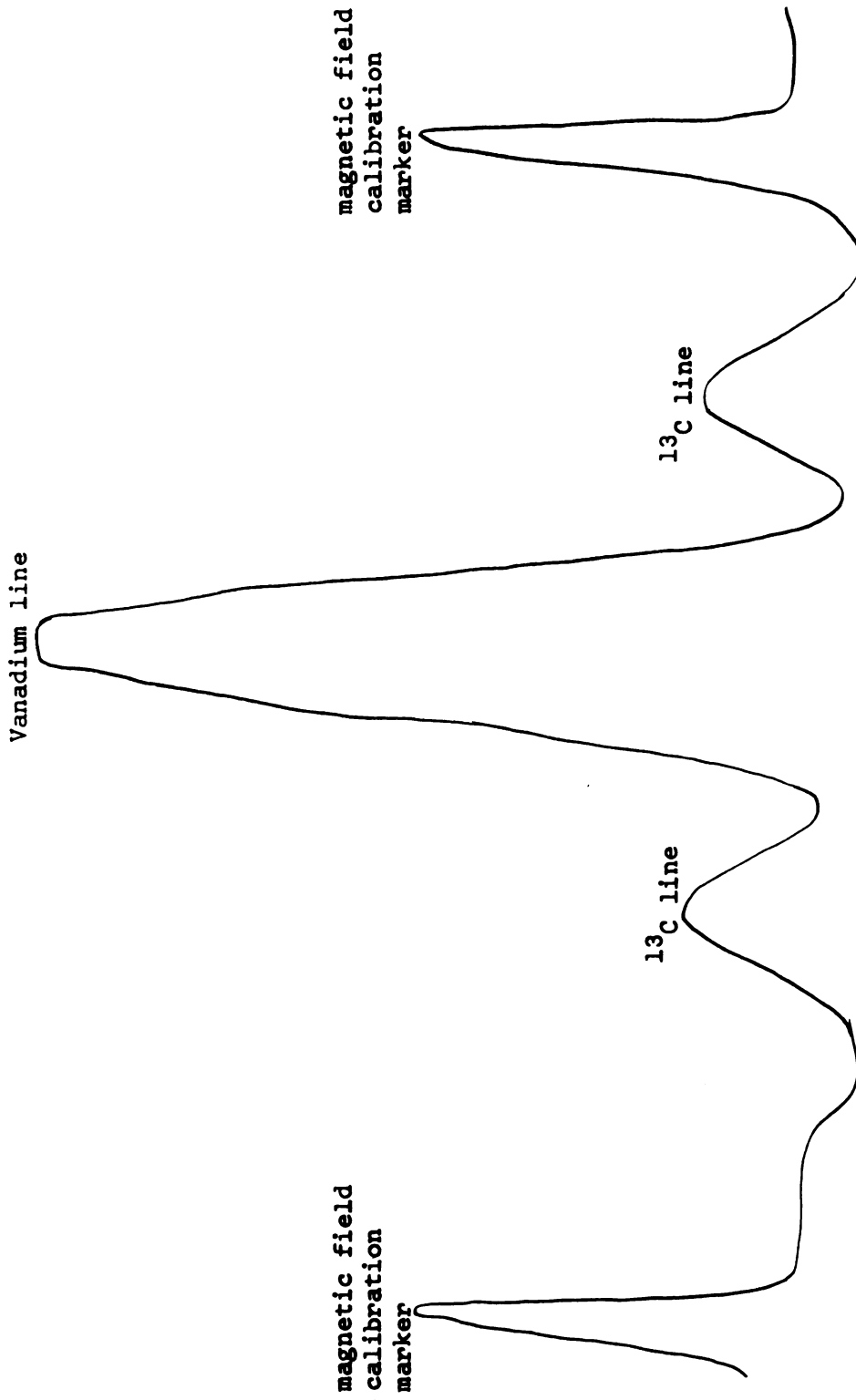


Figure 18. Aqueous solution spectrum of 15% ^{13}C enriched $\text{VO}(\text{CN})_5^{-3}$.

TABLE 15.--Molecular orbital coefficient for vanadyl xy orbital.

	$N^2_{\pi_2}$ a	$N^2'_{\pi_2}$ b	$N^2''_{\pi_2}$ c
$VO(H_2O)_5^{+2}$	0.79	1.00	1.00
$VO(DMSO)_5(ClO_4)_2$ in DMSO	0.81	1.02	0.93
$VOSO_4$ in DMSO	0.79	0.995	0.95
$VOClO_4$ in $HClO_4$	0.79	0.99	1.01
$VO(S^{\square}CF_3AcAc)_2$ in DMF	0.775	0.975	0.92
$VO(CF_3AcAc)_2$ in DMF	0.775	0.97	0.91
$VO(CF_3CF_3AcAc)_2$ in DMF	0.765	0.96	0.945
$VO(NCS)_5^{-3}$ in $CHCl_3$	0.74	0.93	0.90
VO (porphyrin) in THF	0.74	0.93	0.805
$VOCl_5^{-3}$	0.735	0.925	0.92
$VO(AcAc)_2$ in $CHCl_3$	0.72	0.91	0.895
$VO(NCS)_5^{-3}$ in DMF	0.715	0.90	0.88
$VO(CN)_5^{-3}$ in KBr	0.625	0.79	0.70

^aBased on $A_0 = 184$ gauss in Equation (35).

^bBased on $A_0 = 145.14$ gauss in Equation (35). Chosen to make $N^2_{\pi_2} = 1$ for $VO(H_2O)_5^{+2}$.

^cBased on ratio of $A_{isotropic}$ over $A_{isotropic}$ of $VO(H_2O)_5^{+2}$ (119 gauss).

COPPER COMPLEXES

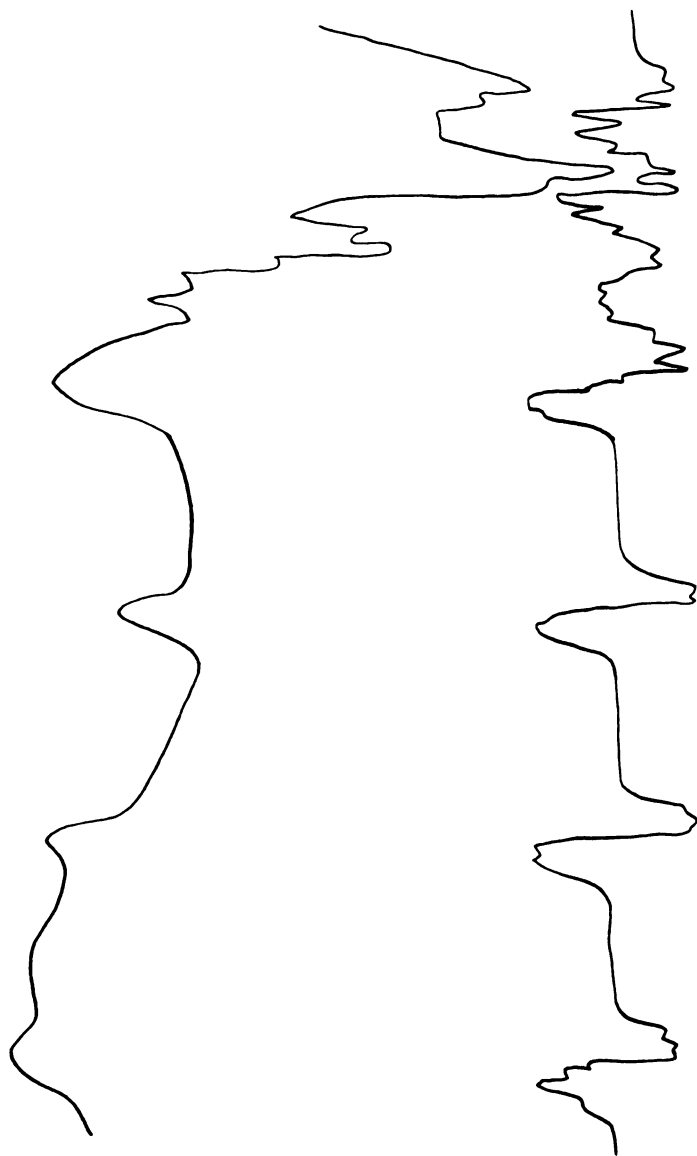
Single Crystal Study of Copper Glycinate in Cadmium Glycinate

g_{\parallel} and g_{\perp} were found by rotating the crystal in two mutually perpendicular directions and observing the ESR signal on the oscilloscope. g_{\parallel} is at the lowest possible magnetic field and g_{\perp} is at the highest possible magnetic field. Spectra of crushed dilute copper glycinate in cadmium glycinate single crystals were also taken as a check on the data obtained from the oriented single crystals. The data are given in Table 16. The spectra are given in Figures 19-21.

TABLE 16.--ESR data^a for bis-(glycino) - copper (II) · xH₂O

	g	g _⊥	g	A ^{Cu}	A _⊥ ^{Cu}	A ^{Cu}	A ^N	A ^N _⊥	A ^N _S
In Cd(gly) ₂ Single Crystal	2.2674 ±0.001	2.0546 ±0.002	2.1255 (Calculated)	133 ±0.5	44.1 ±1.0	73.7 (Calculated)	10.4 ±0.5	6.8 ±0.5	8.0 (Calculated)
In Cd(gly) ₂ Powder	2.266 --	-- --	-- --	135 --	-- --	-- --	-- --	-- --	-- --
In H ₂ O Solution	-- --	-- --	-- --	-- --	-- --	68.8 --	-- --	-- --	-- --

^aA values are in gauss.



Copper(II) glycinate - Cadmium(II) glycinate powder spectrum, (top).

Copper(II) glycinate - Cadmium(II) glycinate single crystal spectrum (bottom).

Figure 19. ESR spectra of copper(II) glycinate.

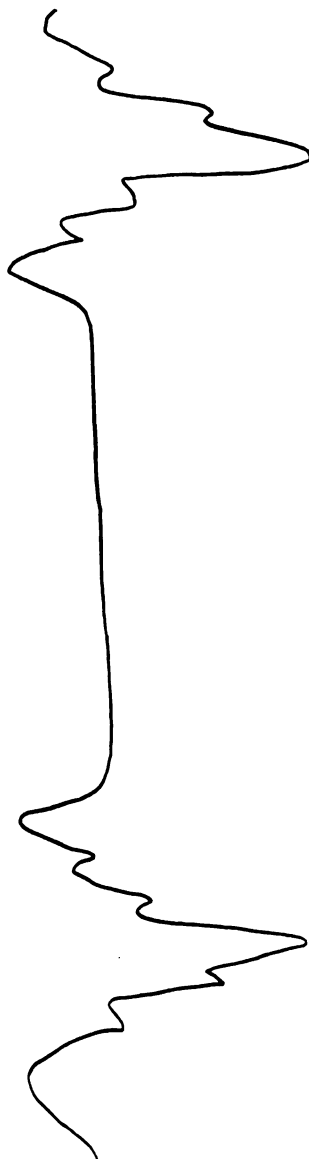


Figure 20. Second derivative ESR spectrum at g_{\parallel} position (lines two and three) of a copper(II) glycinate - cadmium(II) glycinate single crystal.



Figure 21. Second derivative ESR spectrum at g_1 position of a copper(II) glycinate-cadmium(II) glycinate single crystal.

TABLE 17.--ESR hyperfine splittings for copper (II) amino acid complexes

Ligand	A(gauss)	Ligand	A(gauss)
Isoleucine	72.8	α -Alanine	69.6
2-Aminobutyric acid	71.8	Glycine	68.8
Valine	71.8	N-Phenylglycine	68.6
2-Aminoisobutyric acid	71.2	β -Alanine	51.0
Serine	71.0		

Solution Spectra of Copper Amino Acid Complexes

The isotropic copper nuclear hyperfine splitting constants of some water soluble copper amino acid complexes were determined from their solution spectra, see Table 17 above.

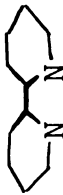
Solution Spectra of Substituted Copper Acetylacetonates

The complexes were dissolved in CHCl_3 . The high precision of measurement of the ESR A values was made possible by recording the spectra on an X-Y recorder whose x axis displacement is proportional to the magnetic field. This was accomplished by using the Hall probe circuit described in Figure 4. The A values are given in Table 18. The frozen solution ESR spectra are given in Figures 22 through 29.

The ESR results were all obtained in chloroform solution since the effect of changing solvent can be larger than the substituent effects; thus, the hyperfine splitting A for copper acetylacetonate in chloroform is $77.2 \times 10^{-4} \text{ cm}^{-1}$ ($g = 2.123$) whereas it is 66.1 in dimethylformamide ($g = 2.138$) and 56.7 in pyridine ($g = 2.148$).

TABLE 18.--Isotropic and anisotropic A values for substituted copper (II) acetylacetonates.

R'	R''	R'''	A	A_{\parallel}	A_{\perp}^c	g	g_{\parallel}	g_{\perp}^c	N_{σ}^2 a	N_{σ}^2 b
CF ₃	H	CF ₃	54.7 cm ⁻¹			2.150				.698
CF ₃	H	Thenoyl	71.6	169	23.0	2.131	2.310	2.042	.763	.887
CF ₃	H	CH ₃	72.5	168	24.8	2.129	2.307	2.040	.763	.875
Phenyl	H	CH ₃	76.4	178	25.4	2.124	2.284	2.044	.777	.879
CH ₃	H	CH ₃	77.2	175	28.2	2.123	2.285	2.042	.779	.862
CH ₃	CH ₃	CH ₃	78.5	185.5	25	2.121	2.269	2.047	.784	.884
		bipyridyl	66.5	169	15.4	2.115	2.260	2.043	.692	.849



^aCalculated using equation (70) with a constant $K_0^{0.5}$.

^bCalculated using $N_{\sigma}^2 = \frac{7}{4} \left[\frac{A_{\parallel}}{A_0} - \frac{A}{A_0} + \frac{2}{3} (g_{\parallel} - 2) - \frac{5}{21} (g_{\perp} - 2) + 0.04 \right]$ with

$A_0 = 0.036 \text{ cm}^{-1}$.

^cCalculated from the solution and parallel values.

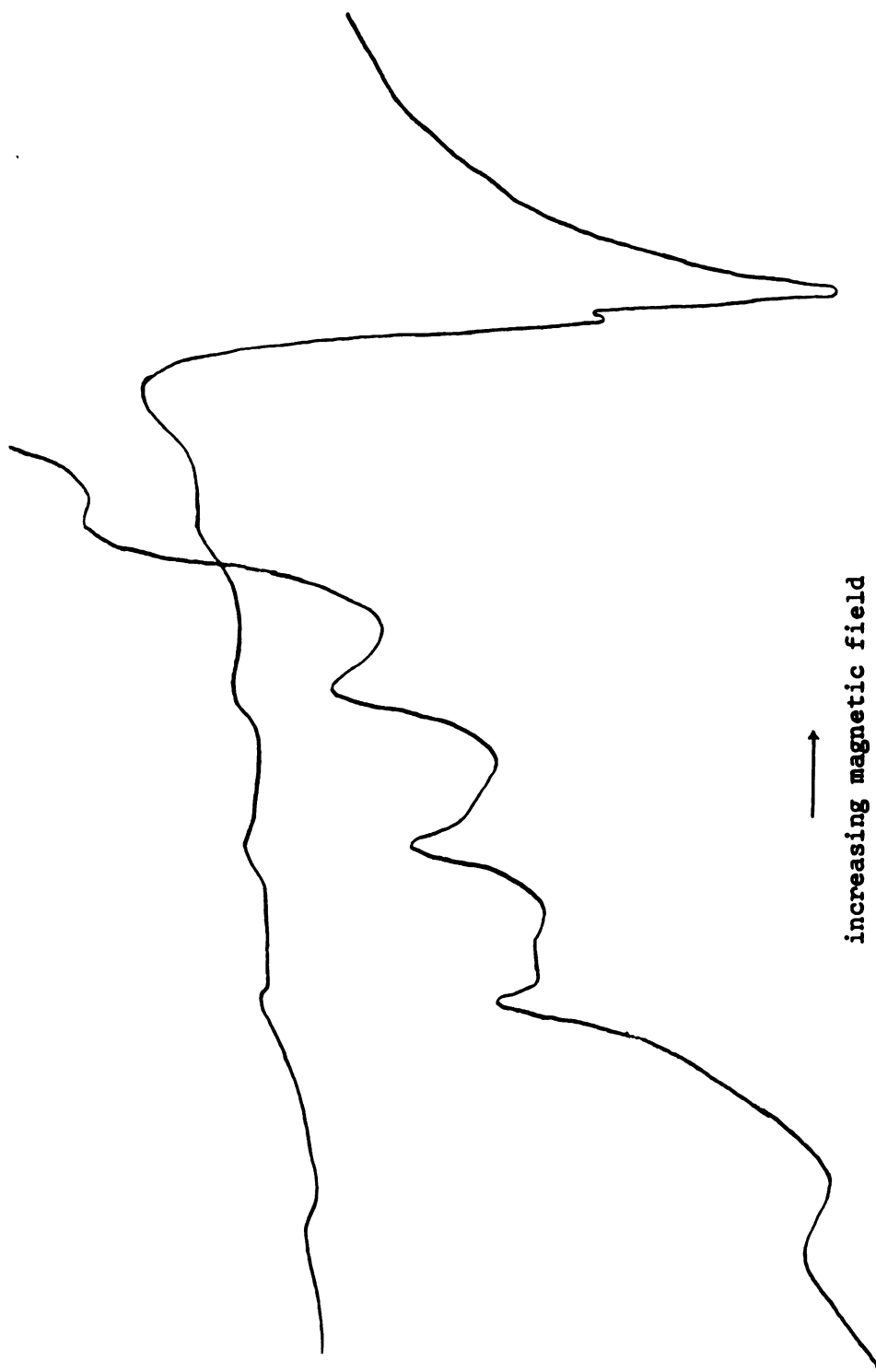


Figure 22. Frozen CHCl_3 solution ESR spectra of copper (II) hexafluoroacetylacetonate.

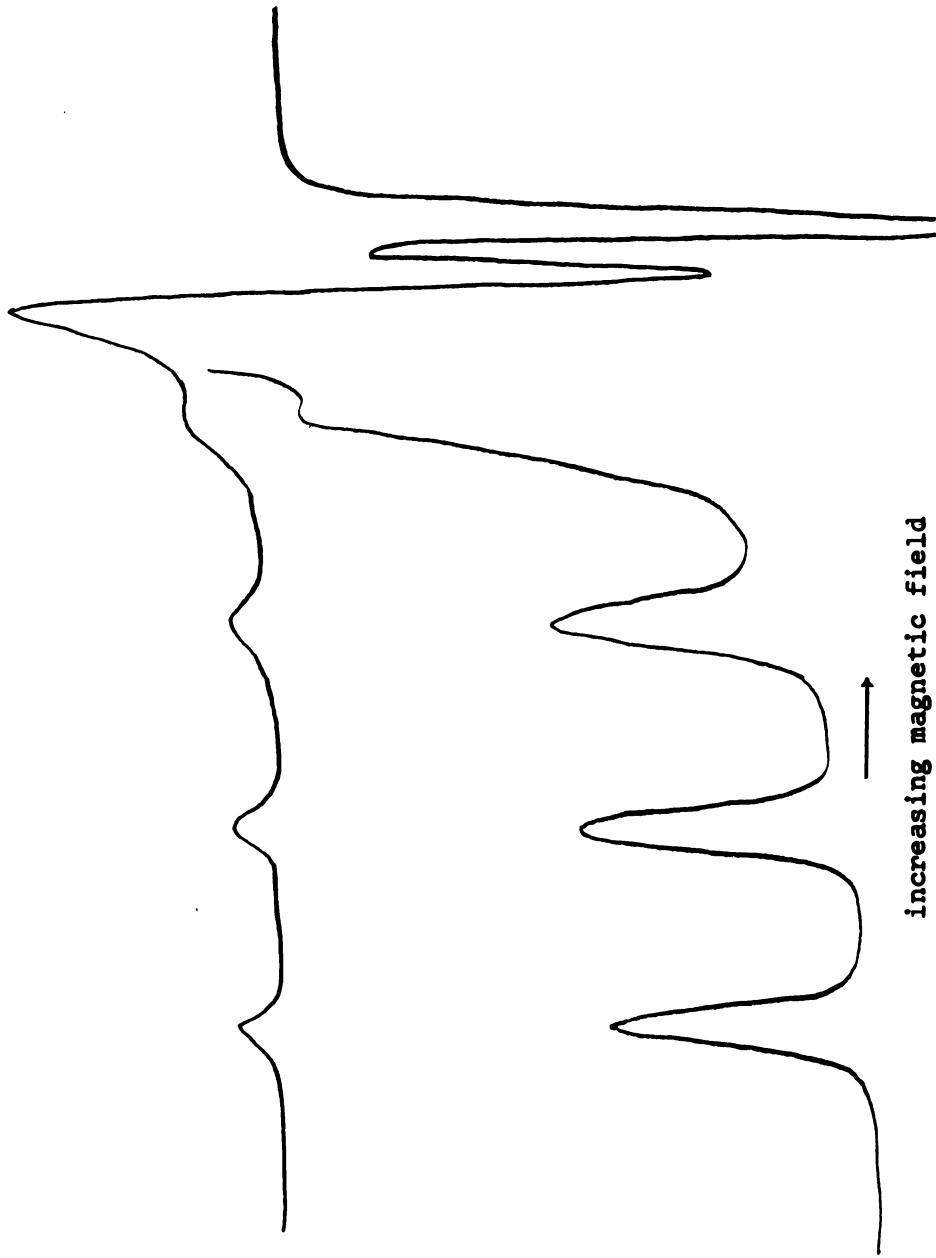


Figure 23. Frozen CHCl_3 solution ESR spectra of copper (II) trifluoroacetylacetonate.

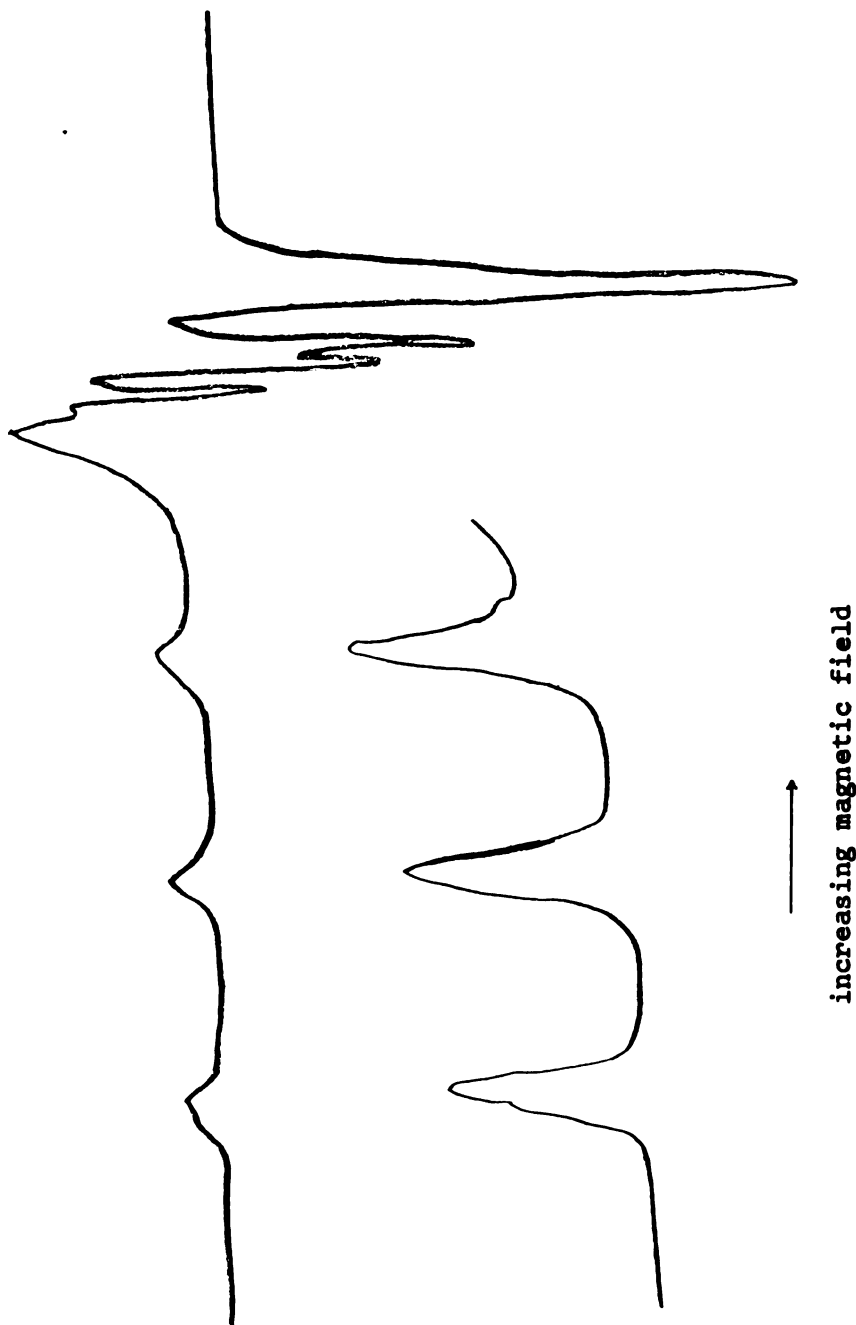
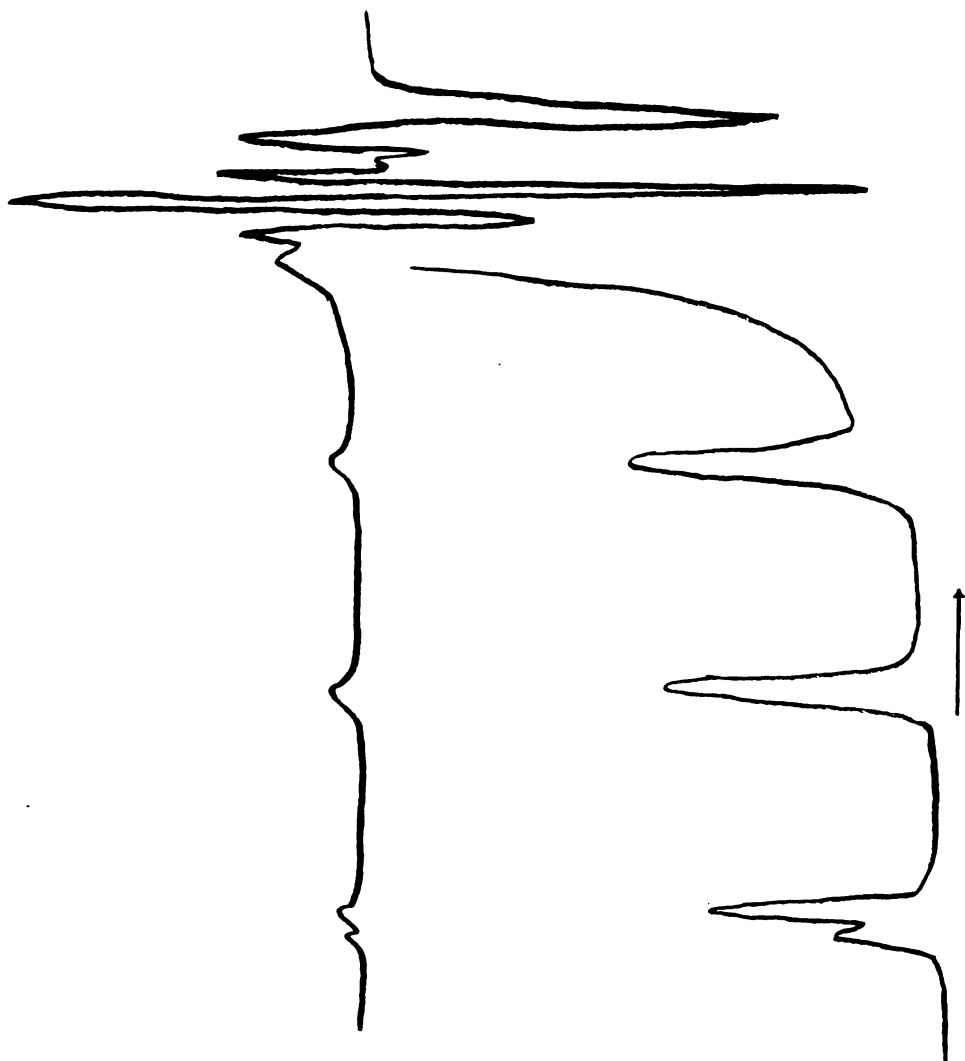
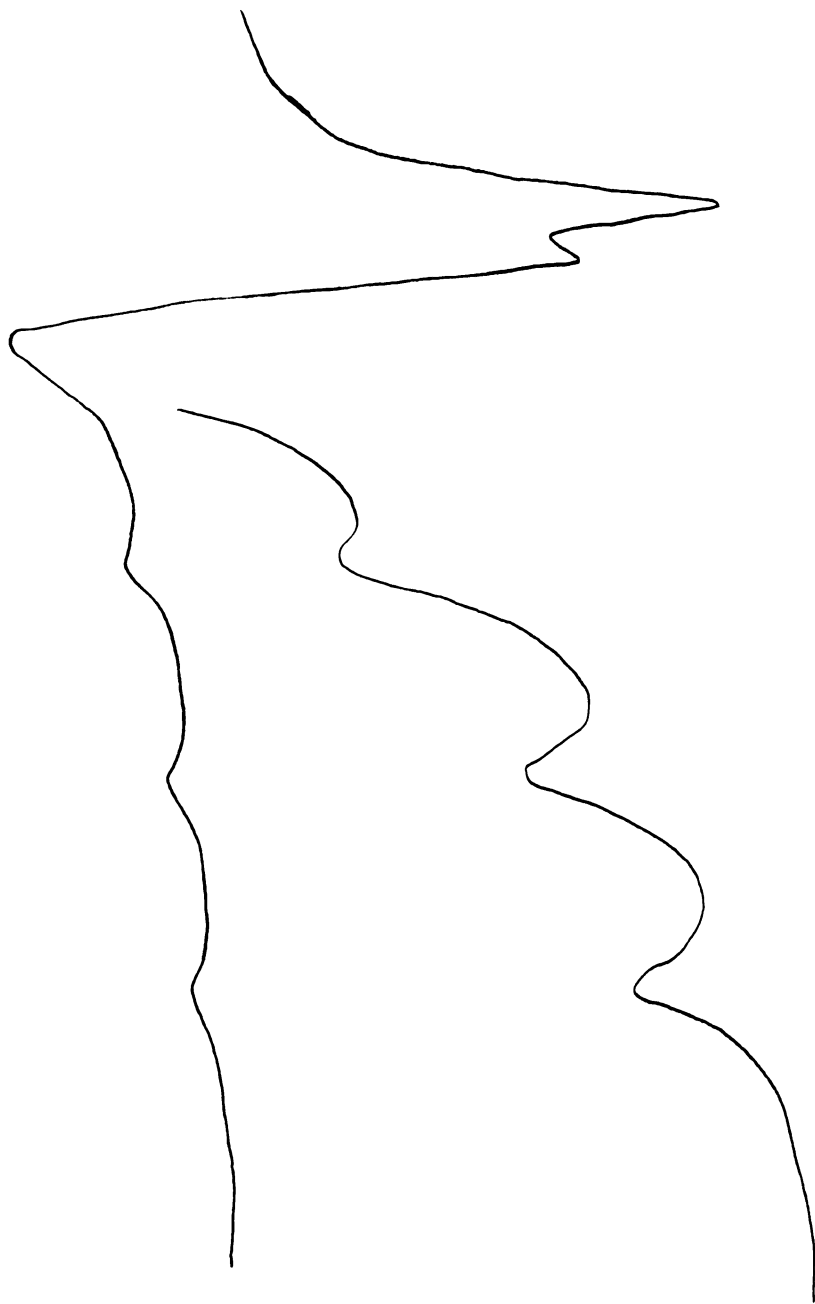


Figure 24. Frozen CHCl_3 solution ESR spectra of copper(II) benzoylacetonate.



increasing magnetic field

Figure 25. Frozen CHCl_3 solution ESR spectra of copper(II) 3-methylacetylacetonate.



increasing magnetic field
Figure 26. Frozen CHCl_3 solution ESR spectra of copper(II) acetylacetonate.

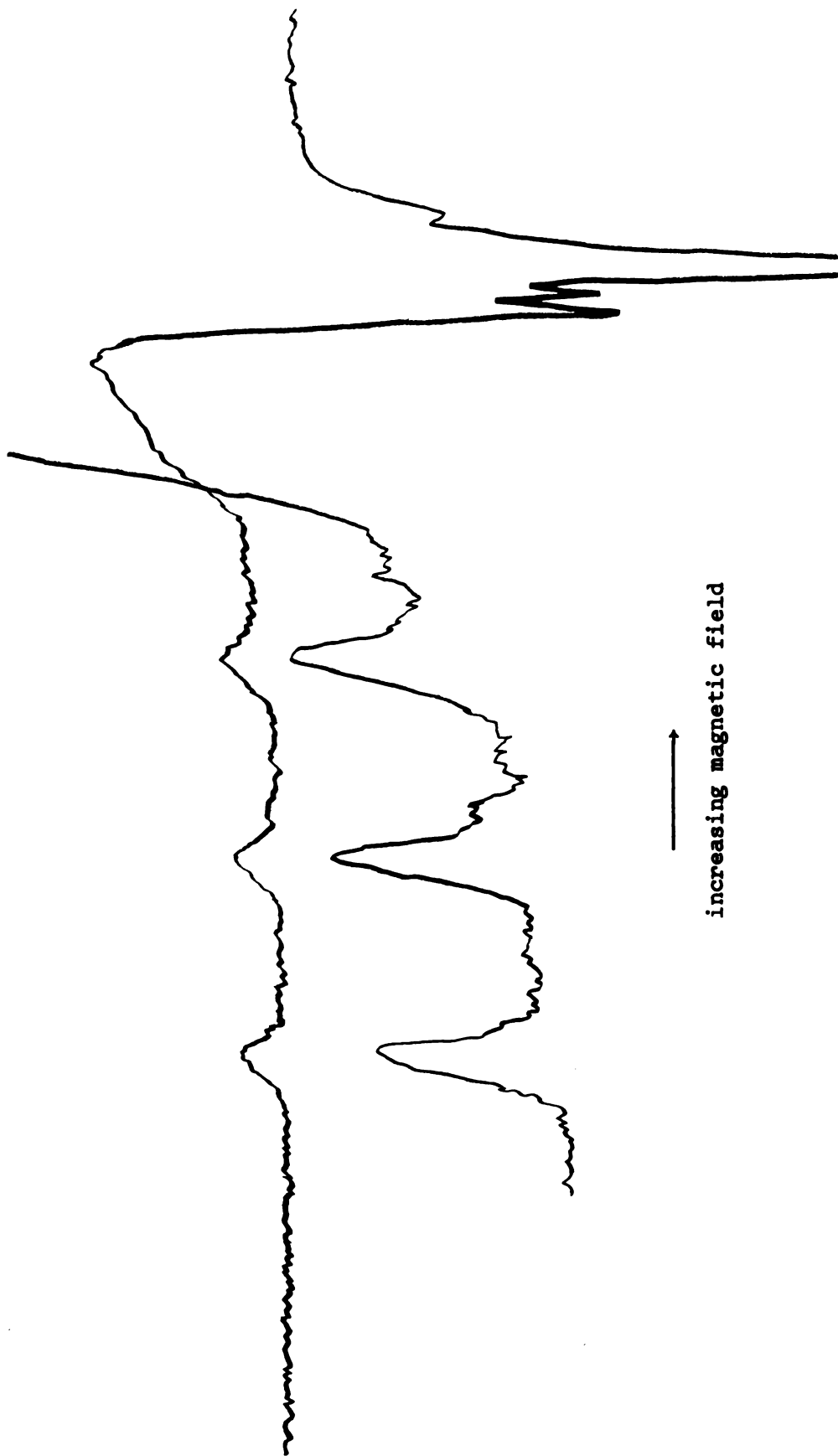
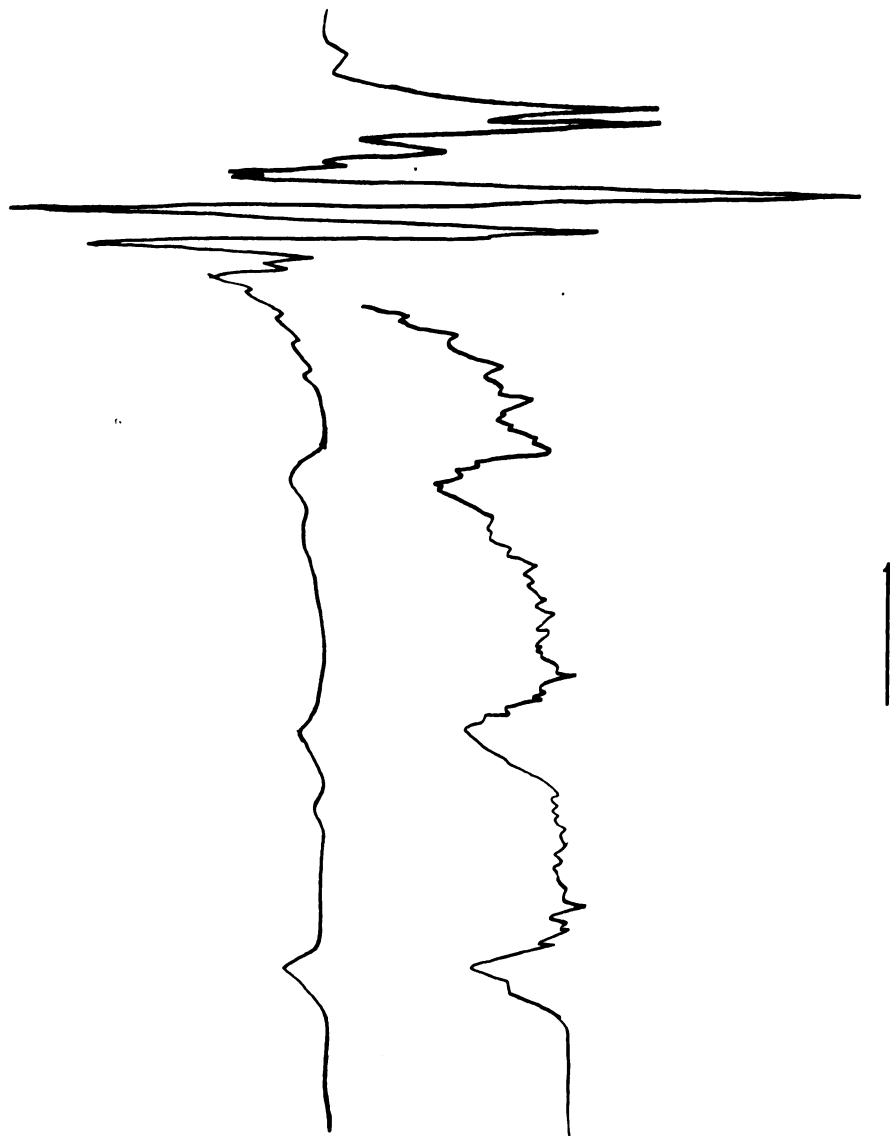


Figure 27. Frozen CHCl_3 solution ESR spectra of copper(II) benzoyltrifluoroacetone.



increasing magnetic field
Figure 28. Frozen CHCl_3 solution ESR spectra of copper(II) dibenzoylmethane.

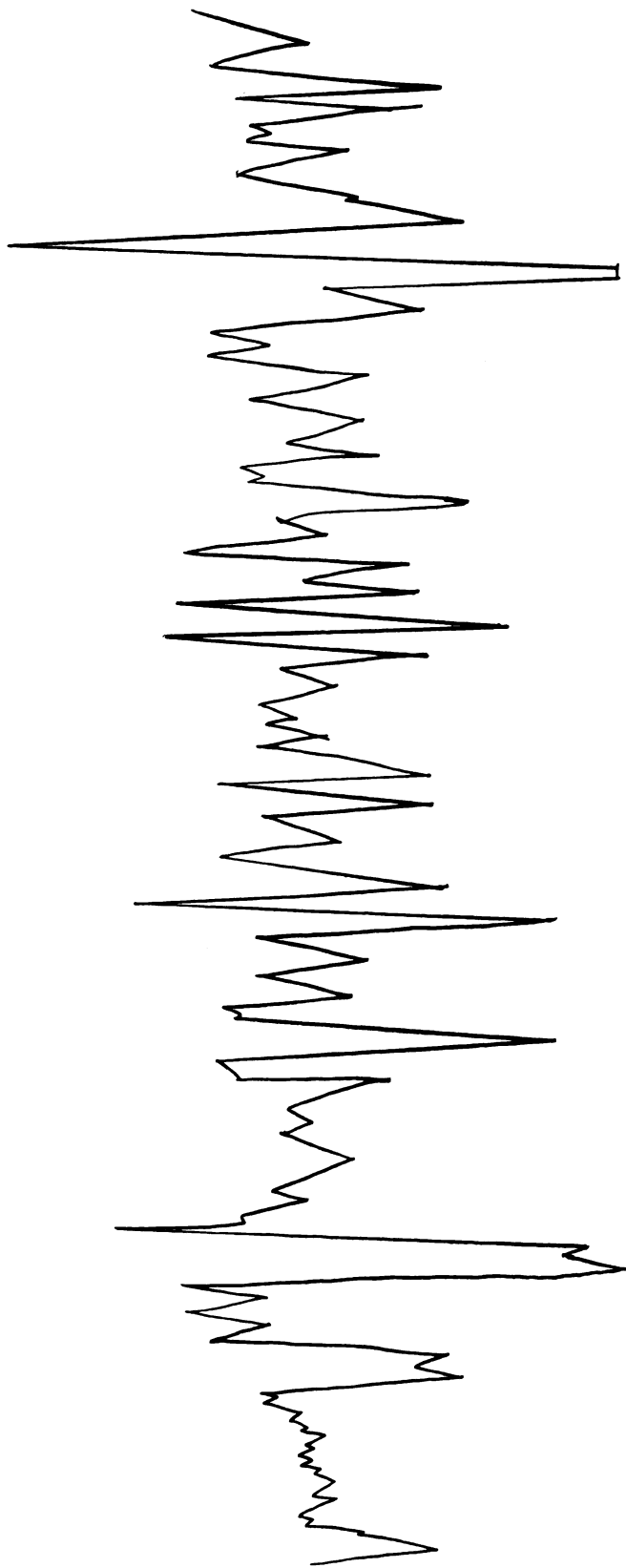


Figure 29. Hyperfine structure observed between $g_{||}$ lines two and three in a frozen CHCl_3 ESR spectrum of copper(II) dibenzoylmethane.

For copper (II) diphenylacetylacetonate a superhyper-fine structure of approximately four gauss was observed on the $A_{||}$ lines in frozen CHCl_3 solution. It was not possible to determine the exact number of lines and relative intensities due to overlapping of the of the sets from each $A_{||}$ copper line (between copper lines two and three thirty lines were observed).

ESR STUDY OF $[\text{Cr}(\text{NO})(\text{NH}_3)_5]\text{Cl}_3$

The ESR spectra of $\text{Cr}(\text{NO})(\text{NH}_3)_5^{+3}$ in an NH_4Cl single crystal are given in Figure 30. From the angular dependence of the spectra it is possible that the condition of $g\beta H \gg D$ is not met. This situation of $D \gg g\beta H$ is discussed in detail by Schulz-Du Bois.¹¹³ The effective g value along the molecular z axis is still g , but the effective g value in the xy plane is approximately 4. This situation is not unusual for Cr^{+3} complexes. In order to obtain precise data one must go to higher klystron frequencies than x-band and higher magnet fields than the 3000 gauss region. A limited amount of information can be obtained by utilizing Schulz-Du Bois' work and looking at the angular dependence at x-band frequencies. However, our main interest in this compound is in the nitrogen hyperfine splittings. Since they were not observed, the spectra were not analyzed further. The ESR spectrum of Mn^{+2} in NH_4Cl has been reported¹¹⁴ and it also has $D \gg g\beta H$.

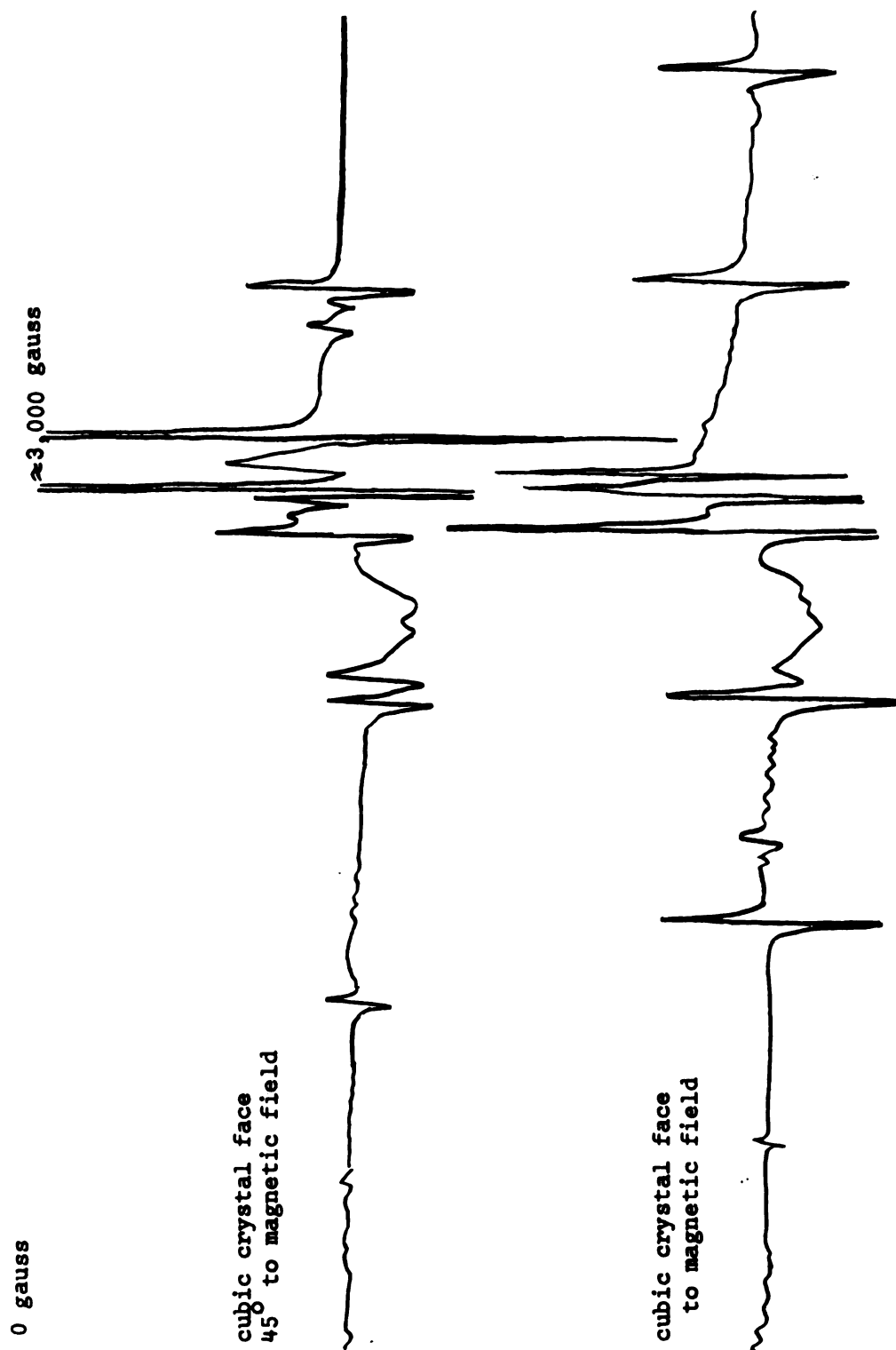
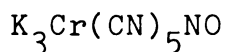


Figure 30. ESR spectra of $\text{Cr}(\text{NO})(\text{NH}_3)_5^{+3}$ in NH_4Cl single crystal.

DISCUSSION



Solution ESR Spectra

There are several possible explanations for the difference in A values of the equatorial and axial carbons. One is axial destabilization of the complex so that the axial cyanide is not held as strongly as the equatorial cyanides. Neither the internuclear distances¹⁰⁹ in $\text{Fe}(\text{CN})_5\text{NO}^{-2}$ nor the rates of cyanide exchange¹⁰⁶ in $\text{Cr}(\text{CN})_5\text{NO}^{-3}$ support this suggestion.

Another possibility is that the unpaired spin density reaches the cyanide π orbitals through the $xy - \pi$ molecular orbital and that the π spin density polarizes the paired s electrons to give the equatorial $A_s^{13\text{C}}$ value while the axial $A_s^{13\text{C}}$ value can only arise from a configuration interaction mechanism of the type given by equation (42). Single crystal work rules out this possibility since the π spin density would only produce an A_s value of 2 gauss (or less) if the ratio of A_p to A_s is similar to that found in organic systems.¹¹⁵ In addition, spin polarization would give A_s a positive value¹¹⁵ while the observed A_s values are negative. It appears that configuration interaction as formulated in equation (46) is the principle mechanism for both the axial and equatorial^{13C} hyperfine splittings. The larger value of the equatorial splitting can be explained by putting the $x^2 - y^2$ energy level below the z^2 energy level since $A_s^{13\text{C}}$ in this mechanism is inversely proportional to the energy difference $E_{(z^2 \text{ or } x^2 - y^2)^*} - E_{(z^2 \text{ or } x^2 - y^2)^b}$.

One cannot estimate the coefficients of the molecular orbitals from equation (46) since the excitation energy for $(x^2-y^2)^b \rightarrow (x^2-y^2)^*$ is not known. The net spin density at the ligand can be calculated from equation (26) (see Table 19.) The nitrogen A_S hyperfine splitting of -5.56 gauss can be accounted for by an explanation similar to that employed for the cyanide hyperfine splittings.

Electronic Configuration and Optical Spectra

Assuming that the $x^2 - y^2$ level can be assigned to a lower energy than the z^2 level on the basis of the isotropic A^{13C} values two possible energy level assignments are given in Table 20. The assignment in Table 20a is supported by the observed charge transfer transitions at $37,000 \text{ cm}^{-1}$ and $44,000 \text{ cm}^{-1}$ which can consistently be assigned as $xy \rightarrow \pi^*(NO)$ and $xz, yz \rightarrow \pi^*(NO)$, respectively, since the difference in energy between these two bands is approximately the observed xz or $yz \rightarrow xy$ energy. The assignment in Table 20b draws support from the ESR g_{\perp} value which can only be reasonably explained by placing the $xy \rightarrow \pi^*(NO)$ charge transfer transition at low energy.

Gray et. al.¹⁶² have recently calculated the energy levels for $Fe(CN)_5NO^{-2}$ and find that the $\pi^*(NO)$ is at low energy. However, their extension to $Fe(CN)_5NO^{-3}$ appears incorrect since the ESR data indicate that the unpaired electron is in the z^2 orbital rather than the $\pi^*(NO)$ as they propose.⁷⁷ The z^2 orbital assignment is supported by the similarity of the anisotropic nitrogen hyperfine splittings¹⁶³ with those found in copper phthalocyanine.¹²⁶ The $^{13C} A$ value of the equatorial cyanides is 10.0 ± 2 gauss.⁷⁷ This is consistent with a z^2 ground state but is too large for an $\pi^*(NO)$ ground state.

TABLE 19. σ orbital spin density (f_s) in sigma ligand orbitals

Atom	$K_3Cr(CN)_5NO$ in H_2O	$K_3VO(CN)_5$ in H_2O	$Na_3Fe(CN)_5NO$ in DMF	$K_3Fe(CN)_6$ in H_2O	$K_3Cr(CN)_6$ in $K_3Co(CN)_6$	K_3CrF_6
Axial	-0.96 ^a	--	+2.8% ^a	--	--	--
Nitrogen	-1.92 ^b	--	+5.6 ^b	--	--	--
Axial	-0.76 ^a	--	--	--	--	--
Carbon	-1.52 ^b	--	--	--	--	--
Equatorial	-1.13 ^a	-1.02 ^a	-0.9 ^a	-1.06 ^a	-2.6 ^a	-0.03 ^a
Atom	-2.26 ^b	-2.04 ^b	-1.8 ^b	-2.12 ^b	-3.2 ^b	--

^aCalculated assuming a pure s orbital.

^bCalculated assuming an sp orbital

TABLE 20a.--Possible energy level assignment for $\text{Cr}(\text{CN})_5\text{NO}^{-3}$

Transition	Theoretical Energy	Observed Energy
xz or $yz \rightarrow x^2 - y^2$	$10Dq + 3Ds - 5Dt + 1715(N_{\pi_1}^2)(N_{\sigma_2}^2) = 22,500 \text{ cm}^{-1}$ $10Dq + 3Ds - 5Dt - 2488(N_{\pi_1}^2)(N_{\sigma_2}^2) = 21,200$	$22,000 \text{ cm}^{-1}$ ---
xz or $yz \rightarrow xy$	$3D_s - 5Dt = 8,300$	---
$xy \rightarrow x^2 - y^2$	$10Dq = 13,700$	13,700
$xy \rightarrow z^2$	$10Dq - 4Ds - 5Dt + 9222(N_{\pi_2}^2)(N_{\sigma_1}^2) = 25,800$	---
xz or $yz \rightarrow z^2$	$10Dq - Ds - 10Dt + (2415)(N_{\pi_1}^2)(N_{\sigma_1}^2) = 30,900$ $10Dq - Ds - 10Dt + (5217)(N_{\pi_1}^2)(N_{\sigma_1}^2) = 31,600$	30,400 ---

Interelectronic repulsion parameters calculated using $F_4 = 71.1 \text{ cm}^{-1}$ and $F_2 = 1056 \text{ cm}^{-1}$ and the equations of Gray and Ballhausen.¹⁶⁴ The values of the terms used are $Ds = 0$, $Dt = -1,660 \text{ cm}^{-1}$, $Dq = 1,370 \text{ cm}^{-1}$, $N_{\pi_2}^2 = .83$, $N_{\sigma_2}^2 = .64$, $N_{\pi_1}^2 \approx .50$ and $N_{\sigma_1}^2 \approx .50$.

TABLE 20b.--Alternate energy level assignment for $\text{Cr}(\text{CN})_5\text{NO}^{-3}$

Transition	Theoretical Energy	Observed Energy
xz or yz \rightarrow $x^2 - y^2$	--	30,400 cm^{-1}
xz or yz \rightarrow xy	--	13,700
xy \rightarrow $x^2 - y^2$	16,400	16,400
xy \rightarrow z^2	--	--
xz or yz \rightarrow z^2	--	--
xy \rightarrow π^* (NO)	--	22,000

$Dq = 1,640 \text{ cm}^{-1}$, Ds and Dt cannot be determined.

Molecular Orbital Coefficients From Single Crystal Data

The experimentally determined hyperfine splittings, A_p , are related to the spin density by equations (14) through (23). Note that $A_\pi = 0$ for nitrogen since $f_{\pi_{xz}} = f_{\pi_{yz}}$. The ligand molecular orbitals chosen are:

$$\phi_{\sigma_2}^* = N_{\sigma_2} [\psi_{x^2 - y^2} - (\lambda_{2s} \psi_{2s})_{13C} - (\lambda_{p_\sigma} \psi_{p_\sigma})_{13C}] \quad (61)$$

$$\phi_{\pi_1} = N_{\pi_1} [\psi_{3d_{xz}} \text{ or } \psi_{3d_{yz}} + (\lambda_{\pi_1} \psi_{p_{\pi N}}) + (\lambda_{\pi_1} \psi_{p_\pi})_{13C}] \quad (62)$$

$$\phi_{\pi_2} = N_{\pi_2} [\psi_{3d_{xy}} + (\lambda_{\pi_2} \psi_{p_\pi})_{13C}] \quad (63)$$

The overlap integrals were estimated by graphical interpolation from the tables of Jaffe and Doak¹¹⁶ using the Z_{eff} values of Hartree¹¹⁷ for carbon and nitrogen atoms.

The values obtained are $S_{2p_{\pi}, 3d} = 0.15$ (Cr-N) and 0.10 (Cr-C); $S_{2p_{\sigma}, 3d_{\sigma}} = 0.20$ (Cr-N) and 0.17 (Cr-C); $S_{2s, 3d_{\sigma}} = 0.10$ (Cr-N) and 0.12 (Cr-C).

For d^5 low-spin complexes the g values are related to the molecular orbitals by equations (29) and (30). These equations were derived for the d^1 case but can be used for d^5 low spin complexes by changing the sign of the spin-orbit coupling constant when the transitions are of the hole type. The value of the spin-orbit coupling constant, λ , for Cr(I) is 212 cm^{-1} .⁶ Since the chromium is already in the low valence state of +1 no correction of the type proposed by Murao⁴⁷ (to account for a reduction in λ due to screening by the partial transfer of the bonding ligand electrons to the metal) was applied.

Estimation of N_{π_2}

A value of $N_{\pi_2} = 0.91$ is obtained from the observed chromium hyperfine splittings (Table 6) by use of equations (24) and (25). Where $A_o = \frac{\beta n \mu_n}{I_n} \langle r^{-3} \rangle = 29$ gauss was computed using $r^{-3} = 2.73 \pm 0.4$ A.U. estimated by the semi-empirical equation of Korol'kov.⁷⁹

From the values of N_{π_2} and $S_{d,\pi}$ (Cr-C) estimated above we obtain $\lambda_{\pi_2} = 0.32$, since $N_{\pi_2} = [1 + 4\lambda_{\pi_2} S_{d,\pi}(\text{Cr-C}) + \lambda_{\pi_2}^2]^{-1}$. The equatorial Cr-C π -covalent bonding is

$$N_{\pi_2}^2 \gamma_{\pi_2}^2 = N_{\pi_2}^2 (\lambda_{\pi_2} - 2S_{d,\pi}(\text{Cr-C}))^2 = 0.012 \quad (64)$$

and so is quite small.

Carbon-Chromium σ -Bonding

The observed value of g_{11} , along with values of $b_2 \rightarrow b_1^* = 13,700 \text{ cm}^{-1}$, $b_1^b \rightarrow b_2$ (charge transfer) = $50,00 \text{ cm}^{-1}$ (approximated). $T(n) = 0.273$ for an s-p hybrid carbon orbital, $S = \frac{\sqrt{3}}{2} (S_{d,s} + S_{d,p_{\sigma}})$, $\lambda_{\sigma} = 1.0$ (by iteration), and the previously estimated constants leads to the value $N_{\sigma_2} = 0.81$ if the

charge transfer correction, equation (22), is used. This is reduced to $N_{\sigma_2} = 0.78$ if the $X_2\Lambda^2$ term of Lacroix and Emch⁵² is used which takes into consideration the spin-orbit coupling constant of the ligand.

The amount of covalent bonding may now be estimated as

$$N_{\sigma_2}^2 \gamma_{\sigma_2}^2 = N_{\sigma_2}^2 [\lambda_{\sigma} - S_{d,\sigma}(\text{Cr-C})] = 0.34 \quad (65)$$

The alternate energy level assignment $b_2 \rightarrow b_1^* = 16,400 \text{ cm}^{-1}$ leads to $N_{\sigma_2} = 0.86$ and $N_{\sigma_2}^2 \gamma_{\sigma_2}^2 = 0.26$. The Cr-C σ -bonds thus have considerable covalent character.

π -Character in the Axial Bonds to Chromium

If it is assumed that the metal d_{xz} and d_{yz} orbitals are involved in π -bonding with nitrogen only, and that charge transfer contributions can be neglected, the amount of electron transfer to the ligand, the π -covalent bonding, is found to be $N_{\pi_1}^2 \gamma_{\pi_1}^2 \approx 0.66$, for the optical assignment $b_2 \rightarrow e = 8,300 \text{ cm}^{-1}$; this value is reduced to ≈ 0.63 if the assignment $b_2 \rightarrow e = 13,700 \text{ cm}^{-1}$ is used.

If only the $xy \rightarrow \pi^*$ (NO) charge transfer correction is considered, $N_{\pi_1}^2 \gamma_{\pi_1}^2 \approx .50$ for the optical assignments $b_2 \rightarrow e = 8,300 \text{ cm}^{-1}$ and $b_2 \rightarrow e(\pi^*) = 37,000 \text{ cm}^{-1}$; but $N_{\pi_1}^2 \gamma_{\pi_1}^2 \approx .35$ for the optical assignments $b_2 \rightarrow e = 13,700 \text{ cm}^{-1}$ and $b_2 \rightarrow e(\pi^*) = 22,000 \text{ cm}^{-1}$. These values qualitatively indicate a highly covalent xz, yz π bond to the nitrosyl nitrogen.

Estimation of Values of A_D

The internuclear distances $^{109}\text{Fe} \cdots \text{N} = 1.63\text{A}^\circ$ and $\text{Fe} - \text{C} = 1.91\text{A}^\circ$ found for $\text{Fe}(\text{CN})_5\text{NO}^{-2}$ should be close to the Cr - N and Cr - C distances in $\text{Cr}(\text{CN})_5\text{NO}^{-3}$. These lead, with equation (17), to the values $A_D^{\text{N}} = 0.47$ gauss and $A_D^{^{13}\text{C}} = 1.06$ gauss.

Unpaired Electron Density on Nitrogen

The observed A_p^N value of + 1.41 is too large to be accounted for by the A_D term alone in equation (14). The anisotropic splitting in excess of the dipolar (A_D) splitting is about + 1 gauss. This can be accounted for by positive spin density in the sigma orbital or negative spin density in the π orbital or the difference between + (-) spin density in the sigma orbital and + (-) spin density in the π orbital if both are appreciable.

The negative spin density in the nitrogen s orbital indicates that the sigma p spin density will also be negative assuming that the sigma orbital is an sp hybrid. With this hybridization we can estimate the contribution of the p part of the sigma orbital to be -0.16 gauss. This value combined with the A_D value of +0.47 gauss and $N_{\pi_2}^2 = 0.83$ leaves a splitting of +1.2 gauss to be accounted for by π spin density. This is a π spin density, f_{π} , of -0.07. Assuming that the spin density arises from configuration interaction Fortman and Hayes¹⁰⁴ have derived an equation similar to equation (46) which accounts for the π spin density.

$$f_{\pi} = - \frac{4 (d_{xy}, d_{xz}) N_{\pi_1}^4 (\lambda_1^N)^2}{3 \quad xz \rightarrow \pi^*(NO)} \quad (66)$$

With the assignment $xz \rightarrow \pi^*(NO) = 45,000 \text{ cm}^{-1}$ (Table 20a), and Fortman and Hayes estimate of $(d_{xy}, d_{xz}) = 3,868 \text{ cm}^{-1}$, one obtains $N_{\pi_1}^4 (\lambda_1^N)^2 = 0.61$ while with $xz \rightarrow \pi^*(NO) = 36,000 \text{ cm}^{-1}$ (Table 20b) one obtains $N_{\pi_1}^4 (\lambda_1^N)^2 = 0.49$. Calculations of this type are not expected to give quantitative estimates of the molecular orbital coefficients. In this light the qualitative agreement between the $N_{\pi_1}^4 (\lambda_1^N)^2$ value (≈ 0.35) obtained from g_{\perp} by the reduction of the spin-orbit coupling constant (equation (30) and the value obtained with equation (66), $N_{\pi_1}^4 (\lambda_1^N)^2 \approx 0.55$ can be interpreted to indicate significant xz and yz chromium - nitrogen π bonding.

Anisotropic ^{13}C Splittings

The equations for the angular dependence of the ^{13}C hyperfine splittings (equations (38), (39), and (40)) indicate that if there is appreciable covalency in the xy π bond such that $|f_{\pi_2 A_p}| \gg |N_{\pi_2 A_D}^2|$ the symmetry will be $A_Z^C \approx A_\sigma^C \neq A_\pi^C$; but if the xy π bond is essentially ionic, $A_Z^C \approx A_\pi^C \neq A_\sigma^C$ since in this case the main contribution to the angular dependence should be $N_{\pi_2 A_D}^2$. In KBr we were not able to determine the axis of symmetry, but in KCl it appears that the A_σ axis is the symmetry axis.

The A_p^C value found with this assignment, $A_p^C = +1.13$ gauss, is consistent with the value calculated for A_D , 1.06 gauss. This interpretation is in agreement with our work on $\text{K}_3\text{Cr}(\text{CN})_6$ where the anisotropic ^{13}C splitting is of the same magnitude as A_D . Fortman and Hayes,¹⁰⁴ in a study of $\text{Cr}(\text{CN})_5\text{NO}^{-3}$ in $\text{K}_3\text{Mn}(\text{CN})_5\text{NO}$, have found that $A_\pi^C \approx A_\sigma^C \neq A_Z^C$. Their analysis indicates that this is due to $f_{\pi_2 A_p}$ being of comparable magnitude to $N_{\pi_2 A_D}^2$.

Using equations similar to (38), (39), and (40) with the assumption that $f_{\pi_1 A_p'} = f_{\sigma_2 A_p'} = 0$ and Marshall's⁷⁵ higher order equations for $N_{\pi_2 A_D}^2$, Fortman and Hayes obtained a p_{xy} spin density (f_{π_2}) of ≈ 0.03 . Equations (38), (39), and (40) allow three separate determinations of $f_{\pi_2 A_p}$. From Fortman and Hayes' analysis one obtains $f_{\pi_2 A_p} = 0.69, 0.96, \text{ and } 1.20$ gauss. The agreement is satisfactory considering the approximations made and the experimental errors; however, if one attempts to further improve the treatment by estimating the $f_{\sigma_2 A_p'}$ contribution from the experimental $f_s A_s'$ and a model of an s-p hybrid orbital, the agreement is lost; and one obtains $f_{\pi_2 A_p} = 1.55, 0, \text{ and } 1.57$ gauss.

Variation of ESR and Infra-Red Data with the Various Alkali Halide Matrices

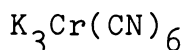
The hyperfine splitting constants and the infra-red frequencies are found to depend on the host lattice. The $[\text{Cr}(\text{CN})_5\text{NO}]^{-3} A_s^N$ values and the NO stretching frequencies for

the complex in KBr and KCl matrices are consistent with the NO group being forced outward (i.e., the C-N distance increased) as the smaller lattice forces the CN-Cr-NO angle from the expected obtuse angle to a more perpendicular one. However, the A_p^N values and the NaCl nitrosyl stretching frequency are inconsistent with this model. The effects of the water molecules of hydration, pellet preparation, and of local charge compensating defects are other possible causes for the variations.

Jones¹²² found that for $K_3Co(CN)_6$ the CN vibration frequencies in various lattices had the values given in Table 21. A stronger metal-carbon σ bond is found to lead to a stronger C-N bond. Therefore, the strongest metal-carbon σ bond is expected in NaCl. The $K_3Cr(CN)_5NO$ data cannot be explained by such a simple model. Further experimentation in this laboratory on other cyanides in alkali halide matrices is planned.

TABLE 21.-- $K_3Co(CN)_6$ vibration frequencies.

Host Lattice			
NaCl	KCl	H ₂ O	Solid $K_3Co(CN)_6$
2145 cm ⁻¹	2127 cm ⁻¹	2127 cm ⁻¹	2150 cm ⁻¹
2140	2119	--	2137
2128	2110	--	2129



Covalent Bonding

The general theory for ¹³C hyperfine splitting in $Cr(CN)_6^{-3}$ was presented on pages 16-17. The value of the overlap integral was estimated by graphical interpolation from the tables of Jaffee and Doak¹¹⁶ and is $S_{3d,2p_\pi} = 0.065$. The internuclear distance used was that of the host lattice

$K_3Co(CN)_6$.¹¹⁸ A_D is calculated to be $0.8N_\pi^2$ gauss using $C = 0.75$.

Using the experimental value of A_p and the calculated value of A_D , we obtain $A_\sigma - A_\pi = A_p - A_D = 0.7 - 0.8N_\pi^2 \approx 0$. The possible error in A_D is such that a quantitative estimate of A_π cannot be made. Qualitatively the results indicate little π bonding in agreement with the analysis by Jones¹¹⁹ of the infrared spectra. McGarvey⁵³ estimates that $N_\pi^2 \approx 0.89$ and that $N_\sigma^2 \approx 0.68$ from the ESR chromium nuclear hyperfine splitting and g value, respectively. From the nephelauxetic ratios^{55,120} one obtains $N_\pi^2 \approx 0.83$ and $N_\sigma^2 \approx 0.72$.

Determination of g_y , D , and E

The energy level equations for Cr^{+3} along the y magnetic axis (see Table 9 for the relationships between y and the crystallographic axes) are:¹¹¹

$$3/2 \text{ to } 1/2 \text{ transition } g_y \beta H = h\nu + D + 3E - \frac{3(D+3E)(E-D)^2}{8(h\nu)^2} \quad (67)$$

$$1/2 \text{ to } -1/2 \text{ transition } g_y \beta H = h\nu - \frac{3(E-D)^2}{4h\nu} \quad (68)$$

$$-1/2 \text{ to } -3/2 \text{ transition } g_y \beta H = h\nu - D - 3E + \frac{3(D+3E)(E-D)^2}{8(h\nu)^2} \quad (69)$$

The experimental values of g_y , D , and E are given in Table 22 along with some literature values. There are two reported room temperature g_y values. The one by Artman et. al.¹²¹ gives a $\frac{\lambda}{\lambda_0}$ value in agreement with expectations. The value reported by Walsh,¹²³ and also found in our crystals, is difficult to explain especially since D and E are either smaller or of the same order of magnitude for our crystals compared to the values for D and E in the crystals for which $g_y = 1.991$. Besides the abnormal temperature effect, Walsh found that the g value first decreased and then increased as the pressure was increased. He postulates that intermolecular

TABLE 22.---Values of ϵ_y , D, and E for $K_3Cr(CN)_6$ in $K_3Co(CN)_6$

	$T = 20^\circ K^{111}$	$T \approx 298^\circ K^{123}$	$T = 298^\circ K^{121}$	$T = 298^\circ K^a$
ϵ_y	1.991 ± 0.001	1.9826 ± 0.0005	1.9912 (two lines seen polytypic crystal)	1.982 ± 0.001
D	0.0831 cm^{-1} ± 0.0010	0.0824 cm^{-1} ± 0.0005	0.07832 0.07866	0.0826 ± 0.001
E	0.0108 cm^{-1} ± 0.0010	0.00765 ± 0.0005	0.009026 0.00970	0.00790 ± 0.001

^aThis investigation.

bond sharing increases as the volume is reduced and that the spin-orbit coupling eventually dominates as the volume becomes smaller. Artman *et. al.*¹²¹ found evidence for polytypism and Raoult¹²⁴ found that aged crystals gave extra ESR lines which were not present in new crystals.

⁵³Cr Hyperfine Splittings

The ⁵³Cr A value varied from 15 to 17 gauss in K₃Cr(CN)₆. Recently McGarvey¹²⁵ observed an anisotropic ⁵³Cr A value in Cr⁺³ acetylacetonate and was able to theoretically account for the anisotropic behavior. He found that the six oxygen atoms surrounding the chromium are distorted from the octahedral configuration by compression along the trigonal axis. Assuming an ionic model he calculated that a distortion of 0.6° in the angle between the trigonal axis and the Cr-O bond was sufficient to account for the anisotropic ⁵³Cr A value. A distortion of this small magnitude would not produce a detectable difference in the resulting non-equivalent ¹³C A values.

ESR STUDIES OF COPPER GLYCINATE

The single crystal, solution, and powder data are given in Table 16. The powder data and single crystal data are in agreement. Solution spectra are not expected to agree since copper glycinate is only soluble in highly polar solvents which can coordinate along the z axis and change the hyperfine splitting constant by as much as ≈ 40%.

Using equations (11) through (28) with A_D = 0.25 gauss one obtains the values of the s and p spin density f_s and f_p, respectively, given in Table 23. The literature data for several other copper complexes are included in Table 23 for comparison purposes. The f'_s and f'_σ values were calculated with the assumption that the σ bond is an sp² hybrid. If this assumption is correct, f'_s should equal f'_σ.

TABLE 23.--Comparison of ligand spin densities for copper complexes.

	A_{II}^a	A_{I}^a	A_S^a	A_p^a	A_D^a	A_o^a	f_s	f_σ	f'_s	f'_σ
Cu glycinate	10.4 ^b	6.8 ^b	8.0	1.2	.25	.95	.0146	.056	.044	.084
Cu phthalocyanine	18.6 ^c	14.2 ^c	15.7	1.47	.33	1.14	.0286	.067	.086	.100
Cu(PyH) ₄ (NO ₃) ₂	16.4 ^d	12.1 ^d	13.5	1.4	.31	1.1	.0246	.065	.074	.0975
Cu(PyH) ₄ (Ts) ₂	13.7 ^d	10.5 ^d	11.6	1.1	.22	0.9	.021	.053	.063	.0795
Cu(PyCH ₃) ₄ (Ts) ₂	14.1 ^d	11.7 ^d	12.5	0.8	.14	.66	.023	.039	.069	.0585
Cu(PyN(CH ₃) ₂) ₄ (Ts) ₂	15.7 ^d	11.7 ^d	13.0	1.3	.28	1.0	.024	.059	.072	.0885
Cu(PyCN) ₆ (ClO ₄) ₂	14.0 ^d	10.5 ^d	11.7	1.2	.25	.95	.021	.056	.063	.084

The symbols following Py in the bracket are the substituents in the 4-position of the pyridine, Ts = paratoluenesulfonic acid anion. Py = pyridine.

^aIn gauss.

^bThis work.

^cReference 126.

^dReference 127.

SOLUTION SPECTRA OF SUBSTITUTED
COPPER ACETYLACETONATES

For the spectrum of a copper (II) complex taken in solution the isotropic nuclear hyperfine splitting \underline{A} has been related to the covalency of the unpaired electron by the equation:

$$A = A_o(-N_o^2 K_o + g-2.0023 + \text{smaller terms}) \quad (70)$$

where N_o^2 is the fraction of time the unpaired electron is on the copper atom, $A_o = \frac{\mu_n \beta_n}{I_n} \left\langle \frac{1}{r^3} \right\rangle$, and K_o is the Fermi contact term due to spin unpairing in the copper s orbitals. In this equation K_o is assumed constant but if this assumption is not justified, the value of \underline{A} will also be influenced by any change in position of the copper d electron energy levels such that the amount of unpaired s electron character at the nucleus changes. For copper complexes K_o is usually considered to be constant and the above equation is considered to be applicable.^{128,129,130}

The ESR \underline{A} values for the substituted copper acetylacetonates decrease with change of substituent in the same manner that the hydroxyl proton NMR chemical shift decreases for the corresponding enol tautomer,¹³¹ with the exception of the phenyl and thenoyl substituents (see Table 24). Here ring current effects might be expected to alter the NMR values. Both sets of data would give the order of electronegativity $CF_3 > Cl > H > CH_3$. If it is assumed that conjugation of the phenyl and thenoyl groups with the Cu-O bond is not important the ESR data would give these groups an electronegativity greater than that of methyl, in agreement with the conclusions from NMR studies. However, Nakamoto et. al.¹³² reported on the basis of some infrared data that phenyl substitution increased the Cu-O bond strength relative to methyl and suggested that release of electrons to oxygen by phenyl would increase the Cu-O π -bonding. They also cited some stability constant data¹³³

TABLE 24.--ESR hyperfine splitting constants and other data for copper acetylacetonates.^a

R'	Substituents R'' R	ESR A Value 10^4 cm^{-1}	g Value	Half- Wave Potential 135	Cu-O Stretching Frequency 135	Cu-O Force Constant 132	NMR Proton Chemical Shift#	Cu Che- late Sta- bility Constant*	MO Co- effi- cient N_0^2
CH ₃	CH ₃ CH ₃	78.5 ± 0.5	2.121	-0.559	--	--	990	--	.784
CH ₃	H CH ₃	77.2 ± 0.5	2.123	-0.487	455 cm^{-1}	2.20	934	9.73	.779
CH ₃	Cl CH ₃	76	--	--	--	--	922	--	--
Phenyl	H CH ₃	76.4 ± 0.5	2.124	-0.384	458	--	980	9.68	.777
Phenyl	H Phenyl	75.3 ± 1.0	2.124	-0.376	462	2.31	1020	9.63	.770
CF ₃	H CH ₃	72.5 ± 0.7	2.129	-0.173	445	--	847	6.59	.763
CF ₃	H Thenoyl	71.6 ± 0.7	2.131	-0.155	--	--	898	6.55	.763
CF ₃	H CF ₃	54.7 ± 1.0	2.150	+0.040	415	1.75	780	2.70	.698

^aThe substituted acetylacetonate is R'CO-CR''-CR'''O.

^bDetermined from equation (70) with a constant K_0 , see Table 18.

* Log K^{136} .

Reference 131.

to support this order of electronegativities but these appear inconclusive since some of the data for diphenylacetylacetonates could not be repeated.¹³⁴ Also steric interactions between phenyl and the α -hydrogen would be expected to reduce the importance of π -bonding.

The N_{σ}^2 values given in Table 24 indicate that the more electronegative the substituent the greater the covalency. This conclusion is not supported by either the polarographic reduction investigation¹³⁵ or the correlation between the stability constants and the basicity of the pure ligands.¹³⁷¹³² The polarographic reduction data were interpreted to indicate that a more negative value of the half-wave potential is evidence for a more covalent bond. This interpretation was supported by the similarity between the half-wave potentials for copper hexafluoroacetylacetonate and copper nitrate. The correlation between the stability constants and the basicity of the pure ligands indicates that electron withdrawing substituents tend to withdraw the bonding oxygen electrons and so decrease the amount of ligand-to-metal electron donation.

It therefore appears that equation (70) cannot be used with a constant K_{σ} to calculate N_{σ}^2 as has been previously assumed. This conclusion is not completely startling as earlier papers on the ESR of copper complexes have indicated that, although the g values were following the expected trend (a g value nearer 2.0023 qualitatively indicates a greater covalency) the A values seemed to be increasing with greater covalency rather than decreasing as expected.^{138,129,139} The consistent trend in the substituted acetylacetonate A values can be explained by considering that K_{σ} consists of two contributions: ^{63,66,26} a negative contribution which arises from the exchange polarization of the electron spin in filled s -orbitals and a positive contribution which arises from unpaired s electron density in the $4s$ copper orbital. Since the experimental A value is negative, an increase in $|A|$ can be explained by an increase in the relative importance

of the negative exchange polarization term over the positive 4s population contribution. There is strong evidence⁶¹ for Mn^{+2} , in which the 4s contribution appears negligible, that the exchange polarization contribution is dependent upon the covalency of the complex. The 4s contribution should have a dependence on both the covalency and the separation between the ground state and the excited 4s level. Because of this dependency of the 4s term on an additional parameter besides covalency it is possible for the relative contribution of the two terms to change, as appears to have occurred in this series, such that the absolute magnitude of the A value actually increases with covalency.

A surprising correlation can be made between solvent effects and substituent effects. A plot of g versus A values is given in Figure 31 for a series of substituted copper acetylacetonates in chloroform solution (circles) and the relationship is seen to be nearly linear. The points for copper acetylacetonate in various solvents (triangles) appear to obey the same relationship and it therefore appears that increasing the basicity of the solvent has the same effect on the d-electron energy levels and on the unpaired electron density on copper as does increasing the electronegativity of the substituents on the ligand. The similarity in ESR parameters for copper hexafluoroacetylacetonate in chloroform solution and for copper acetylacetonate in pyridine solution is also consistent with the similarity between their low-energy optical absorption spectra.^{140,141}

Further evidence that reliable N_{σ}^2 values cannot be obtained from equation (70) when K_0 is constant comes from an ESR study of nitrogen and copper splittings in copper complexes in which there are copper-nitrogen bonds. Thus we may compare copper phthalocyanine and copper glycinate. The former is considered to be highly covalent while the latter should be reasonably ionic. In addition the copper-nitrogen bond lengths for both have been reported.^{126,142} The ESR data and bond lengths are given in Table 25. A smaller copper A value, interpreted with a constant K_0 in equation (70)

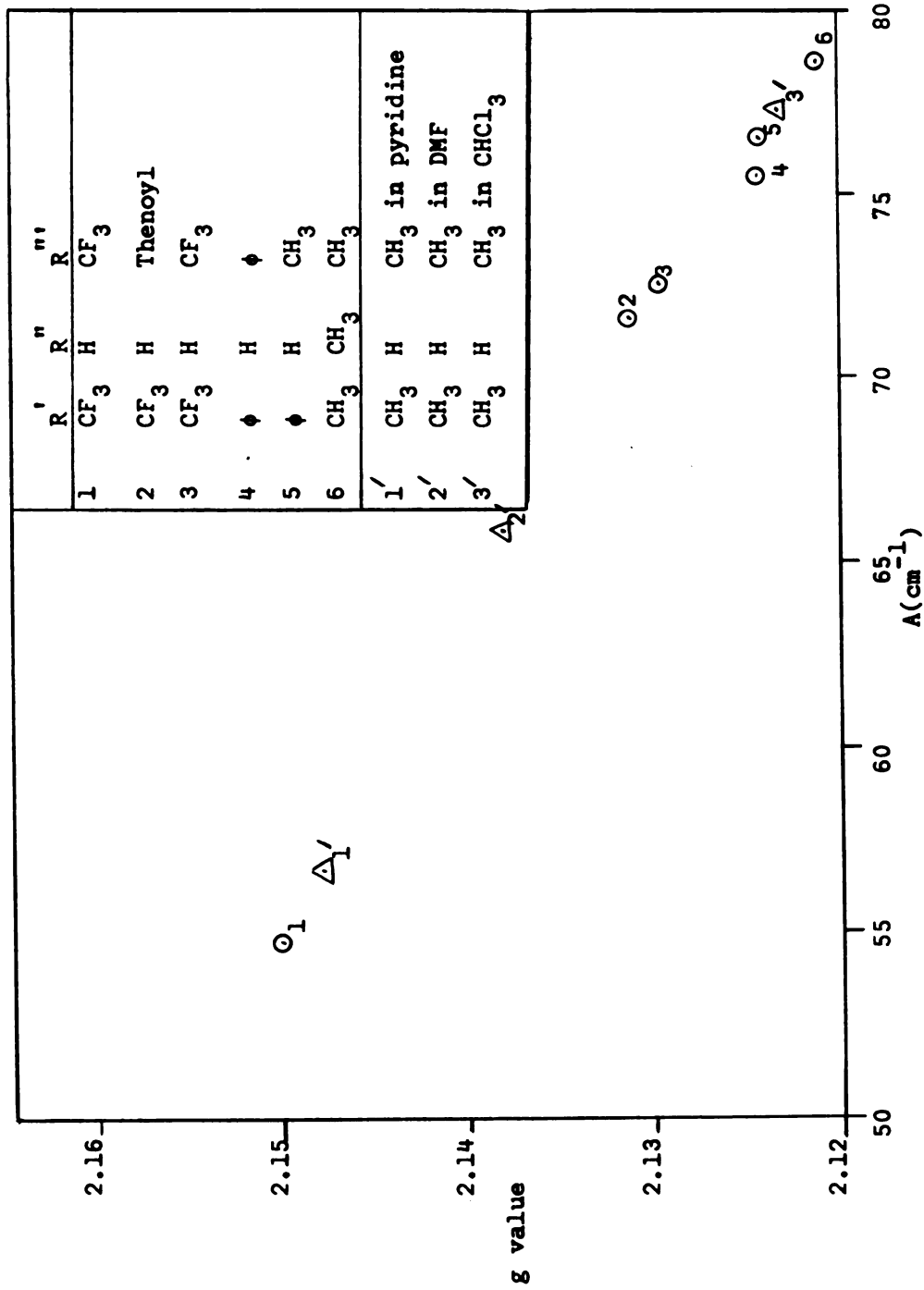


Figure 31. Solvent and substituent effects on copper(II)acetylacetonates.

TABLE 25.--Comparison of copper (II) phthalocyanine and copper (II) glycinate ESR data.

	Cu Phthalocyanine ¹²⁶	Cu Glycinate
g_{\parallel}	2.179	2.267 ± 0.002
g_{\perp}	2.050	2.055 ± 0.003
$A_{\parallel}^{\text{Cu}}$	$202 \times 10^{-4} \text{ cm}^{-1}$	$141 \pm 1.5 \times 10^{-4} \text{ cm}^{-1}$
A_{\perp}^{Cu}	19×10^{-4}	--
A_{\parallel}^{N}	17.8×10^{-4}	$10.0 \pm 0.5 \times 10^{-4}$
A_{\perp}^{N}	14.5×10^{-4}	7.2×10^{-4}
$A_{\text{isotropic}}^{\text{N}}$	15.6×10^{-4}	8.1×10^{-4}
A_{P}^{N}	1.1×10^{-4}	0.9×10^{-4}
Cu-N Distance	1.83 \AA°	$1.984 \text{ and } 2.021 \text{ \AA}^{\circ}$ 142
N_{σ}^2	0.80 ^a	0.72 ^a

^aCalculated from equation 8, reference 129, see also reference 165.

indicates that the unpaired electron should be spending more time on the nitrogen; and therefore, one would expect a larger nitrogen A value for the copper complex with the smaller copper A value which is not what is found. The relative magnitudes of the nitrogen splittings are in agreement with the reported copper-nitrogen bond distances so that again it appears that the use of equation (70) with a single constant value of K_0 leads to contradictory conclusions and so is unjustified.

The anisotropic A values give the correct order of covalency, see Table 18.

SOLUTION SPECTRA OF SUBSTITUTED VANADYL ACETYLACETONATES

The ESR A values are given in Table 11 for a series of substituted vanadyl acetylacetonates. The A values increase as the substituents become more electronegative and also as the solvent (which can coordinate in the sixth position) becomes less basic with the exception of the phenyl substituted acetylacetonates. The behavior of the phenyl substituted complexes is difficult to explain since it is not consistent in the different solvents used. Either a steric effect or an inductive π effect could cause such a behavior if the solvent DMF sufficiently weakened the metal-ligand bonds such that the steric effect or inductive π effect were no longer important. An infrared study of the metal - ligand stretching frequencies for vanadyl acetylacetonate in various solvents has shown that the more basic the solvent the weaker the metal-ligand bond.¹⁴³

The substituent behavior is opposite to the behavior found for the substituted copper acetylacetonates. This is in agreement with the earlier results of Faber and Rogers¹³⁸ on the effects of complexation by a series of ion exchange resins with copper (II) and vanadyl (see Table 26).

The vanadyl trend is that expected from covalency considerations since a larger A value normally indicates a

TABLE 26.--ESR A values for Cu^{+2} and VO^{+2} adsorbed on ion exchange resins.¹³⁸

Adsorbent	VO^{+2} A_{\parallel} (in gauss)	Cu^{+2} A_{\parallel} (in gauss)
IR-100	200	110
Dowex-50	210	115
Charcoal	190	140
IR-4B	175	180

more ionic bond. The solvent effect data, if interpreted similarly, would indicate that the more basic the solvent the greater the ligand-metal covalency. Since the infrared data indicate that the more basic the solvent the weaker the ligand-metal bond, one is led to the conclusion that vanadyl ion prefers (forms stronger) ionic bonds to (than) covalent bonds. This is supported by the limited amount of stability constant data available.¹⁴⁴ Vanadyl oxalate has a higher stability constant than vanadyl acetylacetonate¹⁴⁶ and vanadyl fluoride is more stable than vanadyl chloride.¹⁴⁴ It appears that vanadyl with the electron configuration d^1 is not easily polarized and therefore prefers ionic bonds.

Although the explanation for the change in A values with substituent based on the covalent character of the metal-ligand bonds is plausible, Kivelson and Lee⁷² have suggested that the major dependence of A is on the amount of $4s$ character in the ground state rather than on covalency. The correlation of the optical and ESR spectra, in the following section, gives support to this explanation although it is still possible for the correlation to hold if both the ESR A values and the positions of the optical bonds have a similar dependence on covalency.

In DMF, after sitting for several months, decomposition was detected by the appearance of a second set of lines in the

solution ESR spectra for vanadyl acetylacetonate, vanadyl bisbenzoylacetonate, and vanadyl dibenzoylmethanate. The second set of peaks have a smaller A value than the original set. In the next section this behavior is found to be consistent with the formation of a mixed DMF, acetylacetonate complex of symmetry lower than C_{2v} .

CORRELATION OF OPTICAL SPECTRA WITH THE ESR A VALUES

For a series of vanadyl complexes, Table 27, a linear correlation was found between the ratio of the axial to equatorial crystal field, ρ , (see equations (55) and (56) and the corresponding ESR A values as shown in Figure 32. This correlation serves as evidence that the optical assignments utilized are correct. Of special significance are: (1) the extrapolation to the $VO\text{SO}_4$ in H_2O case indicates that a previous theoretical Wolfsberg-Helmholz calculation of the energy levels¹⁴⁵ is incorrect and (2) the resolving of the question as to whether the highest energy transition is a charge transfer or a d-d transition.¹⁶⁰

With the use of equations (57), (58), and (59) along with the assumption that the ratio of σ_x to π_x in VOX_5 is the same as for the corresponding ligand in $Co(III)$, it is possible to determine the σ and π field strength of the various ligands, see Table 28. The assumption probably overemphasizes the role of equatorial π bonding and underemphasizes the role of axial π bonding since the xz and yz π bonding is currently thought to be axially directed.¹⁶⁸ By comparing the σ_y and π_y values for the vanadyl oxygen atom with the corresponding values of O^{-2} in Co^{+3} compounds¹⁰ (where $\sigma_y = 39,000\text{ cm}^{-1}$ and $\pi_y = 24,000\text{ cm}^{-1}$) it appears that the sigma metal-ligand bonds are of approximately equal strength, but the π bond is considerably stronger in the vanadyl complexes than in the Co^{+3} complexes.

TABLE 27.--Energy levels, hyperfine splittings, and ρ values for vanadyl complexes.

Compound	No. in Fig. 32	Assignment of Optical Transition				ρ	A
		$xy \rightarrow xz, yz$	$xy \rightarrow x^2 - y^2$	$xy \rightarrow z^2$	$xy \rightarrow z^2$		
$VO(CN)_5^{-3}$ in H_2O^{93}	--	--	--	--	1.39	79.9 gauss	
$VO(AcAc)_2$ in CH_3OH	1	13,000 cm^{-1} *	17,450 cm^{-1} *	25,600 cm^{-1} *	.210	102.3 ¹⁵⁰	
$VO(AcAc)_2$ in DMF	2	13,000*	17,000*	25,100*	.185	104.6 ⁹³	
$VO(NCS)_5^{-3}$	3	13,500 ^a	17,200 ^a	23,900 ^a	.145	104.5 ⁹³	
$VO(AcAc)_2$ in CH_3CN	4	14,200*	16,800*	25,800*	.113	105.3 ¹⁵⁰	
$VO(AcAc)_2$ in CH_3COCH_3	5	14,300 ¹⁵⁰	16,700 ¹⁵⁰	25,600 ¹⁵⁰	.088	106.0 ¹⁵⁰	
$VO(AcAc)_2$ in $CHCl_3$	6	14,900*	16,900*	26,000*	.041	106.9 ⁷³	

TABLE 27. --(Continued).

Compound	No. in Fig. 32	Assignment of Optical Transition			ρ	A
		$xy \rightarrow xz, yz$	$xy \rightarrow x^2 - y^2$	$xy \rightarrow z^2$		
VO(Oxalate) ₂ in DMSO ⁹³	7	12,400	16,000	22,900	.046	106.9
VOCl ₅ ^b	8	15,500	16,200	26,000	-.006	109.4
VO(AcAc) ₂ in C ₆ H ₆ ⁹³	9	15,300*	16,900*	25,700*	-.030	108.3 ⁹³
VO(CF ₃ AcAc) ₂ in Benzene ⁹³	10	14,700	16,800	23,500	-.102	110.4
VO(CF ₃ CF ₃ AcAc) ₂ in CHCl ₃ ⁹³	11	13,400	16,200	20,700	-.240	112.6
VOSO ₄ in DMF ⁹³	12	12,600	15,200	18,000	-.382	114.6
VOF ₅ ^c	13	13,300	14,100	18,200	-.450	116.0
VOSO ₄ in Dilute H ₂ SO ₄	--	(13,230)		16,200	--	116

^aOptical spectrum in CH₃CN, Ref. 97; ESR in DMF.

^bOptical spectrum in K₃TlCl₅·2H₂O, Ref. 160; ESR in (NH₄)₂ [InCl₅·H₂O], Ref. 151.

^cOptical data in KBr pellet, Ref. 161, ESR in HF, H₂O, Ref 93.

* Reference 81.

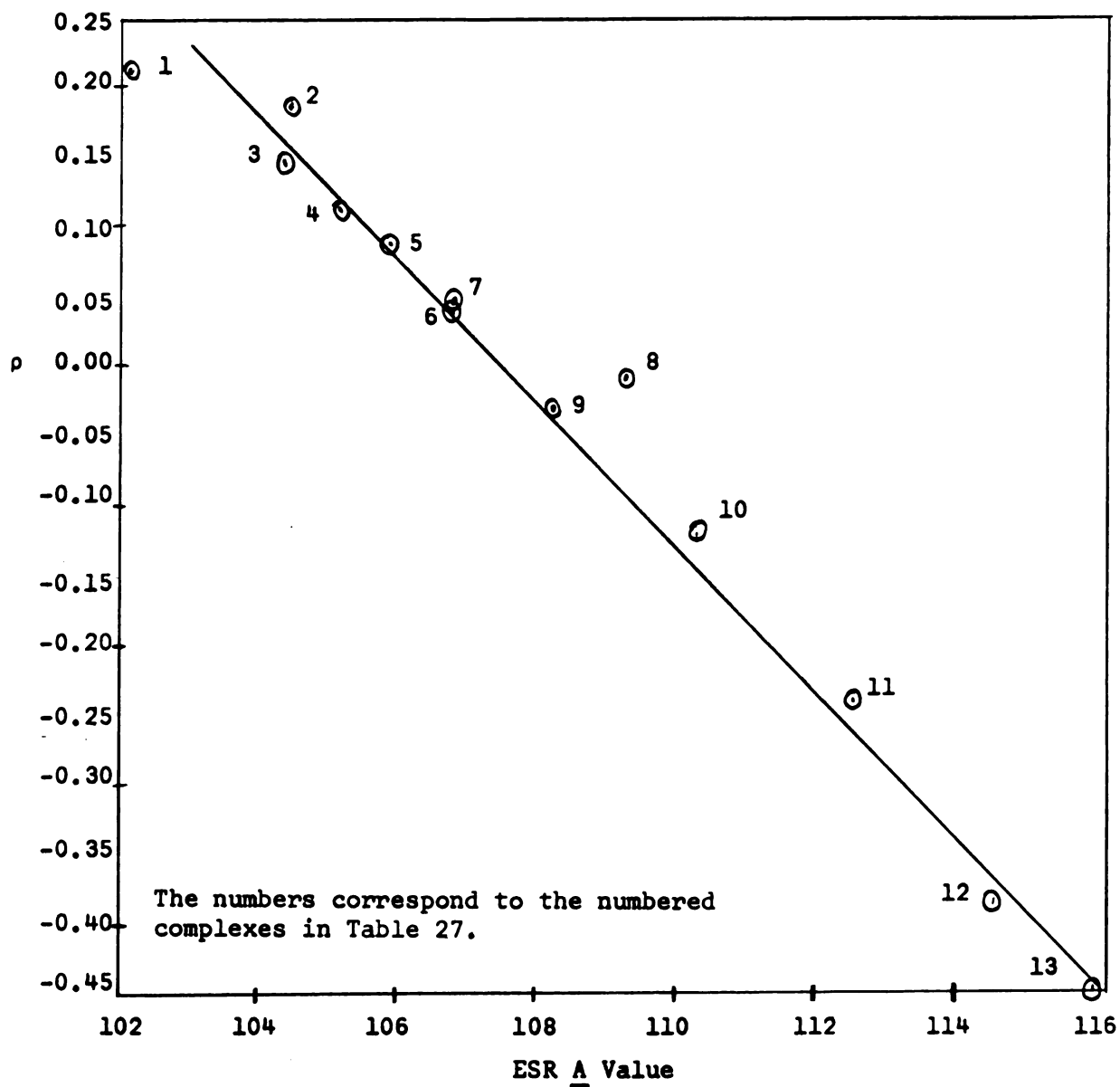


Figure 32. Correlation of ratio of axial to equatorial crystal field, ρ , and ESR A values for a number of vanadyl complexes.

TABLE 28.-- σ and π electrostatic interactions for VYX_5 Compounds

Compound	σ_x	π_x	σ_y	π_y
$VO(NCS)_5^{-3}$	29,480 cm^{-1}	12,280 cm^{-1}	43,580 cm^{-1}	66,280 cm^{-1}
VOF_5^{-3}	22,920	8,820	35,220	62,020
$VOSO_4$	23,540 ^a	7,540 ^a	107,540 ^a	59,540 ^a

^aUsing optical assignment of reference 145.

The correlation cannot be extended to include complexes of lower symmetry than C_{2v} . It appears that as in the copper (II) case, there are two contributions to the hyperfine splitting, a negative contribution from the polarization of filled s orbitals and a positive contribution due to some 4s character. In order for the 4s contribution to be appreciable the symmetry must be lower than C_{2v} since the only vanadium d orbital which can admix with the 4s in C_{2v} or C_{4v} is the d_{z^2} orbital.⁶⁵ This theory is consistent with the available solution data. For vanadyl oxalate in H_2O , with no excess ligand present, a second set of ESR peaks slowly grows with an A value of 90 gauss while the original peaks have an A value of 106.6 gauss. Since there is nothing in the solution which can form a more covalent bond than the oxalate, a higher covalency cannot be used as the explanation for the lower A value. As a check of this interpretation the ESR spectra of several known low-symmetry complexes¹⁴⁷ were obtained. The A values for the tartrate, lactate, malate, and mandelate vanadyl complexes in basic solution were all within the range of 88 to 90 gauss. Also, vanadyl glycinate (in which the glycinate is a chelate ligand with one vanadium-nitrogen and one vanadium-oxygen bond) has an ESR A value of 99.2 ± 1 gauss.⁹³

This explanation of a positive 4s contribution and a negative polarization contribution has been used to account

for the unusually low ESR \underline{A} value, 27.4 gauss, found for $V(C_5H_5)_2$ (bis-cyclopentadienyl vanadium) in benzene.¹⁴⁸ The largely ionic complex $V(NH_4)_2(SO_4)_2 \cdot 6H_2O$ has an \underline{A} value of 94 gauss.¹⁴⁹ The $V(C_5H_5)_2$ case is particularly interesting because proton nuclear magnetic resonance spectra have shown that the electron spin density on each carbon atom is 0.009. This gives a total spin density on the ligands of 0.9. Since the total spin density in the complex is 3 electrons the maximum value of the covalency is 30%. Taking into account the large metal-ligand orbital overlap would decrease this quantity so that it appears that this compound does not have an abnormally high covalency as would be predicted from the small value of the vanadium ESR \underline{A} value.

In Table 29 the published ESR data for $[VS_6C_6(CN)_6]^{-2}$ are compared with the data for $VO(CN)_5^{-3}$. The g values are the same within experimental error, and $A_{||}$ is greater than A_{\perp} for both compounds. On the basis of the low \underline{A} value, $g_{\perp} > g_{||}$, and $A_{||} > A_{\perp}$, and with the assumption of trigonal symmetry, Davison et. al.⁶⁵ suggested that the unpaired electron is in a molecular orbital which is mainly ligand in character since for trigonal symmetry one predicts that $A_{\perp} > A_{||}$ and $g_{||} > g_{\perp}$. The similarity of their data to the data for $VO(CN)_5^{-3}$ suggests that their symmetry is actually distorted tetragonal. The low \underline{A} value can then be explained by the admixture of 4s character rather than an abnormal amount of covalency.

ESR SPECTRA OF VANADYL COMPLEXES

The ESR data for a series of vanadyl complexes, including the anisotropic hyperfine splitting constants, are shown in Table 13. These values can be compared with the previously published ESR data collected in Table 30. A plot of the $g_{||}$ values versus the $A_{||}$ values is given in Figure 33; within the average experimental error of ± 0.005 for the $g_{||}$ values, there appears to be a linear correlation between the $A_{||}$ and $g_{||}$ values for complexes with tetragonal symmetry. With this assumption,

TABLE 29.--Comparison of the ESR data for $\text{VO}(\text{CN})_5^{-3}$ and $[\text{VS}_6\text{C}_6(\text{CN})_6]^{-2}$

	g	$g_{ }$	g_{\perp}	A	$A_{ }$	A_{\perp}
$\text{VS}_6\text{C}_6(\text{CN})_6^{-2}$	1.980	1.974	(1.983)	63.3	100	45
$\text{VO}(\text{CN})_5^{-3}$	1.983	1.972	1.984	79.9	149	51

the $A_{||}$ values could be used to estimate the $g_{||}$ values for additional complexes and possibly give a more accurate value of $g_{||}$ for the complexes in Table 13. This correlation is surprising since the principle dependence of $A_{||}$ is on $N_{\pi 2}^2$ (see equation (35)) while the principle dependence of $g_{||}$ is on

$$\frac{N_{\pi 2}^2 N_{\sigma 2}^2}{\Delta b_{\perp} b_{||}} \quad (\text{see equation (29)})$$

The overlap integrals for some vanadyl complexes are given in Table 31. The relative magnitudes of these overlap integrals should give an approximate indication of the relative magnitudes of the covalency in the bonds involved.

SOLUTION SPECTRA OF COPPER (II) AMINO ACID COMPLEXES

The isotropic ESR A values and some literature data for comparison are given for a series of copper (II) amino acid complexes in Table 32. Using the results of the substituted copper acetylacetonate series as a model, one would predict that the more basic the amino acid, the larger the ESR A value of the corresponding complex, the more stable the complex, and the greater the covalency. There does appear to be a general overall correlation between the basicity of the ligands as measured by the ligand proton dissociation constants and the A values but the correlation does not hold for all of the

TABLE 30.--Literature ESR A values for VO^{+2} complexes.

Compound	A(in gauss)	A_{\parallel} (in gauss)	A_{\perp} (in gauss)
$\text{VO}(\text{porphyrin})^{72}$	96 to 98	173 to 176	56 to 60
$\text{VO}(\text{acetylacetonate})_2^{72,150}$	102 to 108	181 to 191	64 to 69
$\text{VO}(\text{H}_2\text{O})_5^{+2}$	116, 118 120, 116.6	-- --	-- --
$\text{VO}(\text{C}_2\text{O}_4)^{-2}$ ¹¹²	(103)	180 ± 2	65 ± 2
VO^{+4} in amorphous GeO_2 ⁷⁸	(114.2)	194.8 ± 0.1	73.9 ± 0.1
VO^{+4} in tetragonal GeO_2 ⁷⁸	-- --	146.66 ± 0.02	40.90 ± 0.01 (x axis) and 41.854 ± 0.01 (y axis)
VO^{+4} in IR 100 ¹³⁸	--	200	81
Dowex 50	--	210	80
Charcoal	--	190	76
IR 4B	--	175	66
VO^{+4} in $\text{Zn}(\text{NH}_4)_2(\text{SO}_4)_2$ ¹⁵³	-- -- -- --	202.54 -- 202.63 --	$71.15(\text{x axis})$ $78.49(\text{y axis})$ $76.81(\text{x axis})$ $78.49(\text{y axis})$
VOF_2 ¹⁵²	116 ± 3	--	--
VOCl_2 ¹⁵²	--	202 ± 10	76 ± 5
VOCl_5^{-3} ¹⁵¹	(109.4)	173.0	77.6

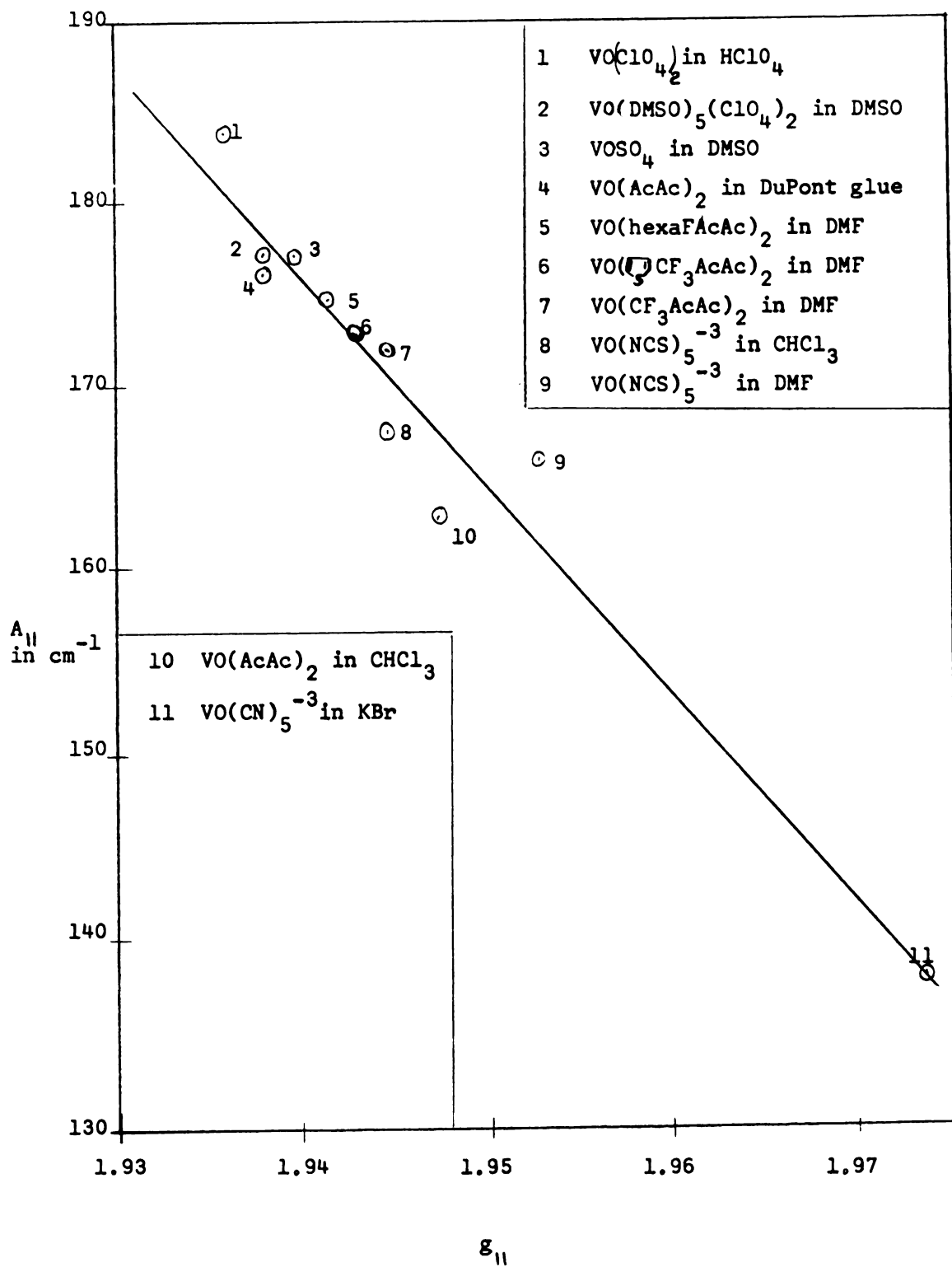


Figure 33. Plot of $A_{||}$ versus $g_{||}$ for a number of vanadyl complexes.

TABLE 31.--Group overlap integrals for some vanadyl complexes.

	$\text{VO}(\text{H}_2\text{O})_5^{+2}$	$\text{VO}(\text{NCS})_5^{-3}$	$\text{VO}(\text{AcAc})_2$	$\text{VO}(\text{CN})_5^{-3}$
V = O Distance (A°)	1.67 ^a	1.62 ^a	1.59 ^a	1.75 ^b
V-ligand Distance (A°)	2.3 ^a	2.04 ^a	1.97 ^a	≈ 1.91
S_{σ_2}	0.168	0.22	0.249	0.284
S_{π_2}	0.056	0.132	0.124	0.26
S_{π_1}	0.124	0.139	0.148	0.105

^aSee Ref. 154.

^bEstimated from infrared data, Ref. 97.

compounds in the series. There appears to be no correlation between the stability constants and the A values; however, there is a correlation between the A values and the separation between the COO stretching frequencies. According to Nakamoto's model,¹⁵⁹ increased covalent character leads to a more asymmetrical carboxyl group and hence to an increase in the frequency separation of the two bands.

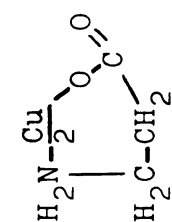
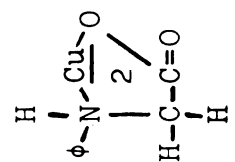
From the available data it appears that the ESR A value increases with increasing covalency, but that the stability of the complexes is dependent upon an additional factor which does not proportionally affect the ESR A value. Irving and Pettit¹⁵⁵ noted the discrepancy between the basicity of the ligands and the stability constants of the complexes and suggested that the discrepancy is probably due to steric effects. This explanation is consistent with the ESR behavior of the bipyridyl complex, see Table 18, which does not follow the smooth correlation which is obtained for the substituted acetylacetonates.

TABLE 32.---ESR data and literature data for copper amine acid complexes.

R	R	ESR \bar{A} Value	Stability Constant (log K_{ML}^2) ¹⁵⁵	Ligand Nitrogen		Ligand Nitrogen Proton Dissociation Constant ¹⁵⁶	Log $K_1 K_2$ ¹³⁶	Cu-N Force Constant	Separation between the COO groups		Metal-Nitrogen Stretching Frequency
				Ligand Carboxyl Proton Dissociation Constant ¹⁵⁶	Ligand Nitrogen Proton Dissociation Constant ¹⁵⁶				Stretching Frequency	Stretching Frequency	
H	$\begin{array}{c} \text{H} \\ \\ \text{CH}_3 - \text{C} - \text{CH}_3 \\ \\ \text{H} \end{array}$	71.8	2.32	9.62	15.1	0.50 ¹⁵⁸	394 cm^{-1}	158			
H	$\begin{array}{c} \text{H} \\ \\ \text{CH}_2 - \text{CH}_3 \end{array}$	71.8	--	--	--	--	--	--	--	--	
CH ₃	CH ₃	71.2	6.84	--	--	--	--	--	--	--	
H	CH ₂ OH	71.0	2.21	9.15	14.6	--	--	--	--	--	
H	$\begin{array}{c} \text{H} \\ \\ \text{CH}_3 - \text{C} - \text{C}_2\text{H}_5 \\ \\ \text{H} \end{array}$	70.0	2.26	9.62	--	--	235 cm^{-1}	--	--	--	

TABLE 32.--(Continued).

R	R'	ESR \bar{A} Value	Stability Constant (log K_{ML_2}) ¹⁵⁵	Ligand Carboxyl Proton Dissociation Constant ¹⁵⁶	Ligand Nitrogen Proton Dissociation Constant ¹⁵⁶	Log K_1 K_2 ¹³⁶	Cu-N Force Constant	Separation between the COO Stretching Frequencies ^a	Metal-Nitrogen Stretching Frequency
H	CH ₃	69.6	6.78	2.34	9.69	15.1	--	220	--
H	H	68.8	6.91	2.34	9.60	15.4	0.62 ¹⁵⁷	206	275 ^b 332 ^c
		68.6	--	1.83	9.13	--	--	--	--
		51.0	--	3.60	10.19	--	--	161	--



^aIn hydrated crystal. ¹⁵⁹ ^bWhen nitrogen are cis to each other. ¹⁵⁷
^cWhen nitrogens are trans. ¹⁵⁷

For comparison the solution ESR A values and stability constants for some copper (II) amine complexes are given in Table 33. For the bidentate ligands a higher A value corresponds to a higher stability constant.

TABLE 33.--ESR and stability constants for copper (II) amine complexes.

Ligand in Water Solution	A (in gauss)		Log $K_1 K_2^c$
$H_2NCH_2CH_2NH_2$ Ethylenediamine	89 ^a	90 ^b	19.72
$H_2NCH_2CH_2CH_2NH_2$ Trimethylenediamine	--	87 ^b	16.9
$H_2NCH_2CH_2OH$ Ethanolamine	87.5 ^a	87 ^b	--
$HN(CH_2CH_2OH)_2$ Diethanolamine	--	83 ^b	--
$HN_2CH_2CH_2NH$ CH ₂ CH ₂ $HN_2CH_2CH_2NH$ Triethylenetetramine	82 ^a	--	20.5
NH_3 Ammonia	81 ^a	78 ^b	12.7($K_1 K_2 K_3 K_4$)
$N(CH_2CH_2OH)_3$ Triethanolamine	77 ^a	74 ^b	--
$H_2N-CH_2-CH_2N(CH_2CH_3)_2$ N,N-Diethylenediamine	77.5 ^a	--	13.7
$(CH_3)_2CH_2NH_2$ Isopropylamine	--	61	--

^aThis work.^bReference 139.^cReference 136, page 286 and 518-523.

SUMMARY

The electron spin resonance spectra of a number of transition metal complexes have been obtained. The interpretation of the spectra has been shown to be more complex than expected. Effects which previously were ascribed to covalency may also have appreciable contributions from excited states so that it now appears that additional information about the symmetry, energy levels, and effects of spin polarization are required in order to accurately describe the covalency of a transition metal complex from its electron spin resonance spectrum.

APPENDIX I

GLOSSARY

1. A, A_S - Isotropic hyperfine coupling coefficient, page 19, 20, 25, 26.
2. A_D - Ligand hyperfine coupling constant due to direct dipole interaction from the electrons on the metal ion, page 20, 21.
3. A_O - Theoretical anisotropic nuclear hyperfine splitting value, page 25, 80.
4. A'_σ, A'_S - Theoretical nuclear hyperfine splitting value for an electron which spent 100% of its time in the orbital indicated by the subscript, page 21.
5. $A_{||}$ - Anisotropic hyperfine coupling coefficient along the chosen axial symmetry axis, page 18, 19, 24, 25, 26.
6. A_{\perp} - Anisotropic hyperfine coupling coefficient perpendicular to the chosen axial symmetry axis, page 18, 19, 24, 25, 26.
7. AcAc- Acetylacetonate, page 65.
8. CF_3 AcAc- Trifluoroacetylacetonate, page 65, 73.
9. D- Zero-field splitting coefficient along the chosen symmetry axis, page 102.
10. Diphenylacetylacetonate-
Dibenzoylmethane, page 89.
11. DMF- Dimethylformamide, page 38, 63, 65, 73.
12. DMSO- Dimethylsulphoxide, page 64, 66, 73.
13. D_s, D_q, D_t - Crystal field splitting parameters, page 28.

14. E- Zero-field splitting coefficient perpendicular to the chosen symmetry axis, page 100.
15. e_g^- Transition metal d orbitals of correct symmetry to form sigma molecular orbitals in an octahedral complex.
16. f_σ, f_π, f_s^- Electron spin density in the σ , π , and s orbital respectively, page 21, 26, 98.
17. g- Spectroscopic splitting factor, page 6.
18. g_{\parallel}^- Spectroscopic splitting factor parallel to chosen axial symmetry axis. page 22, 23, 24.
19. g_{\perp}^- Spectroscopic splitting factor perpendicular to chosen axial symmetry axis, 22, 23, 24.
20. HexaFACAc, $CF_3CF_3AcAc^-$ Hexafluoroacetylacetonate, page 65, 73.
21. I- Nuclear magnetic moment, page 24, 25.
22. K_o^- Fermi contact term contribution to the nuclear hyperfine splitting constant, page 105.
23. m- Component of nuclear magnetic moment, I, page 24, 25.
24. N_σ, N_π^- Molecular orbital coefficient of metal atomic d orbital, page 17, 19, 20, 21, 22.
25. Py- Pyridine, page 103.
26. $S_{d,x}^-$ Metal 3d orbital-ligand x orbital atomic overlap integral, page 20.
27. t_{2g}^- Transition metal d orbitals of correct symmetry to form π molecular orbitals in an octahedral complex.
28. Ts- Paratoluenesulfonic acid anion, page 103.
29. β_n^- Nuclear magneton, page 20.

30. γ - Molecular orbital coefficient which indicates covalent character in excess of that caused by metal-ligand overlap, page 20.
31. λ - Spin-orbit coupling constant, page 6, 24.
32. λ_x - Molecular orbital coefficient of the ligand orbital which includes both covalency and overlap, page 20.
33. μ_n - Magnetic moment of the nucleus, page 20.
34. ν - Klystron frequency, page 24, 61.
35. ρ - Ratio of axial crystal field to equatorial field, page 30.
36.  $\text{CF}_3\text{AcAc-}$ Thenoyltrifluoroacetate, page 66, 73.
37.  - Thenoyl group, page 63.

REFERENCES

1. S. Sugano, and R. G. Shulman, Phys. Rev. 130, 517 (1963).
2. T. P. P. Hall, W. Hayes, R. W. H. Stevenson, and J. Wilkens, J. Chem. Phys., 38, 1977 (1963); 39, 35 (1963).
3. R. Lacroix and G. Emch, Helv. Phys. Acta. 35, 592 (1962).
4. C. J. Ballhausen, "Introduction to Ligand Field Theory," McGraw-Hill, New York, 1962.
5. L. E. Orgel, "An Introduction to Transition-Metal Chemistry," Wiley, New York, 1960.
6. J. S. Griffith, "The Theory of Transition-Metal Ions," University Press, Cambridge, England, 1961.
7. C. K. Jorgensen, "Absorption Spectra and Chemical Bonding in Complexes," Pergamon Press, New York, 1962.
8. C. K. Jorgensen, "Inorganic Complexes," Academic Press, New York, 1963.
9. C. K. Jorgensen, "Progress in Inorganic Chemistry," 4, Interscience, New York, 1962.
10. C. K. Jorgensen, "Advances in Chemical Physics," V, Interscience, New York, 1963.
11. C. K. Jorgensen, "Solid State Physics," 13, Academic Press, New York, 1962.
12. F. A. Cotton, "Chemical Applications of Group Theory," Interscience, New York, 1963.
13. K. Nakamoto, "Infrared Spectra of Inorganic and Coordination Compounds," Wiley, New York, 1963.
14. R. J. Faber, Ph.D. Thesis, Michigan State University, 1957. Title: "Paramagnetic Resonance of Some Adsorbed Transition Metal Ions."
15. K. D. Vos, Ph.D. Thesis, Michigan State University, 1962. Title: "Electron Paramagnetic Resonance Absorption Studies on Solutions of Metals in Ammonia and Amines."

16. S. K. Bolte, Ph.D. Thesis, Michigan State University, 1963. Title: "A Study of the Free Radicals in Irradiated Amides by Electron Spin Resonance Spectroscopy."
17. J. E. Wreede, M. S. Thesis, Michigan State University, 1963. Title: "Hyperfine Splitting in Electron Paramagnetic Resonance Studies of Metal-Amine Solutions."
18. G. E. Pake, "Paramagnetic Resonance," Benjamin, New York, 1962.
19. W. Low, "Solid State Physics," Suppl. 2, Academic Press, New York, 1960.
20. C. P. Slichter, "Principles of Magnetic Resonance," Harper and Row, New York, 1963.
21. S. A. Al'tshuler and B. M. Kozyrev, "Electron Paramagnetic Resonance," Academic Press, New York, 1964.
22. R. S. Anderson, "Methods of Experimental Physics," 3, Academic Press, New York, 1962.
23. K. W. H. Stevens, "Magnetism," 1, Academic Press, New York, 1963.
24. A. Carrington and H. C. Longuet-Higgins, Quart. Rev. 14, 427 (1960).
25. H. S. Jarrett, "Solid State Physics," 14, Academic Press, New York, 1963.
26. R. E. Robertson, "Determination of Organic Structures by Physical Methods," 2, Academic Press, New York, 1962.
27. S. I. Weissman, Ann. Rev. Phys. Chem. 12, 151 (1961)
28. R. G. Shulman, Ann. Rev. Phys. Chem. 13, 325 (1962).
29. M. C. R. Symons, Ann. Repts. Progr. Chem. 59, 45 (1962).
30. W. Low, Ed., "Paramagnetic Resonance," 1, 2, Academic Press, New York, 1963.
31. Colloque Ampere, 9, University of Geneva, Switzerland, 1960.
32. Colloque Ampere, 10, North-Holland, Amsterdam, 1961.
33. Colloque Ampere, 11, North-Holland, Amsterdam, 1962.
34. R. Servant and A. Charru, Ed. "Electronic Magnetic Resonance and Solid Dielectrics," North-Holland, Amsterdam, 1964.

35. J. Phys. Soc. Japan. 17, Suppl. B-1, 1962.
36. J. Appl. Phys. 33, Suppl. 1, 1962.
37. R. D. Feltham, Ph.D. Thesis, U. of Calif., Berkeley, UCRL 3867, 1957.
38. J. E. Drumheller, Ph.D. Thesis, U. of Colorado, 1962.
39. R. Neiman, Ph.D. Thesis, U. of Calif., Los Angeles, 1960.
40. A. V. Guzzo, Ph.D. Thesis, Washington University, St. Louis, 1960.
41. L. Helmholz and A. V. Guzzo, J. Chem. Phys. 32, 302 (1960).
42. L. Helmholz, A. V. Guzzo, and R. N. Sanders, J. Chem. Phys. 35, 1349 (1961).
43. R. Kyi, Ph.D. Thesis, U. of Calif., Berkeley, UCRL 9109, 1960.
44. J. D. Axe, Ph.D. Thesis, U. of Calif., Berkeley, UCRL 9293, 1960.
45. R. G. Hayes, Ph.D. Thesis, Univ. of Calif., Berkeley, UCRL 9873, 1961.
46. J. Owen, Proc. Roy. Soc. (London) A 227, 183(1955).
47. T. Murao, Progr. Theoret. Phys. (Kyoto) 21, 657 (1959).
48. T. M. Dunn, Trans. Faraday Soc. 57, 1441 (1961).
49. W. Marshall and R. Stuart, Phys. Rev. 123, 2048 (1961).
50. P. W. Anderson, "Solid State Physics," 14, Academic Press, New York, 1963, p. 99.
51. R. G. Shulman and S. Sugano, Phys. Rev. 130, 506, (1963).
52. R. Lacroix and G. Emch, Helv. Phys. Acta 35, 592 (1962).
53. B. R. McGarvey, J. Chem. Phys. 41, 3743 (1964).
54. H. Kon and N. E. Sharpless, J. Chem. Phys. 42, 906 (1965).
55. H. A. Kuska and M. T. Rogers, J. Chem. Phys. 41, 3802 (1964).
56. A. Abragam and M. H. L. Pryce, Proc. Roy. Soc. (London) A 205, 135 (1951).
57. A. J. Freeman and R. E. Watson, Phys. Rev. 123, 2027 (1961).

58. J. H. Wood and G. W. Pratt, Jr., Phys. Rev. 107, 995 (1957).
59. V. Heine, Phys. Rev. 107, 1002 (1957).
60. On.Matamura. J. Phys. Soc. Japan 14, 108 (1959).
61. R. S. Title, Phys. Rev. 131, 623 (1963).
62. B. Welber, Phys. Rev., 138, A1481 (1965).
63. E. König, Z. Naturforsch. 19A, 1139 (1964).
64. W. J. Childs, L. S. Goodman, and D. von Ehrenstein, Phys. Rev. 132, 2128 (1963).
65. A. Davison, N. Edelstein, R. H. Holm, and A. H. Maki, J. Am. Chem. Soc. 86, 2799 (1964).
66. R. E. Robertson and H. M. McConnell, J. Phys. Chem. 64, 70 (1960).
67. N. J. Trappeniers and S. H. Hagen, Physica, 31, 122 (1965) and 31, 251 (1965).
68. A. Mukherji and T. P. Das, Phys. Rev. 111, 1479 (1958).
69. A. J. Freeman and R. E. Watson, Bull. Am. Phys. Soc. 6, 234 (1961).
70. R. E. Watson and A. J. Freeman, Phys. Rev. 134, A 1526 (1964).
71. D. E. Ellis, Solid-State and Molecular Theory Group, M.I.T. Quarterly Progress Report No. 55, January 15, 1965, p. 58.
72. D. Kivelson and S. Lee, J. Chem. Phys. 41, 1896 (1964).
73. R. G. Shulman and S. Sugano, J. Chem. Phys. 42, 39, (1965).
74. T. Tsang, J. Chem. Phys. 40, 729 (1964).
75. W. Marshall, "Paramagnetic Resonance," I, Academic Press, New York, 1963, p. 347.
76. E. Simanek and Z. Sroubek, Phys. Stat. Solidi 4, 291 (1964).
77. H. A. Kuska and M. T. Rogers, J. Chem. Phys. 42, 3034 (1965).
78. I. Siegel, Phys. Rev. 134, A 193 (1964).
79. V. S. Korol'Kov, Opt. Spectry. 11, 73 (1961).
80. R. A. D. Wentworth and T. S. Piper, Inorg. Chem. 4, 709 (1965).

81. J. Selbin and T. R. Ortolano, *J. Inorg. Nucl. Chem.* 26, 37 (1964).
82. H. Yamatera, *Bull. Chem. Soc. Japan* 31, 95 (1958).
83. Varian Associates, Palo Alto, California.
84. L. Buss and L. Bogart, *Rev. Sci. Instr.* 31, 204 (1960).
85. Hewlett-Packard Co., Palo Alto, California.
86. Waveline Inc., Caldwell, New Jersey.
87. Micro-Now Instrument Company, Chicago, Ill.
88. National Company, Malden, Mass.
89. Beckman Model 350, Beckman Helipot Division, Fullerton, California.
90. H. A. Kuska and M. T. Rogers, *J. Chem. Phys.* 40, 910 (1964).
91. Instruction Manual V-4502 EPR Spectrometer Systems, Varian Associates, Palo Alto, Calif., p. 5-11.
92. J. B. Spencer and R. J. Myers, *J. Am. Chem. Soc.* 86, 522 (1964).
93. This work.
94. J. L. Burdett, Ph.D. Thesis, Michigan State University, 1963.
95. F. Crusser and E. H. Miller, *J. Am. Chem. Soc.* 28, 1132 (1906).
96. W. P. Griffith, J. Lewis, and G. N. Wilkinson, *J. Chem. Soc.* 1959, 872.
97. L. H. Holmes Jr., Ph.D. Thesis, Louisiana State University, 1961.
98. A. M. Golub and R. A. Kostrova, *Russ. J. Inorg. Chem.* 5, 349 (1960).
99. M. Mori, S. Ueshiba, and S. Kawaguchi, *Bull. Chem. Soc. Japan* 36, 796, (1963).
100. J. P. Greenstein and M. Winitz, "Chemistry of the Amino Acids, 1, Wiley, New York, 1961, p. 569.
101. *Physics Today*, Feb., 49 (1964).
102. I. Bernal and S. E. Harrison, *J. Chem. Phys.* 34, 102 (1961).
103. W. P. Griffith, *J. Chem. Soc.* 1963, 3286.

104. J. J. Fortman and R. G. Hayes, *J. Chem. Phys.* 43, 15 (1965).
105. R. G. Hayes, *J. Chem. Phys.* 38, 2580 (1963).
106. J. B. Spencer and R. J. Myers, *J. Am. Chem. Soc.* 86, 522 (1964).
107. B. Elschner and R. Neubert, "Hochfrequenzspektroskopie" Akademie-Verlag, Berlin, 1961, p. 185.
108. J. Cowen, Physics Department, Michigan State University, Personal Communication.
109. P. T. Manoharan and W. C. Hamilton, *Inorg. Chem.* 2, 1043 (1963).
110. P. Groth, "Chemische Kristallographie," I, Verlag von Wilhelm Engelmann, Leipzig, 1906. p. 418.
111. J. M. Baker, B. Bleaney, and K. D. Bowers, *Proc. Phys. Soc. (London)* B69, 1205 (1956).
112. R. M. Golding, *Mol. Phys.* 5, 369 (1962).
113. E. O. Schulz-Du Bois, *Bell System Tech. J.* 38, 271 (1959).
114. H. Abe and H. Shirai, *J. Phys. Soc. Japan* 15, 1711 (1960).
115. J. R. Morton, *Chem. Rev.* 64, 453 (1964).
116. H. H. Jaffe and G. O. Doak, *J. Chem. Phys.* 21, 196, 258 (1953).
117. D. R. Hartree, "The Calculation of Atomic Structures," Wiley, New York, 1957, p. 67.
118. N. A. Curry and W. A. Runciman, *Acta Cryst.* 12, 674 (1959).
119. L. H. Jones, *Inorg. Chem.* 2, 777 (1963).
120. R. Krishnamurthy and W. B. Schaap, *Inorg. Chem.* 2, (1963).
121. J. O. Artman, J. C. Murphy, J. A. Kohn, and W. D. Townes, *Phys. Rev. Letters* 4, 607 (1960).
122. L. H. Jones, *J. Chem. Phys.* 36, 1400 (1962).
123. W. M. Walsh, *Phys. Rev.* 114, 1485 (1959).
124. G. Raoult, J. C. Parouty, M. Lacombat, and A. M. Duclaux, "Colloque Ampere," 10, North-Holland, Amsterdam, 1961, p. 165.
125. B. R. McGarvey, *J. Chem. Phys.* 40, 809 (1964).

126. S. E. Harrison and J. M. Assour, *J. Chem. Phys.* 40, 365 (1964).
127. A. V. Zelewsky and W. Schneider, "Proc. 8th International Conference on Coordination Chemistry," Springer-Verlag, Wien, 1964, p. 43.
128. H. R. Gersmann and J. D. Swalen, *J. Chem. Phys.* 36, 3221 (1962).
129. D. Kivelson and R. Neiman, *J. Chem. Phys.* 35, 149 (1961).
130. A. H. Maki and B. R. McGarvey, *J. Chem. Phys.* 29, 31 (1958).
131. J. L. Burdett and M. T. Rogers, *J. Am. Chem. Soc.* 96, 2105 (1964).
132. K. Nakamoto, Y. Morimoto, and A. E. Martell, *J. Phys. Chem.* 66, 346 (1962).
133. L. G. Van Uitert, W. C. Fernelius and B. E. Douglas, *J. Am. Chem. Soc.* 75, 457, 2736 (1953).
134. G. S. Hammond, A. W. Moschel, and W. G. Bordium, *J. Phys. Chem.* 64, 1782 (1960)
135. H. F. Holzclaw, Jr., A. J. Carlson, and J. P. Collman, *J. Am. Chem. Soc.* 78, 1838 (1956).
136. A. E. Martell and M. Calvin, "Chemistry of the Metal Chelate Compounds," Prentice-Hall Inc., New York, 1952, Appendix 1.
137. R. L. Belford, A. E. Martell, and M. Calvin, *J. Inorg. and Nucl. Chem.* 2, 11 (1956).
138. R. J. Faber and M. T. Rogers, *J. Am. Chem. Soc.* 81, 1849 (1959).
139. N. N. Tithomirova and K. I. Zamaraev, *Zhurnal Strukturnoi Khimii.* 4, 224 (1963).
140. R. L. Belford, M. Calvin, and G. Belford, *J. Chem. Phys.* 26, 1165 (1957).
141. J. P. Fackler, Jr., F. A. Cotton, and D. W. Barnum, *Inorg. Chem.* 2, 97 (1963).
142. H. C. Freeman, M. R. Snow, I. Nitta, and K. Tomita, *Acta Cryst.* 17, 1463 (1964).
143. K. Nakamoto, Y. Morimoto, and A. E. Martell, *J. Am. Chem. Soc.* 83, 4533 (1961).

144. S. Ahrland and B. Noren, Acta Chem. Scand. 12, 1595 (1958).
145. C. J. Ballhausen and H. B. Gray, Inorg. Chem., 1, 111 (1962).
146. "Stability Constants of Metal-Ion Complexes," Publication number 17, Chemical Society, London, Burlington House, London, 1964.
147. J. Selbin and L. Morpurgo, J. Inorg. Nucl. Chem. 27, 673 (1965).
148. H. M. McConnell, W. W. Porterfield, and R. E. Robertson, J. Chem. Phys. 30, 442 (1959).
149. C. Kikuchi, M. S. Sirvetz, and V. W. Cohen, Phys. Rev. 92, 109 (1953).
150. I. Bernal and P. H. Rieger, Inorg. Chem., 2, 256 (1963).
151. K. DeArmond, B. B. Garrett, and H. S. Gutowsky, J. Chem. Phys. 42, 1019 (1965).
152. N. S. Garif'yanov and S. E. Kamenev, Soviet Physics, JETP, 19, 340 (1964).
153. R. H. Borcherts and C. Kikuchi, J. Chem. Phys., 40, 2270 (1964).
154. J. Selbin, Chem. Rev. 65, 153 (1965).
155. H. Irving and L. D. Pettit, J. Chem. Soc., 1963, 1546.
156. J. P. Greenstein and M. Winitz, "Chemistry of the Amino Acids, 1, Wiley, New York, 1961, p. 486.
157. T. J. Lane, J. A. Durkin, and R. J. Hooper, Spectrochim. Acta 20, 1013 (1964).
158. I. Nakagawa, R. J. Hooper, J. L. Walter, and T. J. Lane, Spectrochim. Acta 21, (1965).
159. K. Nakamoto, Y. Morimoto, and A. E. Martell, J. Am. Chem. Soc. 83, 4528 (1961).
160. R. A. D. Wentworth and T. S. Piper, J. Chem. Phys. 41, 3884 (1964).
161. T. R. Ortolano, J. Selbin, and S. P. McGlynn, J. Chem. Phys. 41, 262 (1964).
162. H. B. Gray, P. T. Manoharan, J. Pearlman, and R. F. Riley, Chem. Communications 1965, 62.

163. D. A. C. McNeil, J. B. Raynor, and M. C. R. Symons, J. Chem. Soc. 1965, 410.
164. H. B. Gray and C. J. Ballhausen, J. Chem. Phys. 36, 1151 (1962).
165. A. K. Wiersema and J. J. Windle, J. Phys. Chem. 68, 2316 (1964).
166. C. A. Bates, Proc. Phys. Soc.(London) 83, 465 (1964).
167. J. S. Van Wieringen, Disc. Faraday Soc. 19, 118 (1955).
168. C. J. Ballhausen and H. B. Gray, Inorg. Chem. 2, 426 (1963).
169. J. Lewis, R. J. Irving, and G. Wilkinson, J. Inorg. Nucl. Chem. 7, 32 (1958).

MICHIGAN STATE UNIVERSITY LIBRARIES



3 1293 01750 6530